(19)日本国特許庁(JP)　(12)公表特許公報(A)　(11)特許出願公表番号
特表2004-502957
(P2004-502957A)
(43)公表日　平成16年1月29日(2004.1.29)

(51)Int.Cl.[7]	F I		テーマコード（参考）
G01N 21/17	G01N 21/17	620	2G059
A61B 1/00	A61B 1/00	300D	2H040
G02B 23/26	G02B 23/26	B	4C061
H04N 5/335	H04N 5/335	V	5C024

審査請求 未請求　予備審査請求 有　（全 186 頁）

(21)出願番号　特願2002-509751(P2002-509751)
(86)(22)出願日　平成13年7月10日(2001.7.10)
(85)翻訳文提出日　平成15年1月10日(2003.1.10)
(86)国際出願番号　PCT/CA2001/000992
(87)国際公開番号　WO2002/004929
(87)国際公開日　平成14年1月17日(2002.1.17)
(31)優先権主張番号　60/217,090
(32)優先日　平成12年7月10日(2000.7.10)
(33)優先権主張国　米国(US)

(71)出願人　503020529
ユニヴァーシティー　ヘルス　ネットワーク
ＵＮＩＶＥＲＳＩＴＹ　ＨＥＡＬＴＨ　ＮＥＴＷＯＲＫ
カナダ国　エム２ジー　２エム９　オンタリオ州　トロント　ユニヴァーシティー　アヴェニュー　６１０　ルーム　７－５０４
(74)代理人　100073184
弁理士　柳田　征史
(74)代理人　100090468
弁理士　佐久間　剛

最終頁に続く

(54)【発明の名称】高分解能コヒーレント光画像化のための方法及び装置

(57)【要約】
試料の表面下微細構造を検査するための方法及び装置が提供される。複数の光放射源からの光が第１の光路に沿って進行する。第１の光路において、装置はそれぞれの光源からの光を第１の光路に沿う複数の焦点のそれぞれに集束させて、第１の光路の選ばれた部分の実質的に連続な覆域を提供する。次いで、試料内に延び込む選ばれた長さの範囲内にある第１の光路上の試料が、第１の光路の選ばれた範囲に沿って走査される。

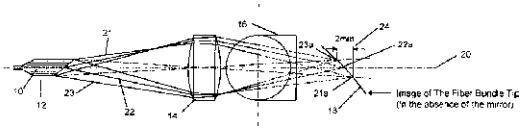

【特許請求の範囲】
【請求項１】
試料の光検のための装置において、前記装置が：
複数の個別光放射源を提供するための光源手段；
前記光源手段から延びる第１の光路；
前記第１の光路の選択された範囲の実質的に連続な覆域を提供するために、前記光放射源からの光を前記第１の光路内の表面の上に位置する複数の焦点のそれぞれに集束させるための、前記第１の光路にある集束手段であって、使用においては、前記選択された範囲内の少なくとも一部に試料を配置することができ、よって前記試料内の複数の点の同時走査を可能にするものである集束手段；
ことを特徴とする装置。
【請求項２】
前記光源手段が一次光源及び、前記一次光源を前記光放射源に結合し、複数本の光ファイバを含む、光結合手段を備えることを特徴とする請求項１に記載の装置。
【請求項３】
前記複数本の光ファイバがファイバ束チップで終端し、前記ファイバ束チップ内の前記光ファイバの末端には前記第１の光路に沿って互いに対して段差が付けられ、前記複数本の光ファイバのそれぞれからの光が相異なる焦点に集束されることを特徴とする請求項２に記載の装置。
【請求項４】
前記第１の光路内に、前記表面の回転運動を可能にするために光放射源からの光を偏向させるための、可回転ミラーを備えることを特徴とする請求項１，２または３に記載の装置。
【請求項５】
前記第１の光路内にミラーを備え、前記光源手段、前記集束手段及び前記ミラーを、結合して、前記表面の直線並進運動を可能にするために直線的に並進させ得ることを特徴とする請求項１，２または３に記載の装置。
【請求項６】
前記第１の光路内に可回転ミラーを備え、前記光源手段、前記集束手段及び前記可回転ミラーを、結合して、前記表面のヘリカル運動を可能にするために直線的に並進させ得ることを特徴とする請求項１，２または３に記載の装置。
【請求項７】
前記表面が複雑な表面であることを特徴とする請求項４，５または６に記載の装置。
【請求項８】
前記ミラーがプリズムの表面であることを特徴とする請求項４，５または６に記載の装置。
【請求項９】
前記ミラーに結合された、前記ミラーを回転させるためのミクロ機械加工電気機械システムを備えることを特徴とする請求項４または６に記載の装置。
【請求項１０】
前記光源手段、前記集束手段及び前記ミラーを直線的に並進させるためのミクロ機械加工電気機械システムを備えることを特徴とする請求項５または６に記載の装置。
【請求項１１】
前記一次光源と前記光ファイバとの間の複数の光結合器、前記光結合器に結合された光遅延発生器及び前記光結合器に結合された検出器手段をさらに備え；前記光結合器は、前記一次光源からの光の一部を前記第１の光路に沿って送り、また前記一次光源からの光の一部を前記光遅延発生器に送り；前記光遅延発生器は第２の光路を提供し；ここで前記第１及び第２の光路に沿って前記光結合器に戻る光の間に干渉効果が生じ；前記光結合器が前記第１及び第２の光路に沿って戻った光を前記検出器手段に送ることを特徴とする請求項２，３または４に記載の装置。

【請求項１２】
複数の一次光源及び複数のツリー型結合器を備え、前記複数のツリー型結合器のそれぞれは、前記複数の一次光源の内の１つと関係付けられ、前記１つの一次光源を前記光結合器の内の少なくとも１つに結合することを特徴とする請求項１１に記載の装置。
【請求項１３】
回収光を前記検出器手段に与えるために前記光結合器と前記検出器手段との間に配置された、複数の光サーキュレータを備えることを特徴とする請求項１２に記載の装置。
【請求項１４】
複数本の光ファイバが前記光結合器を前記光遅延発生器に結合し、前記光遅延発生器は回折格子及び走査ミラーを有し、前記走査ミラーは軸を有し；前記回折格子が前記複数本の光ファイバのそれぞれからの光を前記走査ミラー上に直線的に配向されるスペクトル成分に分解し；前記スペクトル成分の中点が前記スペクトル成分を位相変調するために距離x_dだけ前記走査ミラーの前記軸からオフセットされていることを特徴とする請求項１１に記載の装置。
【請求項１５】
前記複数の光結合器のそれぞれを位相変調器に結合するための第１の複数本の光ファイバ及び前記位相変調器のそれぞれを前記光遅延発生器に結合するための第２の複数本の光ファイバを備え、前記光遅延発生器は回折格子及び走査ミラーを有し、前記走査ミラーは軸を有し；それぞれの光ファイバについて、前記位相変調器が前記光を位相変調し、前記回折格子が前記位相変調された光を前記走査ミラー上に直線的に配向されるスペクトル成分に分解し、前記スペクトル成分の中点が前記走査ミラーの軸上に向けられ；それぞれの光ファイバからの前記スペクトル成分が別の光ファイバからの光の前記スペクトル成分と間隔をおいて配置されていることを特徴とする請求項１１に記載の装置。
【請求項１６】
複数本の光ファイバを備え、前記複数本の光ファイバのそれぞれは前記複数本の光ファイバのそれぞれからの光を第１の光ファイバに結合するために前記複数の光結合器のそれぞれをツリー型結合器に結合し、前記第１の光ファイバは前記結合された光を位相変調するための位相変調器に結合され；前記位相変調器を前記光遅延発生器に結合するための第２の光ファイバを備えることを特徴とする請求項１１に記載の装置。
【請求項１７】
前記装置が、身体の内部検査のための内視鏡として構成され；前記第１の光路、前記集束手段及び前記ミラーが前記内視鏡内に備えられ；前記内視鏡が、少なくとも１つの白色光照明用チャネル、白色光内視鏡前面観察用チャネル、空気ノズル及び水ノズルの内の１つのためのチャネル、及び吸引／生検チャネルの内の少なくとも１つを備えることを特徴とする請求項４，５または６に記載の装置。
【請求項１８】
前記内視鏡が動径、並進またはヘリカル走査を行うように適合されていることを特徴とする請求項１７に記載の装置。
【請求項１９】
前記内視鏡が駆動機構としてミクロ機械加工電気機械システムをさらに備えることを特徴とする請求項１８に記載の装置。
【請求項２０】
試料の光検のためのＮチャネル装置において、前記Ｎチャネル装置が複数の光ネットワーク及び基準アームを備え、前記複数の光ネットワークのそれぞれが、前記Ｎチャネル装置のための１つのチャネルを提供し、前記基準アームを共有することを特徴とするＮチャネル装置。
【請求項２１】
前記光ネットワークが、検出器、光結合手段及び試料アームを備え、前記光結合手段が、前の光ネットワークから光を受け取り、次の光ネットワークに光を送るように構成されていることを特徴とする請求項２０に記載のＮチャネル装置。

【請求項２２】
前記試料アームが偏光制御手段、可変遅延素子及び試料を備えることを特徴とする請求項２１に記載のＮチャネル装置。
【請求項２３】
前記基準アームがツリー型結合手段、位相変調手段及び光遅延手段を備えることを特徴とする請求項２０に記載のＮチャネル装置。
【請求項２４】
試料の光検のための２チャネル装置において、前記２チャネル装置が、請求項２０，２１，２２，２３に記載の光ネットワークを２つ備え、さらに光源及び前記２チャネル装置の方向を案内するための可視光源を備えることを特徴とする２チャネル装置。
【請求項２５】
試料の光検のための方法において、前記方法が：
（ａ）　複数の個別光放射源から、第１の光路に沿う、光を提供するステップ；
（ｂ）　前記第１の光路内に集束手段を提供するステップ；
（ｃ）　前記第１の光路の選択された範囲の実質的に連続な覆域を提供するために、前記第１の光路内の表面に沿う複数の焦点のそれぞれに前記光放射源からの前記光を集束させるステップ；
（ｄ）　前記第１の光路内に少なくとも一部が位置する試料を提供するステップ；及び
（ｅ）　前記試料内の複数の点を同時に走査するステップ；
を含むことを特徴とする方法。
【請求項２６】
一次光源から光を提供するステップ及び前記光を複数本の光ファイバを介して前記複数の個別光放射源に送るステップを含むことを特徴とする請求項２５に記載の方法。
【請求項２７】
前記複数本の光ファイバをファイバ束チップに終端させるステップ、前記光ファイバの末端を共通平面内で前記ファイバ束チップに設けるステップ、前記第１の光路に沿って前記光ファイバの末端に互いに段差を付けるステップ、及び前記光ファイバからの光を共通レンズにより集束させるステップを含むことを特徴とする請求項２６に記載の方法。
【請求項２８】
請求項２７に記載の方法において：
（ａ）前記第１の光路内に可回転ミラーを提供するステップ；
（ｂ）前記第１の光路を偏向させるステップ；
（ｃ）前記複数の焦点を一表面上に配置するステップ；
（ｄ）軸方向走査を実施するステップ；
（ｅ）前記表面を移動させるために前記ミラーを回転させるステップ；及び
（ｆ）前記ステップ（ｄ）を少なくとも２回反復し、それぞれの反復の間に前記ステップ（ｅ）を実施するステップ；
を含むことを特徴とする方法。
【請求項２９】
請求項２７に記載の方法において：
（ａ）前記第１の光路内にミラーを提供するステップ；
（ｂ）前記第１の光路を偏向させるステップ；
（ｃ）前記複数の焦点を一表面上に配置するステップ；
（ｄ）軸方向走査を実施するステップ；
（ｅ）前記表面を移動させるために、前記集束手段、前記複数の光放射源及び前記ミラーを、結合して、直線的に並進させるステップ；及び
（ｆ）前記ステップ（ｄ）を少なくとも２回反復し、それぞれの反復の間に前記ステップ（ｅ）を実施するステップ；
を含むことを特徴とする方法。
【請求項３０】

請求項２７に記載の方法において：
（ａ）前記第１の光路内にミラーを提供するステップ；
（ｂ）前記第１の光路を偏向させるステップ；
（ｃ）前記複数の焦点を一表面に配置するステップ；
（ｄ）軸方向走査を実施するステップ；
（ｅ）前記表面を移動させるために、前記ミラーを回転させると同時に、前記集束手段、前記複数の光放射源及び前記ミラーを、結合して、直線的に並進させるステップ；及び
（ｆ）前記ステップ（ｄ）を少なくとも２回反復し、それぞれの反復の間に前記ステップ（ｅ）を実施するステップ；
を含むことを特徴とする方法。

【請求項３１】
前記ミラーとしてプリズムの表面を提供するステップを含むことを特徴とする請求項２８，２９または３０に記載の方法。

【請求項３２】
複数の結合器を介して前記一次光源から前記複数本の光ファイバに光を供給するステップ；前記光結合器に接続された光遅延発生器を提供し、第２の光路を提供するステップ；干渉パターンを形成するため、前記第１及び第２の光路に沿う前記結合器への光の送り戻しを可能にするステップ；及び、前記干渉パターンの検出のため、前記光結合器において前記第１及び第２の光路から受け取った光を検出手段に送るステップを含むことを特徴とする請求項２８，２９または３０に記載の方法。

【請求項３３】
複数の一次光源を提供し、前記複数の一次光源のそれぞれに対して、それぞれのツリー型結合器を提供するステップ；及び前記複数の一次光源のそれぞれを前記それぞれのツリー型結合器を介して前記光結合器のそれぞれに結合するステップを含むことを特徴とする請求項３２に記載の方法。

【請求項３４】
回収光を前記検出手段に与えるために、前記光結合器と前記検出手段との間に光サーキュレータ手段を提供するステップを含むことを特徴とする請求項３２に記載の方法。

【請求項３５】
請求項１から２４のいずれかに記載の装置を、少なくとも１つの白色光照明用チャネル、白色光内視鏡前面観察チャネル、吸引／生検チャネル並びに空気ノズル及び水ノズルの内の１つのためのチャネル、の内の少なくとも１つを備える、身体の内腔の検査のために適合された内視鏡として提供するステップを含むことを特徴とする請求項３３に記載の方法。

【請求項３６】
前記光放射源を含む媒体と前記試料との間の屈折率の変化があり、それぞれの焦点に対して、前記試料内の実際の前記光放射源のそれぞれのコヒーレンスゲートと前記焦点の位置との間の前記屈折率変化による変位間隔が：
（ａ）前記光放射源の前記焦点が前記光放射源を含む前記媒体から前記試料内に延びる光路に沿って配列されるように、前記第１の光路において前記複数の光放射源からの光を走査するステップ；
（ｂ）前記焦点のそれぞれについて反射光を検出するステップ；及び
（ｃ）隣接する焦点に比較して反射光に大きな変化がある焦点の位置を突き止めるステップ；
にしたがい、前記ステップ（ｃ）で位置が突き止められた前記焦点が前記試料と前記光放射源を含む前記媒体との間の界面の位置を示すことにより；
得られることを特徴とする請求項３０，３１または３２に記載の方法。

【請求項３７】
前記方法が、選択された走査域に対して適切な空間分解能を得るために、それぞれの軸方向走査について前記ステップ（ａ）から（ｃ）を繰り返すステップをさらに含むことを特

徴とする請求項３６に記載の方法。
【発明の詳細な説明】
【０００１】
発明の分野
本発明は高分解能光画像化のための方法及び装置のいずれにも関する。さらに詳しくは、本発明は内視鏡への組込に適する高分解能画像化の提供に関する。
【０００２】
発明の背景
現代の医用画像化手法は、健康管理への応用に重要になっている。Ｘ線コンピュータ連動断層撮影（ＣＴ）、磁気共鳴画像法（ＭＲＩ）及び超音波画像法のような手法は、現代の医療センターのほとんどで利用できる主要な断層撮影法である。可視光内視鏡検査法は、気管支鏡検査または結腸鏡検査のような処置に広く用いられる別の主要な画像化手法である。これらの手法のそれぞれは、様々な物理的原理を採用し、検査下の生物学的組織の様々な特性を様々な分解能で測定する。さらに、これらの手法は生体内で普通に実施できる。第３のタイプの画像化手法である光学顕微鏡検査法も、未だに診療医学において広く利用されている。しかし、現時点では光学顕微鏡検査法は切除または摘出試料の詳細な検査に限られ、生体内では用いられていない。多くの情況において、光学顕微鏡検査法によって与えられる優れたコントラスト及び分解能は、生体組織摘出及びこれに続く光学顕微鏡による組織検査が診断に対する黄金律的標準と見なされるほどである。
【０００３】
低分解能断層撮像手法を、高分解能画像化、生体組織検査法または介入処置とともに使用するような、上記の手法の併合が絶えず研究され、評価されている。そのような手法の評価は、技術上の実行可能性、臨床上の恩恵及び費用に基づいている。
【０００４】
光コヒーレンス断層撮影法（ＯＣＴ）は、生物学的組織のような混濁した高散乱性の媒質において高分解能深度プロファイル測定を可能にする、電磁放射の低コヒーレンス特性に基づく比較的新しい画像化手法である。生物医学的画像化におけるＯＣＴの利用は、現在いくつかの公立及び私企業の研究所で研究されている。ＯＣＴの主要な利点は、組織の表面下部位からの反射深度を局限化できるという能力にある。この局限化は用いられる光源のコヒーレンス特性により本質的に決定され、選択された近赤外線（ＩＲ）源（例えば、レーザまたは増幅自然放出発光装置）に対して２から２０μｍもの狭い範囲とすることができる。このことから、ＯＣＴで達成し得る深度分解能の尺度が与えられる。コヒーレンス性とは無関係に、横方向分解能は画像化深度におけるビーム断面積及び取得データの横方向間隔により決定される。文献における横方向間隔の一般値は５から３０μｍの範囲にある。この混濁組織を損なわない優れた断層画像化能力に対して払われなければならない代償は、多重散乱及び吸収により光のコヒーレンス及び侵入深度がともに低下して、ＯＣＴ画像化深度がほぼ２ないし３ｍｍになるので、画像化深度が制限されることである。
【０００５】
現在のＯＣＴの実施態様のほとんどは、入射コヒーレント光ビームをミラーをもつ基準光路（すなわち基準アーム）及び被検試料をもつ試料光路（すなわち試料アーム）に導く５０／５０ビームスプリッタによる、マイケルソン干渉法に基づく。この方式の自由空間光学系及びファイバ光学系実施態様のいずれもが現在用いられている。基準アームのミラーからの反射ビーム及び試料アームの組織からの反射ビームが同じスプリッタで結合されて、生じる光エネルギーの１／２が検出器に当たる。２本のビームの光路長が光源のコヒーレンス長の範囲内で一致する場合を除いては、一般に２本の光束の非コヒーレントな重畳がおこる。この限界距離内では、２本の光束のコヒーレントな重畳により、特定の深度における組織の反射率に比例する強さの干渉縞をもつ干渉パターンが得られる。次いで、試料の深度プロファイル測定が、基準アーム長を走査することにより、さらに正確には、基準アームにおいて時間遅延を用いて（これは基準アームを長くすることと等価である）基準アームの光路長を走査することにより、達成される。大きな背景拡散反射に埋もれてい

る上記のかすかな振幅変調を測定して定量するために、ダイナミックレンジがほぼ７０から１１０ｄＢの、様々な検出方法が開発されている。さらに、ビームの横方向並進及び基準ミラーの軸方向移動により、所望の視野にわたる２次元反射率画像を構成することが可能になる。デコンボリューションによる画像処理の実施のような、最終画像の品質を向上させる手段も研究されてきた。

【０００６】

上述は通常の反射率ＯＣＴ画像化の簡単な説明である。その他の変形には、例えば、フロー（ドップラー）画像化及び（ＯＣＴ光学系及び／または信号処理手法がさらに複雑化するという犠牲は払うものの）偏光画像化がある。これらの別の手法による画像は普通、通常のＯＣＴによる画像とともに得られ、よっていくつかの画像の重ね合わせまたは融合が可能である。技術開発及び／または臨床への実施がさらに進めば、医学におけるＯＣＴの臨床上の有用性を高めるに十分な情報内容を付け加えることができる。

【０００７】

しかし、研究開発され実験室ではうまくはたらいたＯＣＴシステムの構成及び手法の多くは、そのままでは胃腸または気管支の内視鏡検査のような生体内画像化に適していない。むしろ、そのようなＯＣＴシステムは、皮膚科、眼科及び歯科での応用により適するといえる。対照的に、生体内ＯＣＴ画像化は、速度、分解能、コントラスト、侵入深度及び機器寸法の課題に取り組まなければならない。画像は患者の動きの影響を無視できるに十分に迅速に得られなければならず、それでも適切な軸方向及び横方向分解能が得られ、内視鏡として有用であるに十分に小さい機器寸法が維持されなけらばならない。生体内内視鏡検査に課せられた困難な課題を克服するための、強力な近ＩＲ源、基準アーム長を高速で変化させる手段及び特注の遠端光学装置の開発が行われ、成功している。

【０００８】

最新のＯＣＴ技術は、単一モード光ファイバを従来の白色光内視鏡のアクセサリーチャネルに組み入れられた遠端断層観察光学系とともに採用している。画像を構成するため、ＯＣＴファイバの観察方向がほぼ２ｍｍの距離にわたり前後に直線的に走査され、また柔軟なガイドワイヤまたはインターロック付歯車機構によって毎秒数回転で回転される。この並進または回転と同時に、深度方向走査（すなわちＡ－走査）をおこさせるために内視鏡の外にある基準アームの長さが光位相遅延により迅速に変えられる。現在、これらのＯＣＴシステムは通常のビデオレートまでのフレームレートで動作するが、より一般的には毎秒４から８フレームで動作し、１フレームは２から３ｍｍの深度までの十分な周辺観察像を提供する。得られる分解能値は、深度（軸）方向でほぼ５から２５μｍであり、横方向ではほぼ２０から４０μｍである。さらに、横方向分解能は一般に、等比発散により、ＯＣＴ装置のファイバチップからの距離が大きくなるにつれて低下する。これらのＯＣＴシステムは、雑音レベルが高く、画像化速度が速いために、ダイナミックレンジが生体外システムに対応するダイナミックレンジより若干低い。

【０００９】

最新のＯＣＴ技術に基づくと、コヒーレント生体内ＯＣＴシステムが臨床画像化に成功するに十分であるかは疑問である。画像は確かに有用であるが、“光生検”という逃げ水のような目標が実現されるべきであるならば、かなりの改善が必要である。例えば、軸方向及び横方向の分解能は改善できる。軸方向分解能の改善には通常、より良好な低コヒーレンス光源（すなわちＣＷ（連続波）及びパルス光源）の使用が含まれるが、最適に近い、深度可変の、横方向分解能の問題は処理が一層困難である。体外システムでは、速度及び物理的寸法の制限が緩和され、横方向解像度は高ＮＡ（開口数）対物レンズを用いてビームを数μｍまで集束させることにより改善される。従来のＯＣＴ走査とは対照的に、この場合には、光路長差の振動を小さくしてあらかじめ選択された深さで横（面内）方向に画像化を行い、続いて深度を必要なだけ少量増分して次の画像化を行うことができる。高ＮＡ対物レンズは屈折率整合液を介して組織に結合されることが多い。ＯＣＴを高ＮＡ遠端光学レンズとともに用いる手法は総じて光コヒーレンス顕微鏡法（ＯＣＭ）として知られる。しかし、ビームウエスト位置における改善された横方向解像度は、強集束ビームの焦

点深度が非常に浅いため、他の深度においては横方向ぼけという犠牲を払うことになる。したがって、様々な深度に集束させるためにレンズ－表面間隔を変えなければならない。さらに、動的トラッキング方式では、コヒーレンスゲート（コヒーレンスゲート内では試料アームからの光ビームと基準アームからの光ビームとの間でコヒーレント干渉が可能である）の位置とビームウエストの位置が同じ深度に保たれる必要がある。横方向分解能改善のための上記の手法は、寸法及び速度要件のため、生体内内視鏡については試みられてこなかった。

【００１０】

発明の概要

本発明は、以降内視顕微鏡と称することとする、顕微的分解能をもつ内視鏡光コヒーレンス断層撮影（ＯＣＴ）装置を提供するという概念に基づく。内視顕微鏡の考え得る臨床上の応用の考察の結果、以下のパラメータ及び特徴が、現在の生体内ＯＣＴシステムと同時にこれらのパラメータ及び特徴を達成することは困難であることから、弁別された。

【００１１】

１．高分解能

細胞レベル及び細胞より小さいレベルの分解能を達成するためには、内視顕微鏡は、好ましくは軸方向及び横方向のいずれにおいても５μｍより小さい構造を解像すべきである。既存の生体内ＯＣＴシステムのほとんどとは対照的に、等比発散による、画像化されている組織の深度にともなう横方向分解能の実質的な低下が生じてはならない。

【００１２】

２．大視野

内視顕微鏡の適切な視野は、光軸の軸方向及び横方向においてほぼ２ｍｍ×２ｍｍである。この視野で臨床上の応用には十分であると考えられる。画像全体にわたり軸方向及び横方向のいずれにおいても５μｍ分解能を達成するためには、それぞれのフレームに対して８００回をこえるＡ－走査（すなわち深度走査）が行われなければならない。得られる画像は、６４０，０００をこえる画素をもつであろう。この画素数は既存の生体内ＯＣＴシステムより数桁大きい。

【００１３】

３．小寸法内視鏡チップ

既存の生体内ＯＣＴシステムのほとんどは、既存の内視鏡の計装チャネルの制約に基づいて設計されている。この結果、そのようなシステムの外径はほぼ２から３ｍｍに抑えられ、このため撮像システムの開口数が制約される。このことから、生体内条件下で高い横方向分解能を得ることが困難になる。このような制約は技術上不要であり得るし、考察している臨床上の応用におけるＯＣＴ／ＯＣＭの恩恵の十全な活用を制限し得る。したがって、例えば３ｍｍないしそれ以上のような、より大きな外径を、２０ｍｍより短い硬質チップ長とともに、内視鏡に用いることができる。

【００１４】

４．高画像化速度

内視顕微鏡は生体内条件下で高分解能の大面積画像化に用いられるであろうから、生理学的運動による組織の運動があるので、運動アーティファクトが考慮されなければならない。これらの運動アーティファクトは良好な画像品質を保証するために除去されるべきである。したがって、内視顕微鏡は、典型的な生理学的運動速度が５ｍｍ／秒であるとすれば、画像１フレームを好ましくは１２．６ミリ秒以内に取得できるべきである。これは、毎秒６３，０００回のＡ－走査に相当する。この画像化速度は現在の生体内ＯＣＴシステムに比べて１桁より大きい。

【００１５】

５．現在利用可能な内視鏡画像化法との統合

臨床上の有用性を向上させるため、好ましくは従来の白色光画像化が内視顕微鏡に統合されるべきである。さらに、好ましくは、内視顕微鏡の誘導の下に切除生検が行われ得るように、計装チャネルが設計されるべきである。おそらくは、水及び空気の送配のための計

装チャネルも利用可能にされることも好ましい。

【００１６】

上に略述した内視顕微鏡のための高等な要件は既存のＯＣＴ／ＯＣＭ設計とは相容れない。例えば、内視顕微鏡に６ｍｍの外径が許容され、Ｇ．Ｊ．ティアニー（Ｔｅａｒｎｅｙ），Ｍ．Ｅ．ブレジンスキー（Ｂｒｅｚｉｎｓｋｉ），Ｂ．Ｅ．ボウマ（Ｂｏｕｍａ），Ｓ．Ａ．ボッパート（Ｂｏｐｐａｒｔ），Ｃ．ピトリス（Ｐｉｔｒｉｓ），Ｊ．Ｆ．サザーン（Ｓｏｕｔｈｅｒｎ），及びＪ．Ｇ．フジモト（Ｆｕｊｉｍｏｔｏ）（「光コヒーレンス断層撮影法による生体内内視鏡光生検」，サイエンス（Ｓｃｉｅｎｃｅ），１９９７年６月２７日，第２７６巻，ｐ．２０３７～２０３９）により説明されるような単一回転ファイバに基づく、遠端光学系構造が用いられれば、５μｍの横方向分解能が走査のどの１つにおいても組織内の１つの特定の深度で達成され得るが、そのような横方向分解能は他の深度ではビーム発散により低下するであろう。さらに、所要の小寸法ビームウエストをつくるには高ＮＡシステムが必要となるであろうから、Ｌ．Ｍ．シュミット（Ｓｃｈｍｉｔｔ），Ｓ．Ｌ．リー（Ｌｅｅ），及びＫ．Ｍ．ユン（Ｙｕｎｇ）（「厚い組織における分解能が高められた光コヒーレンス顕微鏡」，Ｏｐｔｉｃｓ Ｃｏｍｍｕｎｉｃａｔｉｏｎｓ，１９９７年，第１４２巻，ｐ．２０３～２０７）により説明されるようなある種の動的補償を実施しなければ、かなりの（例：２ｍｍ）距離にわたる深度においてコヒーレンスゲートと焦点とが一緒にとどまることはないであろう。したがって、上述した内視顕微鏡の要件の内のいくつかを達成するためには、（プローブ／組織間隔を変化させる）動的集束及び（光路長差を変化させる）動的補償が用いられなければならない。しかしこれらの集束及び補償手法では、実用装置の実現が面倒になり、高画像化速度要件を満たすことが一層困難になり得る。画像化速度を初めに満たすことを試みると、Ａ．Ｍ．ローリンズ（Ｒｏｌｌｉｎｓ），Ｍ．Ｄ．クルカーニ（Ｋｕｌｋａｒｎｉ），Ｓ．ヤズダンファー（Ｙａｚｄａｎｆａｒ），Ｒ．ウング－アルニャウィー（Ｕｎｇ－ａｒｎｙａｗｅｅ），及びＪ．Ａ．イザット（Ｉｚａｔｔ）（「生体内ビデオレート光コヒーレンス断層撮影法」，Ｏｐｔｉｃｓ Ｅｘｐｒｅｓｓ，１９９８年９月１４日，第３巻，第６号，ｐ．２１９～２２９）によって説明されるように、画像分解能、特に横方向分解能が、装置の臨床上の有用性が損なわれる程度まで低下する。

【００１７】

本発明は、既存の生体内または生体外ＯＣＴ／ＯＣＭシステムに現在実施されているようなシリアル走査の代わりに、複数本のファイバ（すなわちチャネル）を採用して画像の様々な部分のパラレル走査を可能にするＯＣＴを有する内視顕微鏡を提供する。それぞれのチャネルが非常に狭い軸方向範囲にかけてだけ高分解能ＯＣＴデータを収集する、組織内の様々な深度に集束される多パラレルチャネルを使用すれば、動的集束または動的補償を用いずに、視野全体にわたる密配置焦点列を得ることができる。これにより装置の構造が大いに簡素化され、この場合には、使用される光コンポーネントのほとんどを固定型とすることができて、高速動作を容易化することができる。さらに、ファイバ光学ベースのＯＣＴ手法では寸法が本質的に小さいから、多チャネル概念を屈曲性内視鏡装置で実施することが可能になり、一方で、患者の外部にある内視鏡の近端部には、光源、検出器及びその他の装備のための余裕ができる。

【００１８】

本発明の第１の態様にしたがえば試料の光検のための装置があり、本装置は：

複数の個別光放射源を提供するための光源手段；

光源手段から延びる第１の光路；及び

第１の光路の選択された範囲の実質的に連続な覆域を提供するために光放射源からの光を第１の光路内の面上に位置する複数の焦点のそれぞれに集束させ、使用時には、試料の少なくとも一部を前記選択された範囲内に配置することができ、よって試料内の複数の点を同時に走査することを可能にするための、第１の光路内の集束手段；

を備える。

【００１９】

本発明の第２の態様にしたがえば試料の光検のためのＮチャネル装置があり、本Ｎチャネル装置は複数の光ネットワーク及び１つの基準アームを備え、光ネットワークのそれぞれはＮチャネル装置のための１チャネルを提供し、基準アームを共有する。

【００２０】

本発明の第３の態様にしたがえば試料の光検のための方法が提供され、本方法は：

（ａ）　第１の光路に沿う、複数の個別光放射源からの光を提供するステップ；

（ｂ）　第１の光路内に集束手段を提供するステップ；

（ｃ）　第１の光路の選択された範囲の実質的に連続な覆域を提供するために、光放射源からの光を第１の光路内の面に沿う複数の焦点のそれぞれに集束させるステップ；

（ｄ）　第１の光路内に少なくとも一部が配置された試料を提供するステップ；

及び

（ｅ）　試料内の複数の点を同時に走査するステップ；

を含む。

【００２１】

本発明とともに使用するための試料がいかなる生物学的組織も、あるいはその他の適当な材料も含み得ることは当然である。

【００２２】

本発明のさらなる目的及び利点は、添付図面とともになされる、以下の説明から明らかになるであろう。

【００２３】

発明の詳細な説明

本発明の一層の理解のため及び本発明がどのようにしてに実行され得るかを示すため、例として、本発明の好ましい実施形態を示す図面がここで参照される。

【００２４】

以下の説明においては、撮像源により用いられる波長及び装置に用いられる光コンポーネントの物理的寸法のような、様々な特定の寸法及びその他のパラメータが記述される。これらの寸法及びパラメータは説明のためでしかなく、本発明を制限するものでないことは当然である。特定のパラメータ、寸法等は目的とする本発明の応用に依存して選択することができる。

【００２５】

図１を参照すれば、本発明は、多束単一モードファイバ１０，ファイバ束チップ１２，集束レンズ１４及びミラー１６を有する内視鏡コヒーレント光顕微鏡を備える装置を提供する。多束単一モードファイバ１０及び集束レンズ１４は静止しており、一方ミラー１６は回転可能である。したがって、ミラー１６は回転のために既知の態様で取り付けられている。ミラー１６のための回転機構の詳細はこれ以上説明されないが、従来の機構とすることができる。（ほぼ５０本のファイバとすることができる）多束単一モードファイバ１０は、ファイバ束チップ１２においてアレイを形成する。このアレイは開豁されて、図２に示されるように、“階段”パターンに配列される。ファイバ束チップ１２から放射される光は集束レンズ１４で集束され、ミラー１６で反射される。集束レンズ１４は、直径を５ｍｍ（すなわちφ＝５ｍｍ）とし、焦点距離を５ｍｍ（すなわちｆ＝５ｍｍ）とすることができる。ミラー１６は、５ｍｍの直径及び４５°で開豁された前面を有することができる。ファイバ束チップ１２の焦点の拡大像が図３に示される。

【００２６】

図１ａは、多束単一モードファイバ１０から例として任意に選ばれた３本のファイバからの３本のビーム２１，２２及び２３を示す。多束単一モードファイバ１０が順次にずらされている、すなわち階段配列になっているという性質により（図２参照）、ビーム２１，２２及び２３のそれぞれが相異なる点から発し、したがってミラー１６が用いられていないときには、表面１８上の相異なる点２１ａ，２２ａ及び２３ａに集束レンズ１４により集束される。ファイバ束チップ１２の多束単一モードファイバ１０の全てが表面１８上の相異なる点に集束されるビームを生じるという、同じ効果が得られることは理解されよう

。参照数字２４で示されるように（また図３に示されるように）、多束単一モードファイバ１０が５０本の光ファイバからなっており、それぞれのファイバからの光がほぼ４０μｍの狭い範囲内に集束され、焦点が（集束レンズ１４の軸２０に沿って測定して）４０μｍずつ間隔をおくように、それぞれのファイバの末端がずらして配置されていれば、合わせて２ｍｍの範囲すなわち深度がカバーされる。集束レンズ１４の軸２０は第１の光路の一部である。

【００２７】

ミラー１６が存在すると、光ビーム２１，２２及び２３は図１ｂ及び１ｃに示されるように集束される。すなわち、３つの焦点２１ｂ，２２ｂ及び２３ｂは第１の光路の外延を形成する軸２６に沿って垂直方向すなわち深度方向に間隔をおいて配される。図１ｃの端面図が示すように、３つの焦点２１ｂ，２２ｂ及び２３ｂは、ミラー１６の運動に対して円周方向にも間隔をおいて配される（すなわち、３つの焦点は横方向に間隔をおいて配される）。３つの焦点２１ｂ，２２ｂ及び２３ｂは表面２７上に落ちて、第１の光路の選択された範囲の画像化を容易にする。表面２７は複雑な表面であっても、平坦な表面であってもよい。多束単一モードファイバ１０が５０本の個別ファイバからなっていれば、ファイバ束チップ１２からの全ての個別ファイバの焦点は、相応した間隔をおいて配されることになろう。あるいは、反射された焦点２１ｂ，２２ｂ及び２３ｂは必ずしも軸２０に垂直である必要はなく、軸２０に対して大角をなしていればよい。

【００２８】

ミラー１６の回転の結果、表面２７は移動する。これにより、図１ｃに示されるように、好ましい２ｍｍ×２ｍｍの大きさの正方形の走査領域２８をカバーする、２次元Ｂ－走査画像３０を得ることが可能になる。このＢ－走査画像３０は走査領域２８に対して得ることができる画像の例を示す。

【００２９】

例えば多束単一モードファイバ１０のコア及びクラッド層の直径を変えることにより、多束単一モードファイバ１０の構造を変えれば、表面２７が変化する。さらに、多束単一モードファイバ１０の代わりに光導波路ウエハを用いることもできる。

【００３０】

代替実施形態において、図１ｄに示されるように、集束レンズ１４及びファイバ束チップ１２と結合して直線的に移動するミラー１６’でミラー１６を置き換えることができる。直線並進には逆進運動を組み入れ得ることが好ましい。力学用語を用いれば、図１ａに描かれるファイバ束チップ１２は動径走査運動を利用する。動径走査運動は、食道または大腸のような、寸法がより大きい器官の走査に適切である。しかし、動径走査に必要な駆動機構は複雑であるため、ファイバ束チップ１２の直径が大きくなり、血管のような内径の小さい器官の内視顕微鏡観察はできないであろう。したがって、動径走査の代わりに直線並進走査を行うように適合された、同様のファイバ束チップ１２’を備える、図１ｄに示される代替実施形態が用いられることになろう。

【００３１】

図１ｄに示されるように、上記の２つの走査方法の間の主要な違いは、ミラー１６’が回転せず、ファイバ束チップ１２’の全体が水平軸に沿って、例えば４ｍｍの範囲にわたり、好ましくは可逆運動で並進されなければならないことである。機械的には、直線並進走査運動は動径走査運動ほど複雑ではない。さらに、直線並進走査は血管のような内径の小さい器官内の内視顕微鏡観察により一層適する。しかし、大腸のような、より大きないくつかの器官に対しては、直線並進走査は位置決めが困難なためそれほど適切ではない。

【００３２】

別の代替実施形態において、上記の走査運動の両者を組み合せてヘリカル走査を行う内視顕微鏡観察装置を作成することができる。ヘリカル走査運動は、ミラー１６，集束レンズ１４及びファイバ束チップ１６の直線並進と組み合された、ミラー１６の回転運動を含むことになろう。そのような内視顕微鏡観察装置は、ヒトの大腸のような、ある種の器官の画像化により一層適し得る。ヘリカル走査内視顕微鏡観察装置は、図１ａに示される装置

を直線並進させることにより実施できる。

【００３３】

また別の代替実施形態において、ファイバ束チップ１２をミクロ機械加工電気機械システム（ＭＥＭＳ）駆動機構を用いるように変更することができる。上述した実施形態ではミラー１６の何らかの形態の運動が必要であるから、機械的駆動機構が全実施形態で必要となる。したがって、内視鏡外部にモーターが配備され、機械的連結駆動機構またはワイヤが内視鏡の全長に沿って配置される。しかし、多チャネルファイバ光学構造は、そのような機械的駆動手段に束縛されない。実際、多チャネルシステムで実現可能な空間分解能は極めて高いため、機械的駆動手段が用いられる場合には、振動誘起偏光依存性のような、機械的駆動手段からの悪影響が本発明の十全な潜在能力を制限しかねない。したがって、電気的駆動型マイクロマシン光学装置を用いて走査を容易にする、ＭＥＭＳ電気的駆動機構を採用することができる。ＭＥＭＳ実施態様はミラー１６のような並進させられる物体の近傍を除いて装置軸に沿う振動を低減するから、本実施態様は、機械的駆動機構により生じ得る悪影響をおそらくは回避し得る。ＭＥＭＳ実施態様は、小形化及び性能に関する利点も提供し得る。

【００３４】

別の代替実施形態においては、ファイバ束チップがミラー１６を必要としないようにすることができる。ファイバ束チップ１２及び集束レンズ１４の結合体を軸回転可能なように取り付けることができる。そうすれば、軸回転運動により、試料内に広がる複数の面の各部分に沿って複数の焦点を導き、走査領域２８のＢ－走査画像３０を構成するように、ファイバ束チップ１２と集束レンズ１４との結合体を適合させることができる。

【００３５】

また別の実施形態において、ミラー１６をプリズム表面とすることができる。装置の他のコンポーネントは、図１ａから１ｄで先に説明され、示された装置にしたがうことになろう。

【００３６】

光路を、直線、彎曲線、及び曲線とし得ることもまた当然である。さらに、光路を、長さ、幅及び高さを有する３次元光路とすることができる。走査運動（すなわち、動径、直線またはヘリカル走査）に依存して、その上に焦点が乗る面の方位も変化し得る。さらに、光路は１つの光放射源または複数の光放射源（すなわち、複数の光源またはそれぞれが光を伝送する複数本のファイバ）からの光を含むことができる。

【００３７】

次に図２ｂ及び２ｃを参照すれば、多束単一モードファイバ１０からなるファイバ束チップ１２の拡大図が示される。多束単一モードファイバ１０のそれぞれのファイバは、直径が、例えば、それぞれ５μｍ及び４０μｍの、コア１０ｂ及びその周りのクラッド層１０ａからなる。多束単一モードファイバ１０のそれぞれの末端は、それぞれのファイバを通る光の焦点が間隔をおいて配されるように、４０μｍずつ段差を付けることができる。但し、４０μｍ以外の段差を用いることもできる。

【００３８】

次に図３を参照すれば、ファイバ束チップ１２における、多束単一モードファイバ１０のそれぞれのファイバについて、Ａ－走査が、２ｍｍの画像化深度のほぼ全体にわたってとられるが、ビーム径がほぼ最小（参照数字３４に示される）であって軸上の位置に対して実質的に変化しない、それぞれのファイバの焦点近傍におけるほぼ４０μｍの短い軸方向範囲だけにとどめられる。本例の構造における、この４０μｍという範囲は、参照数字３１で示される。Ａ－走査は、ファイバ束チップ１２内の多束単一モードファイバ１０のそれぞれのファイバにより同時に行われる。事実上、多重Ａ－走査は様々な動径方向において試料組織内の２ｍｍの深度全体をカバーするが、多束単一モードファイバ１０のそれぞれのファイバについては、４０μｍの焦点深度３１に対応するそれぞれのＡ－走査区画だけが画像の構成に用いられる。焦点域３１に示されるように、ビーム２１ｂ，２２ｂ及び２３ｂのそれぞれは、焦点３８，３７及び３６について明瞭な“砂時計”形を既知の態様

で示す。ビーム２１ｂ，２２ｂ及び２３ｂのそれぞれに対して、遠視野ビーム広がりが線３２で示され、近視野ビーム広がりが線３４で示される。

【００３９】

ミラー１６を回転させる目的は、Ｂ－走査（すなわち図１の走査領域２８の）画像を生成するために、Ａ－走査方向に垂直な方向における動径（すなわち横方向）走査を生じさせることである。得られる、多束単一モードファイバ１０の個々のファイバの焦点の動径走査パターンが、図４に示される。ミラー１６の開豁面がＢ－走査画像がとられるべき位置“Ａ”及び“Ｃ”の方向に実質的に向けられているときにだけ連続走査面が存在することは、注目に値する。動径走査パターン上の他の位置においては、個々のＡ－走査間の“デッドスペース”が非常に大きいため、組織の十分なサンプリングができない。したがって、本発明は、２ｍｍ×２ｍｍの画像が得られる範囲内で、実質的に“Ａ”または“Ｃ”位置において、約２０°のセクター角でセクター走査を行うために、セクター走査画像化装置を備える。本例においては、与えられた形状寸法により、セクター角をさらに大きくすると適切な断層画像を形成するには大きすぎる“デッドスペース”が生じるであろう。

【００４０】

図４ｂおよび４ｃはそれぞれ、ビーム焦点３６，３７及び３８を平面図及び端面図で示す。図示されるように、また先に示した図に対応して、個々の焦点３６，３７及び３８は軸２０に垂直な動径平面において間隔がとられている。図４ｃに示されるように、軸２６に沿う端面図において、焦点３６，３７及び３８は深度に関して間隔がとられているが、重なり合って連続走査面すなわち走査領域２８を形成している。

【００４１】

走査面すなわち走査領域２８に垂直な、図４ａで“Ｂ”及び“Ｃ”で表示される位置の方向に、実質的にミラー１６の開豁面が向けられると、図４ｄ（パターンの平面図）及び図４ｅ（パターンの側面図）に示されるパターンが得られる。ここで、焦点は参照数字４０，４１及び４２で表示される。図４ｄに示されるように、焦点４０，４１及び４２はそれぞれ、ファイバ束チップ１２におけるファイバ間隔に対応する間隔がとられる、個別の面４０’，４１’及び４２’にある。面４０’，４１’及び４２’は軸２０に垂直である。図４ｂから４ｅにおいて、矢印４４は動径走査方向を示す。

【００４２】

図１ｄに示される直線並進システムについては、“デッドスペース”がなく、したがって直線並進システムは大きさがほぼ２ｍｍ×２ｍｍの画像に適する画像化を行うことができる。

【００４３】

内視顕微鏡システムの例示的構成においては、生体内画像化に対して、生理学的運動による組織運動の最大速度を５ｍｍ／秒に選んだ。近回折限界集束レンズ（すなわち、非常に小さな焦点を結ぶことで理想レンズに近いレンズ）を集束レンズ１４として選んだ。近回折限界集束レンズはメレス・グリオ社（Ｍｅｌｌｅｓ Ｇｒｉｏｔ Ｉｎｃ．）から入手した。さらに、複数の単一モードファイバ１０のそれぞれの単一モードファイバには、コア径が５μｍ（すなわちϕ_c～５μｍ）であり、動作波長が０．８６μｍのファイバを用いた。さらに、本構成では、ほぼn_c＝１．４４７のコア屈折率及びΔｎ＝０．００５のコア－クラッド層間屈折率差を組み入れている。これらの値を用いれば、ファイバのＮＡは式（１）：

【数１】

$$NA = n_c(2\Delta n)^{1/2} = 0.145$$

で与えられ、ファイバの許容角θ_aは式（２）：

【数２】

$$\theta_a = \sin^{-1}(NA) = 8.32° = 0.145\text{ラジアン}$$

で与えられる。

【００４４】
本構成ではさらに、複数本の単一モードファイバ１０からの光を集束するために用いられる、倍率１対１及び遠視野ビーム発散角がθ$_a$と同等の、理想レンズの概念を導入する。したがって、中心波長がλ$_0$の光ビームに対して、焦点におけるビーム径φ$_f$は式（３）：
【数３】

$$\phi_f = 2w_0 = 2\frac{\ddot{e}_0}{\delta e_a} = 3.95\text{im} \approx \phi_c$$

で与えられる。スポット径φ$_f$はコア径（φ$_c$＝５μｍ）とほぼ等しく、よって効率的な光結合が得られる。焦点深度は２（πｗ$_0$^{2}／λ$_0$）＝２７．２ｍｍであり、焦点３６，３７及び３８に対する焦点域の末端におけるビーム径φ$_f$’は式（４）：
【数４】

$$\phi_f' = 2\sqrt{2}w_0 = 5.59\text{mm}$$

で与えられる。パラメータφ$_f$及びφ$_f$’は軸方向における焦点位置の４０μｍの範囲内における振幅に関して定められるから、光強度（すなわち光振幅の２乗）に基づくビーム径は、実際上、５μｍより小さくなり得る。
【００４５】
上記の計算は主光軸上で有効な理想光学に基づく。φ＝５ｍｍ，ｆ＝５ｍｍで作動距離が８．２ｍｍの、市販のレンズ系を用いれば、２ｍｍ×２ｍｍの画像をカバーするに必要なオフアクシス角は約５°であることが市販のレイトレーシングソフトウエアを用いてわかった。集束レンズ１４のフィルファクターをほぼ８０％としたレイトレーシング結果は、オンアクシスＲＭＳ焦点が半径５．３μｍにあり、５°オフアクシスＲＭＳ焦点が半径１０．３μｍにあることを示す。特注レンズ系はより優れた性能を有するはずである。
【００４６】
図１に示されるように、全光学系の作動距離、すなわち集束レンズ１４から装置の焦点までの距離は、レンズ系の焦点距離、集束レンズ１４の直径及び集束レンズ１４とミラー１６との間の間隙長により定まる。上で論じた市販レンズ系を用いれば、作動距離は約２．３５ｍｍである。画像の中心からミラー１６の回転軸までの距離は約５．４７ｍｍである。動径方向で２ｍｍの走査を達成するためには、セクター走査角は、光学系の形状寸法により定まり、ほぼ±１０．４°、すなわち全体で約２０°になるはずである。
【００４７】
現時点で既存の生体内ＯＣＴシステムは、生物学的に許容し得る毎秒４ないし８フレームを得るために４ないし８回転／秒（ＲＰＳ）で動径走査を行う。本実施形態の構成については、回転速度として４．４ＲＰＳが選ばれる。回転速度はＡ－走査の繰返しレート及び５μｍの横方向解像度を得るに必要なＡ－走査回数に依存する。したがって、本発明の装置の画像化速度は４．４フレーム／秒であるが、様々なエンドユーザの用途によっては別の画像化速度が選択されることもあり得る。個々のフレームのそれぞれの画像化時間は、回転速度及びセクター走査角により定まり、１２．６ミリ秒である。したがって、与えられたフレームに対して、システムは１２．６ミリ秒間信号を取得し、その間にデータ処理が行われるフレーム間時間は約２１５ミリ秒である。これらのパラメータは、本システムに用いられる（後に説明される）光遅延発生器の性能に依存する。
【００４８】
上記の計算は光波長８６０ｎｍで動作する光源及び特注単一モードファイバに基づいてなされたが、１３００ｎｍのような別の波長で動作する光源及び市販ファイバを用いる実施態様も可能であり得る。図５ａは、波長１３００ｎｍで動作する、市販ファイバ（コーニング（Ｃｏｒｎｉｎｇ）ＳＭＦ－２８）を用いた、この５チャネルファイバ束チップに対するビームスポット図を示す。ファイバ束チップのファイバ段差は１２５μｍである。これらのファイバからの光ビームは、直径が５ｍｍで焦点距離が４．５ｍｍのレンズにより

集束されて、ほぼ０．６５ｍｍの焦点域をカバーする。得られる横方向画像化分解能はほぼ１０μｍである。図５ｂは、波長８９０ｎｍで動作する、コア径が５μｍでクラッド層径が４０μｍの特注ファイバを用いた、１５チャネルファイバ束チップに対するビームスポット図を示す。このファイバ束チップのファイバ段差は４０μｍである。中央の５チャネルのビームスポットだけが示される。得られる横方向画像化分解能はほぼ０．６５ｍｍの焦点域にわたりほぼ５μｍである。

【００４９】

図５ｃは、図５ａの５チャネルファイバ束チップに対する、ビームスポット径対焦点域に沿う距離を示す。図５ｃは、０．６５ｍｍの焦点域全体にわたりビームスポット径が一様に１５μｍより小さいことを示す。図５ｄは、図５ｂの１５チャネルファイバ束チップに対する、ビームスポット径対焦点域に沿う距離を示す。図５ｄは、０．６５ｍｍの焦点域全体にわたりビームスポット径がほぼ５μｍであることを示す。

【００５０】

次に図６を参照すれば、本発明の装置の基本光学素子の概略の全体的レイアウトには、複数の光源５０，複数のツリー型結合器５２，複数の３ｄＢ結合器５４，ファイバ束チップ５６，複数の検出器５８，複数の復調器６０及び光遅延発生器６４が含まれる。レーザとすることができる複数の光源５０は、複数のツリー型結合器５２に結合される。チップ５６のファイバ（すなわちチャネル）のそれぞれに十分な光を確実に与えるためには１つより多くのレーザが必要となり得る。ツリー型結合器５２のそれぞれは複数の３ｄＢ結合器５４の内のいくつかにそれぞれの光源５０を結合する。複数の３ｄＢ結合器５４は、複数の光源５０からの光のほぼ１／２を前方に伝送するためにファイバ束チップ５６に結合される。ファイバ束チップ５６は図１のファイバ束チップ１２及びその他の光学素子（すなわち、集束レンズ１４及びミラー１６）を備える。複数の光源５０からの光のもう一方の１／２は検出器５８に後方反射され、検出器５８は続いて、サンプリングされたデータを処理してＢ－走査画像３０を生成するために機能する、コンピュータ６２に復調器６０を介して結合される。光遅延発生器６４は、遅延反射信号を検出器５８に与えるために、３ｄＢ結合器５４により用いられる。チップ５６で検査されている試料は参照数字６５で表示される。

【００５１】

図６に示されるレイアウトにおいては、３ｄＢ結合器５４の代わりに、１ｄＢまたは１０ｄＢ光結合器等を用いることができる。さらに、ツリー型結合器５２により３ｄＢ結合器５４のそれぞれに、したがってそれぞれのファイバに伝送される光の強度は同じである必要はなく、実際には、３ｄＢ結合器がファイバ（すなわちチャネル）に深い組織内走査を容易にする光を与えるかまたは浅い組織内走査を容易にする光を与えるかに依存して選ばれる。組織内深くを走査するためには高強度光が必要である。したがって、組織内深くを走査する光をファイバに送るツリー型結合器５２及び３ｄＢ結合器５４は、より多くの光を与えるように適合される。

【００５２】

図７ａ及び７ｂは光遅延発生器６４をさらに詳細に示す。既存の生体内ＯＣＴシステムにおけるものと同様の光遅延発生器６４は、個別のファイバのそれぞれのコヒーレンスエンベロープを用いるＡ－走査を行うために用いられる。光遅延発生器６４は、回折格子６６，レンズ６７，走査ミラー６８及びミラー６９を備える。高速深度走査は、ファイバ束チップ１２の多束単一モードファイバ１０からの擬単色光を回折格子６６上に分散させ、分散光を振動ミラー６９上に集束させることによって、光遅延発生器６４により達成できる。このことは、Ｇ．Ｊ．ティアニー、Ｂ．Ｅ．ブーマ及びＪ．Ｇ．フジモト（「回折格子ベース位相制御線による高速位相及び群遅延走査」，Ｎａｔｕｒｅ Ｍｅｄｉｃｉｎｅ，１９９８年，第４巻，第７号，ｐ．８６１～８６５）により説明されるように、周波数すなわちフーリエドメインにおいて線形ランプを印加する効果を有する。回折格子６６における反射波長の再結合により、実空間時間遅延がつくられる。走査ミラー６８の角度が数°の範囲の回転により急速に振動して基準アームにおける時間遅延を急速に変化させ、試

料の高速繰返し深度操作を可能にする。

【００５３】

多束単一モードファイバ１０の内の１本のファイバからの光７０が図７ａに示される。光７０は、回折格子６６により、スペクトル成分７１，７２及び７３で表されるスペクトル成分に分散される。スペクトル成分７１は光７０の最短波長を表し、スペクトル成分７３は光７０の最長波長を表し、スペクトル成分７２は光７０の中心波長を表す。光７０のこれらのスペクトル成分は光遅延発生器６４内で垂直方向に配列される。同様な態様で、多束単一モードファイバ１０の他のファイバからの光も分散され、それぞれのファイバからの分散光には垂直方向に間隔がとられて、垂直方向に配列される。多束単一モードファイバ１０のそれぞれのファイバからの分散光の位相変調を容易にする、与えられたファイバについての、走査ミラー６８のピボット軸からの分散光の中心波長のオフセットはx_dで表わされる。あるいは、x_dがゼロである場合には、多束単一モードファイバ１０のそれぞれのファイバからの光を位相変調するため、多束単一モードファイバ１０のそれぞれのファイバに対して位相変調器が必要になる。このことには、走査ミラー６８の大きさを縮小でき、したがってより高いフレームレートを用い得るという利点がある。さらに、位相変調器は電気的に制御され、よって非常に安定な信号が生成され得る。

【００５４】

次に図７ｂを参照すれば、多束単一モードファイバ１０のそれぞれのファイバからの分散光が走査ミラー６８上に７５，７６，７７及び７８のように縦列をなして垂直方向に配置されるように、多束単一モードファイバ１０がファイバ束チップ１２に配列される。あるいは、横列のような、別の順序配置を多束単一モードファイバ１０のそれぞれのファイバからの光のスペクトル成分に対して用いることもできる。

【００５５】

図６に示されるように、単一の光遅延発生器を多束ファイバに遅延を導入するために用いることができる。単一の光遅延発生器に結合され得るチャネルの数の決定における制限要因は走査ミラーの物理的大きさであり、したがってチャネル数は光遅延発生器の共鳴周波数により制限される。市販の共鳴光走査器は１６ｋＨｚまで動作可能である。したがって、４ｍｍ×５ｍｍの大きさの走査ミラー６８を用いることができる。ファイバ束アレイの大きさは約２ｍｍであるから、１つの光遅延発生器にアレイ全体を適合させることができる。したがって、本発明の実施形態に対し、光走査角αを±２°として、f_r＝１６ｋＨｚで動作する光走査器を有する単一の光遅延発生器が用いられる。本実施形態には、ピッチがｐ＝３．３３μｍ、中心周波数がλ_0＝０．８６μｍ、焦点距離がf_l＝２１ｍｍの回折格子も組み込まれる。したがって、自由空間群光路長差Δ_{lg}は式（５）：

【数５】

$$\Delta l_g = 4\alpha\left(f_l\frac{\lambda_0}{p} - x_d\right) = 0.618\text{mm}$$

で与えられ（ローリンズ等（１９９８年）による）、またピーク対ピーク値は１．２４ｍｍである。式（５）において、x_d＝１ｍｍはλ_0スペクトル線と共鳴ミラーのピボット軸との間の変位である。ピークＡ－走査速度$V_{A最大}$は式（６）：

【数６】

$$V_{A最大} = 2\pi\Delta l_g f_r = 62.1\ \text{m/秒}$$

で与えられ、Ａ－走査速度V_Aは式（７）：

【数７】

$$V_A = V_{A最大}\cos(2\pi f_r t)$$

にしたがって変化する。コヒーレンス長l_cが５μｍでガウス型発光スペクトルをもつ光源を選べば、等価発光帯域幅Δλは式（８）：

【数８】

$$\Delta\lambda = \beta\frac{\lambda_0^{\,2}}{l_c} = 98\text{nm}$$

で与えられ、ここでガウス型エンベロープに対してはｂ＝０．６６である。

【００５６】

共鳴ミラーの大きさが次に決定される。一次回折を有する回折格子をもつ光遅延発生器に対して、回折角θ（λ）は式（９）：

【数９】

$$\theta(\lambda) = \sin^{-1}(\lambda/p)$$

で与えられる。レンズのフーリエ面における（$\lambda_0 - \Delta\lambda/2$）から（$\lambda_0 + \Delta\lambda/2$）までのスペクトルの広がりΔｘは式（１０）：

【数１０】

$$\Delta x = 2f_l\left[\theta(\lambda_0 + \Delta\lambda/2) - \theta(\lambda_0 - \Delta\lambda/2)\right] = 1.3\text{mm}$$

で与えられる。

【００５７】

ミラー幅は４ｍｍであるから、変位x_dの値をほぼ１ｍｍとして共鳴ミラーの一辺上にスペクトルを適合させることができる。このことが図７ａ及び７ｂに示されている。システムの個々のチャネルのキャリア周波数f_cは式（１１）：

【数１１】

$$f_c = \left(4x_d\alpha \cdot 2\pi f_r/\lambda_0\right)\cos\left(2\pi f_r t\right)$$

で与えられ（ローリンズ等（１９９８年））、最大で１６．３ＭＨｚである。

【００５８】

干渉像（すなわち干渉縞パターン）の帯域幅Δｆは式（１２）：

【数１２】

$$\Delta f = \frac{\Delta\lambda}{\lambda_0^{\,2}} \cdot 4\pi\alpha f_r \cdot 2\left(f_l\lambda_0/p - x_d\right)\cos\left(2\pi f_r t\right)$$

で与えられ、最大で８．４ＭＨｚである。

【００５９】

f_c（ｔ）＞Δｆ（ｔ）であるから、急峻な周波数カットオフは必要であるが、通常の整流及び低域フィルタ方式によって適切な復調を行うことができる。（単一チャネルで行われるＡ－走査深度）D_A＝４０μｍが最高キャリア周波数に一致し、よってD_Aにわたるキャリア周波数変動が最小化されるように、システムの個々のチャネルを設定することが好ましい。キャリア周波数は時間に関して正弦的に変動し、変動Δf_cは式（１３）：

【数１３】

$$\Delta f_c = f_c\left\{1 - \cos\left[\sin^{-1}\left(D_A/\Delta l_g\right)\right]\right\} = 34\text{kHz}$$

によって与えられ、f_cの約０．２％である。

【００６０】

別の位置においても、信号を適切に復調することはできるが、キャリア周波数の変動はより大きくなるであろう。信号を復調するため、アナログ高速整流器及び１０極低域フィルタを復調器６０に組み込むことができる。実際上は、信号の中心がＤＣにおかれ、帯域幅がΔｆになるように、信号周波数が下方偏移される。復調エンベロープ信号は次いで適切なサンプリングレートでデジタル化される。現時点で既存のデータ取得（ＤＡＱ）カードは、約６０ｄＢのＳＮＲ（信号対雑音比）で、毎秒３０メガサンプル（ＭＳ／秒）で動作する。Δｆ＝８．４ＭＨｚの干渉像スペクトルに対してガウス型形状を選べば、６０ｄＢ点は約１４．５ＭＨｚにある。したがって、そのような信号のデジタル化に対するナイキ

ストレートはほぼ２９ＭＳ／秒である。したがって、現時点で既存のＤＡＱカードはエイリアシングを生じずにエンベロープ信号をデジタル化できるであろう。

【００６１】

最高キャリア周波数においてエンベロープ信号をデジタル化するためのサンプリングレートを３０ＭＳ／秒とすれば、軸方向における空間サンプリング間隔は$\Delta_{軸方向}=V_{A最大}/S=2.07\mu m$である。試料を通って上下を繰り返すＡ－走査を示す走査経路８０が図８に示される。サンプリング点が参照数字８２で表示される。２．０７μｍの軸方向間隔が参照数字８４で表示される。横方向における空間サンプリング間隔は、横方向すなわちＢ－走査速度及び光遅延発生器６４の光走査器の共鳴周波数により決定される。ミラーの回転軸からの動径距離ｒが５．４７ｍｍである画像の中心において、動径サンプリング間隔$\Delta_{動径}$は式（１４）：

【数１４】

$$\Delta_{動径}=V_{動径}/2f_r=2\pi\Omega r/2f_r=4.73\mu m$$

により与えられる。図８に、この間隔が参照数字８６で表示される。最浅深度を走査するファイバについての横方向空間サンプリング間隔は３．８６μｍであり、最深チャネルについての横方向空間サンプリング間隔は５．５９μｍである。したがって、画像中心における画素寸法は、軸方向２．０７μｍ×横方向４．７３μｍである。横方向画素寸法は画像の深度にわたって３．８６μｍから５．５９μｍまで変化する。ミラー１６の回転速度を変えることにより、フレームレートを犠牲にして、横方向サンプリング間隔を変えることができる。共鳴周波数がより高い光走査器を用いても、サンプリング間隔を縮小することができる。

【００６２】

パルス光源（例えば波長８６０ｎｍで発光する１５ないし２０フェムト秒パルスレーザ）に対しては、コヒーレンス長はほぼ４．５μｍないし６μｍであろう。軸方向空間サンプリング間隔は約２μｍであり、これはコヒーレンス長の１／２より小さいから、画像は軸方向で問題なくサンプリングされる。集束レンズ１４として近回折限界集束レンズを用いれば、ビームスポット径は約５μｍになるはずである。横方向空間サンプリング間隔が３．８６μｍから５．５９μｍまで変化するから、ビームウエスト径が約５μｍであるとすれば、画像の分解能はサンプリング分解能を若干下回る。しかし、空間サンプリング間隔は最終画像分解能と等価ではなく、最終画像分解能は局所的コントラスト及び雑音レベルの影響も受ける。局所的コントラストは画像において隣接画素として表れる試料の２点の間の反射率の差である。これらの２つの点の反射率が同様であれば、すなわち局所的コントラストが低ければ、これらの点を分解することは困難であろう。

【００６３】

画像化速度は運動ぶれを小さくするに十分に高速であるべきである。標的速度（すなわち組織運動）が一般に５ｍｍ／秒であるとすれば、１フレーム時間（経過時間１２．６ミリ秒）内に標的は特定の方向に６３μｍまで移動することができ、これは５μｍの設計分解能よりかなり大きい。本実施形態においては、コヒーレンスゲートを４０μｍの距離にかけて走査するに必要な時間である０．６マイクロ秒内に画像の１本の線が形成されるようにして、Ａ－走査が全てのチャネルにおいて同時に行われる。２つの連続するＡ－走査間の時間は、システムのミラー１６の回転速度及び１画像当りのＡ－走査数で定まる、約１６マイクロ秒である。すなわち、１６マイクロ秒間の移動量は０．０８μｍであり、これは分解能よりかなり小さいから、得られる画像は鮮明になるはずである。したがって、画像には運動ぶれがないはずであるが、それでも運動アーティファクトは存在し得る。生じる運動アーティファクトはおそらく、組織構造の寸法及び標的速度に依存して６３μｍもの大きさになり得る、画像化される組織構造の形状寸法上の変形であろう。この運動アーティファクトは、空気－組織界面が複数の光源５０からの光に及ぼす効果による。

【００６４】

図９に示されるように、画像化される組織内部の、装置の個々のファイバの焦点は、組織

内の焦点の位置の距離d_0、組織表面の屈折率が１であるか否か、及び（一般にほぼ１．４である）組織の実屈折率にしたがって変化し得る。したがって、実焦点は組織表面下の距離d_fにあり、d_fは式（１５）：

【数１５】

$$d_f = d_0 \cdot \frac{\tan\theta_1}{\tan\theta_2} = d_0 \cdot \frac{\tan\theta_a}{\tan\left[\sin^{-1}\left(\frac{n_1}{n_2}\cdot\sin\theta_a\right)\right]}$$

で与えられる。ここで、θ_1は個々のファイバの許容角θ_aに等しいとされ、θ_2は組織外部（すなわち空気）の屈折率$n_1 = 1$及び組織内部の屈折率$n_2 = 1.4$により定まることになろう。

【００６５】

コヒーレンスゲート位置d_cは式（１６）：

【数１６】

$$d_c = \frac{n_1}{n_2}\cdot d_0$$

にしたがって変化する。したがって、光の進行速度は媒質の屈折率が大きくなるほど遅くなるという事実により、$n_1 = 1$の（すなわち組織が存在しない）媒質内では一致する、焦点と光ビームのコヒーレンスゲートとの間に、光路の不一致が存在する。この不一致の大きさΔｄは式（１７）：

【数１７】

$$\Delta d = n_2\left(d_f - d_c\right) = \frac{n_2 d_0 \tan\theta_a}{\tan\left[\sin^{-1}\left(\frac{\sin\theta_a}{n_2}\right)\right]} - d_0$$

で表される。組織の屈折率$n_2 = 1.4$から、$\Delta d = 0.97 d_0$が得られる。この不一致問題は高ＮＡ－ＯＣＭシステムに対して共通であり、既存の高ＮＡ－ＯＣＭシステムの多くは何らかの形態の動的補償、すなわち基準光路長を動的に変えることによるΔｄの補償を用いるが、高画像化速度でのそのような動的補償は困難である。したがって、本発明の実施形態の一態様は、検出された干渉像信号の‘適応トリガ印加’を用いることである。

【００６６】

上に示したように、自由空間群光路長差はピーク間で$2\Delta l_g = 1.24$ｍｍであり、これは４０μｍでしかない有用なＡ－走査範囲よりかなり大きい。このため、コヒーレンスゲートが焦点を通過するときにだけトリガをかけて干渉像を得ることができるから、上記の不一致を処理する余裕が残される。

【００６７】

図９に示されるように、それぞれのファイバチャネルに対する作動距離d_Wはn_2にしたがって変化するが、n_2はほぼ一定である。したがって、どこに組織表面があるかがわかれば、d_0を決定することができ、続いてΔｄを決定することができる。

【００６８】

組織表面の斜視図及び任意の軸線９０を示す図１０を参照すれば、組織表面を走査するように指定されたチャネル１が、走査領域２８において軸線９０を最初に通過するチャネルである。チャネル１及び２の焦点が、軸線９０を通過する多束単一モードファイバ１０（すなわち複数のチャネル）からの光の概略表示９４に参照数字９１及び９２で表示される。最終チャネル、すなわち本例ではチャネル５０の焦点は参照数字９５で表示され、画像における最深層を走査するように指定される。表示９４の全体のプロファイルは、その範囲内ではコヒーレンスゲートと焦点距離を一致させることができる、適応トリガ域を定め

る。５０のチャネルの内の１つ、すなわちチャネル“ｖ”は、空気－組織界面が擬似的にミラーとしてはたらき、入射光を反射するから、強く判然とした正反射を受けることになろう。組織表面の下では、組織が入射光を散乱させ、吸収する混濁媒質としてはたらく。すなわち、チャネル“ｖ”が、チャネル“ｖ”より前のチャネルは全て雑音レベルにある信号を返すであろうから、この特定の軸線９０に対するd_0を決定するであろう。したがって、“適応トリガ印加”法は‘隣りの’チャネルに比較して反射の大きな増加があるチャネルを識別することにより組織表面の位置を突き止めるために、隣接するチャネルについて検出された反射光を比較するステップを含む。次いでこの情報が引き続くチャネルのそれぞれに順次伝えられ、焦点とコヒーレンスゲートとの間の不一致を小さくするために、それぞれのチャネルに対するトリガ点が前記情報にしたがって設定される。

【００６９】

例として、チャネル“ｖ”が１３チャネルであれば、チャネル１から１２は組織表面より上の自由空間の走査に設定され、チャネル１３は組織表面の走査に設定され、引き続くチャネルは、それぞれのチャネルの光ビームの焦点とコヒーレンスゲートとの間の不一致は生じずに組織内部の走査に設定されるように、装置が較正される。画像化の間、図１０に参照数字９６で表示されるように、組織表面の位置について$\Delta d_0 = \pm 0.5$ｍｍの許容範囲を設けることができる。この許容範囲は、次に説明されるように、Ａ－走査性能及びエンベロープ検出器の周波数応答に関係する。

【００７０】

$\Delta d_0 = 0.5$ｍｍとすれば、補償を必要とする不一致$\Delta d'$は式（１８）：

【数１８】

$$\Delta d' = 0.693 \times 0.5 = 0.347\text{mm}$$

で与えられる。このことは、最高キャリア周波数において干渉像信号をトリガする代わりに、実キャリア周波数f_c'が式（１９）：

【数１９】

$$f_c' = f_{c\text{最高}} \cos\left(\sin^{-1}\left(\Delta d' / \Delta l_g\right)\right) = 13.5\text{MHz}$$

で与えられなければならないことを意味し、この実キャリア周波数は最高キャリア周波数の約８３％であり、これにともなって干渉像信号帯域が変わる。エンベロープ検出器の周波数応答は動的に調整できるとしても、エンベロープ検出器の応答は固定するが、カットオフ周波数に１７％の許容差をもつように設計する方が、より簡単であり、高速である。このようにすれば、適応トリガ印加方式全体が固定型コンポーネントだけを含み、補償の全てが電気的に行われて高速画像化要件を満たす。

【００７１】

図６に示される光コンポーネントは、以下のように選ぶことができる。Ｓ．Ａ．ボッパート，Ｂ．Ｅ．ボウマ，Ｃ．ピトリス，Ｊ．Ｆ．サザーン，Ｍ．Ｅ．ブレジンスキー，及びＪ．Ｇ．フジモト（「生体内細胞光コヒーレンス断層撮像」，Ｎａｔｕｒｅ Ｍｅｄｉｃｉｎｅ，１９９８年７月，第４巻，第７号，ｐ．８６１～８６５）に基づけば、ほぼ２ｍｍないし３ｍｍの深度までの画像化を可能にするために、２ｍＷの組織入射パワーを用いる非内視鏡ＯＣＴシステムにおいて、１００ｄＢをこえるＳＮＲを達成することができる。用いられた光源は、コヒーレンス長が５．１μｍの、中心波長１２８０ｎｍで動作する、カーレンズ－モードロック固体Cr^{4+}：フォルステライトレーザである。しかし、本発明の実施形態はこのタイプの光源にも、広帯域超発光ダイオードのような、その他のいかなるタイプの光源にも限定されない。例えば、別の可能性には、ほぼ４．５μｍないし６μｍのコヒーレンス長を提供するであろう、８６０ｎｍを中心としてほぼ１００ｎｍの帯域をもつ、白色発光Ｃｒ：ＬｉＳＡＦ光源がある。このダイオードポンピング型モードロック固体レーザは、８６０ｎｍで動作させたときに、繰返レート約１００ＭＨｚ及び平均パワー３０ｍＷで動作するはずである。パルスエネルギー変動は１％未満になるはずである。図６に参照数字５０で表示される、いくつか（例えば２つまたは４つ）の上記レー

ザは、５０チャネルの所要パワーを全て供給する必要がある。組織のより深い部分を走査するチャネルにはチャネル当たりほぼ１ないし２ｍＷの入射パワーが必要であろうし、より浅い部分を走査するチャネルにはそれほどのパワーは必要ではないであろう。ツリー型結合器５２は、光源パワーを上記要件に合せて分割するように構成することができる。最高キャリア周波数は１６．３ＭＨｚであるから、それぞれの干渉縞は少なくとも６つのレーザパルスを含むであろう。したがって干渉縞パターンは十分にサンプリングされるはずである。

【００７２】

それぞれのチャネルに対して、個別の光受信器すなわち検出器５８を用いて、干渉縞を検出することができる。最大検出器帯域幅は１２５ＭＨｚであるが、本発明の装置では、検出器帯域幅は、キャリア周波数及び干渉像の帯域幅により定まるように、３０．８ＭＨｚで十分であり得る。

【００７３】

本発明の代替実施形態は、装置の複雑性を軽減し、コストを低減するために光コンポーネントを共有するという概念に関わる。図１１ａを参照すれば、干渉像のＡＣ成分が干渉像のＤＣ成分から分離されてＡＣ成分だけが増幅される、一般的な平衡検波型単チャネル干渉計１５０が示される。単チャネル干渉計１５０は、光ファイバ及び３ｄＢ結合器１４０，１４２及び１４４のネットワークを介して接続される、広帯域ＩＲ（赤外）光源Ｌ，可視波長案内光Ｇ，平衡検波器ＢＤ，偏光制御器ＰＣ，位相変調器φＭＯＤ及び光遅延発生器ＯＤＧを備える。“ｘ”はファイバネットワークのデッドエンドを表す。可視波長案内光Ｇは単チャネル干渉計１５０が指し示している方向を示す（すなわち画像化される方向を示す）緑色レーザとすることができる。単チャネル干渉計１５０は試料Ｓに結合される。

【００７４】

図１１ａの構成を拡張して、図１１ｂに示されるような、２チャンネル干渉計１６０を構成することができる。下付添字は２本のチャネルにおけるコンポーネントを表す。下付添字のないコンポーネントはそのコンポーネントが両チャネルに用いられていることを示す。２チャネル干渉計１６０は、レーザＬ’，可視波長案内レーザＧ’，２対１ツリー型結合器ＴＣ１，偏光制御器$ＰＣ_1$，$ＰＣ_2$及び位相変調器φＭＯＤ’，可変遅延素子$ＶＤ_1$及び$ＶＤ_2$，光遅延発生器ＯＤＧ’，検出器$ＢＤ_1$及び$ＢＤ_2$，並びに３ｄＢ結合器１６２，１６４，１６６，１６８，１７０及び１７２を備える。可変遅延素子$ＶＤ_1$及び$ＶＤ_2$はそれぞれのチャネルに対してコヒーレンスゲート位置を調節するために組み込まれる。２本のチャネルは、組織試料の相異なる位置にある２つの点とすることができる、試料$Ｓ_1$及び$Ｓ_2$に結合される。本例において、光源Ｌ’は２本のチャネル間で共有され、チャネル１の光パワーはチャネル２の光パワーの２倍である。したがって、チャネル１はチャネル２より深い組織領域を走査するために用いられるべきである。２対１ツリー型結合器ＴＣ１は、両チャネルが（位相変調器φＭＯＤ’及び光遅延発生器ＯＤＧ’を含む）同じ基準アームを共有できるように用いられる。同じ基準アームを共有できるという能力により、１つの位相変調器を多束単一モードファイバ１０（すなわち全チャネル）からの光の位相変調を行うために用いることができる。２本のチャネルからの光がツリー型結合器ＴＣ１により１本のファイバに結合されて同じ位相変調器φＭＯＤ’に送られることに注意されたい。したがって、２チャネル干渉計１６０のコストが低減され、複雑性が軽減される。

【００７５】

図１１ｂに基づけば、汎用光ネットワークを図１１ｃに示される光ネットワーク１８０のようなＮチャネルＯＣＴシステムを構成するために用い得ると考えられる。光ネットワーク１８０は、第ｎチャネル１８２のための光ネットワーク及びｎ本のチャネルの全てに共有される基準アーム１８４を備える。第ｎチャネル１８２のための光ネットワークは、検出器$ＢＤ_n$，３ｄＢ結合器１９４，１９６及び１９８並びに偏光制御器$ＰＣ_n$及び、試料$Ｓ_n$に結合された、可変遅延素子$ＶＤ_n$を含む試料アームを備える。第ｎチャネル１８２

のための光ネットワークは、第（ｎ－１）チャネルから光源光１８６を受け取り、３ｄＢ結合器１９４を介して光源光１８８を第（ｎ＋１）チャネルに送り出す。第ｎチャネル１８２のための光ネットワークは、第（ｎ－１）チャネルから案内光パワー１９０を受け取り、３ｄＢ結合器１９６を介して案内光パワー１９２を第（ｎ＋１）チャネルに送り出す。本実施形態において、光源（図示せず）は、等比級数的または別の適切なパワー分割方式にしたがうパワー配分によりＮ本のチャネルのそれぞれの間で共有することができる。Ｎ対１ツリー型結合器$ＴＣ_n$，位相変調器φＭＯＤ”及び光遅延発生器ＯＤＧ”を含む基準アーム１８４は、Ｎ本のチャネルのそれぞれの間で共有される。

【００７６】

図１１ａ，１１ｂ及び１１ｃに示される構成図のそれぞれでは、検出器に結合された３ｄＢ結合器から送られる試料及び基準アームからの反射光の間の干渉による干渉パターンの光の一部が失われるという事実を問題としてかかえている。本例では、３ｄＢ結合器が用いられているから、干渉パターンの光の５０％が失われる。例えば、図１１ａにおいては、干渉パターンの光の５０％だけが３ｄＢ結合器１４０及び１４２から検出器ＢＤに送られる。このため、低強度の干渉パターンに対しては特に、干渉パターンの検出が一層困難になる。これを処理するため、光サーキュレータのような非相反光素子を、３ｄＢ結合器だけが用いられた場合には失われていた部分光を検出器に送るために用いることができる。

【００７７】

図１２ａ，１２ｂ及び１２ｃを参照すれば、単チャネルＯＣＴ装置２００，２チャネルＯＣＴ装置２１０及び、ＮチャネルＯＣＴ装置２２０のための光ネットワークの、光サーキュレータを備える代替実施形態が示される。図１２ａ，１２ｂ及び１２ｃにおいては、検出のためにより強度の高い干渉信号を与えるため、干渉パターンの光を回収して検出器ＢＤ，$ＢＤ_1$，$ＢＤ_2$及び$ＢＤ_n$のそれぞれに導くため、光サーキュレータＣ，$Ｃ_1$，$Ｃ_2$及び$Ｃ_n$が用いられる。３つの実施形態の残りのコンポーネントは、図１１ａから１１ｃに示される、単チャネルＯＣＴ装置１５０，２チャネルＯＣＴ装置１６０及び，ＮチャネルＯＣＴ装置１８０のための光ネットワークのコンポーネントと同様である。光を回収して回収光を検出器に与えるために光サーキュレータを用いるという概念は図６の装置にも適用でき、この場合、光サーキュレータは３ｄＢ結合器と検出器との間に配することができる。

【００７８】

図１１ｃ及び１２ｃに示される構成図によりエレガントな設計が導かれるが、コンポーネント（すなわち位相変調器）を共有する並列干渉計では、非常に大きなチャネルクロストークを生じることがあり、そのようなクロストークは結果として画像劣化を引き起し得る。しかし、チャネル間のファイバ長を一致させないことで、クロストークを効果的に処理できる。電気的クロストークは標準的な遮蔽及び接地法を用いて処理できる。以下で光クロストークを説明する。

【００７９】

次に図１３ａを参照すれば、チャネルクロストークを調べるために組み上げた２チャネルＯＣＴシステム２３０が示される。２チャネルＯＣＴシステム２３０は、レーザ$Ｌ_E$，検出器$Ｄ_1$及び$Ｄ_2$，ビームスプリッタ$ＢＳ_1$及び$ＢＳ_2$，１対２ツリー型結合器$ＴＣ_E$，位相変調器$ＰＭ_E$，光遅延発生器$ＯＤＧ_E$，ビームコリメータ$ＢＣ_1$及び$ＢＣ_2$，並びに試料をシミュレートする２つのミラー$Ｓ_1$及び$Ｓ_2$を備える。２チャネルＯＣＴシステム２３０では、所望の画像化信号はチャネル１光路及びチャネル２光路からくる。チャネル１に対する所望の画像化信号は、光路：

$Ｌ_E \rightarrow ＢＳ_1 \rightarrow Ｓ_1 \rightarrow ＢＳ_1 \rightarrow Ｄ_1$　　（２０）

からの光が、光路：

$Ｌ_E \rightarrow ＢＳ_1 \rightarrow ＯＤＧ_E \rightarrow ＢＳ_1 \rightarrow Ｄ_1$　　（２１）

からの光とコヒーレントに干渉するときに生じ、検出器$Ｄ_1$で検出される。チャネル２に対する所望の画像化信号は、光路：

$L_E \rightarrow BS_2 \rightarrow S_2 \rightarrow BS_2 \rightarrow D_2$ （２２）
からの光が、光路：
$L_E \rightarrow BS_2 \rightarrow ODG_E \rightarrow BS_2 \rightarrow D_2$ （２３）
からの光とコヒーレントに干渉するときに生じ、検出器D_2で検出される。さらに、２本のチャネルにおけるＯＣＴ画像化は、$BS_1 \rightarrow S_1$光路長が$BS_1 \rightarrow ODG_E$光路長に等しく、$BS_2 \rightarrow S_2$光路長が$BS_2 \rightarrow ODG_E$光路長に等しいときに限りおきる。そうでなければ、上述した所望の画像化経路ではない２つ（またはさらに多く）の様々な経路からの反射光の強めあう干渉により画像劣化がおこり得る。

【００８０】

図１３ａに示される光ネットワークに基づけば、２種類の主要なクロストーク源があり得る。一次クロストーク源はおそらく、（ミラーまたは試料により）一方のチャネルのビームスプリッタから他方のチャネルのビームスプリッタ及び検出器に反射されるコヒーレント光であろう。そのようなクロストークは画像化信号強度に等しい強度を有し、おそらくかなりの画像劣化を生じさることになろう。一方のチャネルから他方のチャネルへの反射は、光遅延発生器ODG_Eあるいは試料S_1またはS_2でおこり得る。したがって、光路：
$L_E \rightarrow BS_1 \rightarrow S_1 \rightarrow BS_1 \rightarrow D_1$ （２０）
からの光が、光路：
$L_E \rightarrow BS_2 \rightarrow ODG_E \rightarrow BS_1 \rightarrow D_1$ （２４）
からの光と干渉し得る。あるいは、光路：
$L_E \rightarrow BS_2 \rightarrow S_2 \rightarrow BS_2 \rightarrow D_2$ （２２）
からの光が、光路：
$L_E \rightarrow BS_1 \rightarrow ODG_E \rightarrow BS_2 \rightarrow D_2$ （２４）
からの光と干渉し得る。

【００８１】

試料アーム１及び２は通常、試料アームが組織試料の相異なる点（すなわち相異なる深度）に向けられるであろうから、図１３ａに示されるように分離されていることはないであろう。試料アームが分離されていない場合には、チャネル１からチャネル２に、及びこの逆に、反射がおこることになろう。そのような場合には、光路：
$L_E \rightarrow BS_2 \rightarrow S_2 \rightarrow BS_1 \rightarrow D_1$ （２６）
からの光が、光路：
$L_E \rightarrow BS_1 \rightarrow ODG_E \rightarrow BS_1 \rightarrow D_1$ （２１）
からの光と干渉し得る。あるいは、光路：
$L_E \rightarrow BS_1 \rightarrow S_1 \rightarrow BS_2 \rightarrow D_2$ （２７）
からの光が、光路：
$L_E \rightarrow BS_2 \rightarrow ODG_E \rightarrow BS_2 \rightarrow D_2$ （２３）
からの光と干渉し得る。

【００８２】

ビームスプリッタ及びコネクタ挿入点のような望ましくない位置においても反射がおこり得ることを想起するべきである。そのような反射は、これらの経路からの光がかなりの強度を有する干渉縞を生じれば、画像雑音に寄与し得ると考えられる。しかし、この種の雑音は低強度であるから、おそらくは、先に説明したチャネルクロストークに対しては二次的であろう。

【００８３】

システムの解析により、そのような後方反射の干渉に対する最悪事態のシナリオにはコネクタからの一回反射が関わることが明らかになった。例えば、以下の光路：
$L_E \rightarrow BS_1 \rightarrow S_1 \rightarrow BS_1 \rightarrow D_1$ （２０）
からの光が、光路：
$L_E \rightarrow BS_2 \rightarrow ODG_E \rightarrow PM_E \rightarrow ODG_E \rightarrow BS_1 \rightarrow D_1$ （２８）からの光と干渉し得る。

【００８４】
いずれか２つの経路からの光の干渉に対しては４つの帰結が考えられ、帰結は光路長差に依存する。第１に、光路長が同じであれば、検出器における干渉縞の強度は試料の反射率だけに基づく真の信号強度より高くなるであろう。この種の画像雑音は雑音として検出できず、画像全体にわたり測定される試料強度を変えることになろう。幸いにして、光路長が正確に一致することはほとんどあり得ない。第２の可能性は、光路長が光源のコヒーレンス長の範囲内で一致し得ることである。この状況では、干渉縞エンベロープの幅が広がり、したがって軸方向分解能が低下することになるであろう。この状況はおこりそうもないが、鏡面深度プロファイルの半値幅を測定することにより検出できる。第３の可能性には、光源L_Eのコヒーレンス長より大きく、光遅延発生器ODG_Eの走査深度より小さい距離だけ異なっている、光路長が関わる。この状況は、光遅延発生器ODG_Eによる１回の深度掃引内の分離した２つのコヒーレンスエンベロープとして現れ得る。最後の、最もありそうな可能性は、光路長が光遅延発生器ODG_Eの走査深度より大きく異なり、雑音すなわち無関係な干渉縞はシステムで検出されないであろうことである。

【００８５】
上記の一次型のチャネルクロストークは、ファイバ光学系の製作上おこりそうもないはずである。$BS_1 \rightarrow ODG_E$光路長及び$BS_2 \rightarrow ODG_E$光路長は本質的に、ビームスプリッタBS_1及びBS_2から至るファイバピグテイルの長さにより、あらかじめ定められる。$BS_1 \rightarrow S_1$光路長及び$BS_2 \rightarrow S_2$光路長は計画的に、あらかじめ定められた対応する基準アーム長に一致させられる。一般的に製作されたファイバ長は数１０ｍｍ異なっており、これは光遅延発生器ODG_Eの走査深度より少なくとも１桁大きい。したがって、この種のクロストークが２チャネルシステムで問題となるはずはない。

【００８６】
挿入点反射の場合には、$PM_E \rightarrow ODG_E$光路長が光路$BS_1 \rightarrow S_1$と光路$BS_2 \rightarrow ODG_E$との間の光路長差に一致すれば、干渉縞及び画像劣化が生じ得る。この場合も、ファイバ長が約３００ｍｍであり、一方光遅延発生器ODG_Eの走査深度は２ｍｍしかないから、この種の二次雑音はおこりそうもないはずである。さらに、そのような干渉縞強度はシステム雑音で見えなくなってしまうであろう。第２に、用いられる装置は最大で０．６ｄＢの挿入損失（言い換えれば、最大で０．６ｄＢの反射）を有し、したがって、そのような信号は図１３ａの構成に用いられる検出限界より小さい。

【００８７】
２本のチャネルに同じファイバ及び光コンポーネントを用い得ることを示すため、ＯＣＴシステム２３０を評価した。試料アーム光路長及び光遅延発生器ODG_E基準アーム光路長がそれぞれのチャネルで一致し、干渉縞列が検出器D_1及びD_2のそれぞれで見られるように、試料アームミラーS_1及びS_2を配置した。位置合せのため及び光が、チャネル１からチャネル２を含むファイバに、及びこの逆に、反射する可能性を排除するため、試料S_1及びS_2に対する試料アームは分離したままにした。光遅延発生器は位相変調及び群遅延のいずれの生成にも用いることができる（ティアニー等（１９９７年））が、図１３ａに示した構成では、光遅延発生器ODG_Eを群遅延（すなわち深度走査）に用い、基準アームの位相変調器PM_Eを位相遅延を生じさせるために用いた。

【００８８】
図１３ａの実験構成では、ＡＦＣテクノロジーズ社（ＡＦＣ Ｔｅｃｈｎｏｌｏｇｉｅｓ Ｉｎｃ．）製の１３１０ｎｍ，９ｍＷ光源（モデルＢＢＳ１３１０）を、光源L_Eに備えた。光源L_Eの中心波長は１３１０ｎｍであり、測定したスペクトル広がりは±４０ｎｍであった。測定した光源L_Eのコヒーレンス長は１０μｍであった。検出帯域中心が１３１０ｎｍにあり、帯域幅が１００ｎｍ以上の、１５５Ｍｂｐｓパーキン・エルマー（Ｐｅｒｋｉｎ Ｅｌｍｅｒ）ＩｎＧａＡｓ光ダイオード受信器を検出器D_1及びD_2に用いた。ＪＤＳユニフェーズ（ＪＤＳ Ｕｎｉｐｈａｓｅ）４３ＭＨｚ位相変調器を位相変調器PM_Eに用いた。ビームスプリッタBS_1及びBS_2には、メトロテック（ＭｅｔｒｏＴｅｋ）社製を用いた。ビームコリメータBC_1及びBC_2には、オズ・オプティックス（

ＯＺ Ｏｐｔｉｃｓ）社製を用いた。上記またはその他の部品製造業者からの、代わりの適当なコンポーネントを用いることもできる。

【００８９】

光遅延発生器ODG_Eは、ＣＶＩスペクトラル・プロダクツ（ＣＶＩ Ｓｐｅｃｔｒａｌ Ｐｒｏｄｕｃｔｓ）社製の１３１０ｎｍ用１５０本／ｍｍブレーズド回折格子を用いて、コリメート光を分散させた。光を振動ミラー上に集束させるため、直径が３０ｍｍで焦点距離が１００ｍｍのメレス・グリオ社製ガラスダブレットレンズを用いた。８ｋＨｚで動作し、±１°の機械角すなわち±２°の光学角にわたって走査する共鳴走査器には、ＥＯＰＣ（エレクトロ－オプティカル・プロダクツ・コーポレーション（Ｅｌｅｃｔｒｏ－Ｏｐｔｉｃａｌ Ｐｒｏｄｕｃｔｓ Ｃｏｒｐｏｒａｔｉｏｎ））社製を用いた。この角度設定は試料S_1及びS_2に対する試料アームにおける約１ｍｍの深度走査に対応する。走査深度は２本のチャネルの光路長の不一致に関して重要な要件である。例えば、光路長が１ｍｍより大きく異なれば、２本のチャネル間のクロストークは最小になるはずであり、適切な遮蔽及び接地法により電気的クロストークも処理されるはずである。

【００９０】

図１３ｂ及び１３ｃは、図１３ａに示される構成上で行われた実験の結果を示す。図１３ｂは、チャネル１及びチャネル２の検出器D_1及びD_2からのオシロスコープトレースを示す。図１３ｂは、光遅延発生器ODG_Eの周期内において２本のチャネルが若干異なる位置に配されていること、すなわち、相異なる深度における画像化をシミュレートするために試料アームミラーS_1及びS_2を少量だけ計画的にオフセットさせたことを反映する、光遅延発生器ODG_Eの周期内の相異なる点において、干渉縞が生じていることを示す。図１３ｂは、それぞれのチャネルに強い画像化信号があり、いかなるクロストークの形跡もないことを示す。矢印２３２及び２３４は、組織試料の２つの相異なる点に相当させ得る、２つの相異なる試料からの反射を示す。さらに、それぞれの検出パルスのエンベロープの半値幅は光源L_Eのコヒーレンス長に相当しており、このことはそれぞれのチャネルの光信号が光源L_Eから発したことを示す。図１３ｃは、試料点の内の一方を他方の試料点に対して移動させた場合の実験結果を示す。この場合にも、クロストークは観測されなかった。

【００９１】

本発明の別の実施形態においては、多チャネルＯＣＴ法を診療に用い得るように、本明細書で先に開示された光ファイバネットワークが内視鏡に組み込まれる。本装置のファイバ束チップ１２の大きさのため、ファイバ束チップ１２は、（大径の治療用内視鏡には組み込み得るが）従来の診断用内視鏡の作業チャネルには適合しないであろう。したがって、別の設計手法がとられた。ファイバ束チップ１２を従来の診断用内視鏡の作業チャネルに収容するように設計する代わりに、従来の診断用内視鏡の機能の全てをファイバ束チップ１２の周りに配するように設計した。図１４に示されるように、本発明の内視顕微鏡を組み込んでいる（図６のチップ５６に相当する）ＧＩ内視鏡３００の一実施形態は、直径がほぼ１１ｍｍである。これは、直径が８～９ｍｍの従来の診断用内視鏡より若干大きい。ＧＩ内視鏡３００は、従来の前面観察白色光画像化に加えて、上で開示された内視顕微鏡撮像能力を有する。したがって、ＧＩ内視鏡３００の使用者は図１６に示されるような２ｍｍ×２ｍｍ断層画像を得ることができるはずである。

【００９２】

ＧＩ内視鏡３００は２．７ｍｍ径の吸引／生検チャネル３０２を備える。吸引／生検チャネル３０２の末端は、注目する組織領域３０６に向けられた開口３０４を提供するように曲げられる。吸引／生検チャネル３０２の軸は、注目する組織領域３０６の中心から約６．７ｍｍにおくことができる。２本のチャネル３０８及び３１０が白色光照明のために設けられ、チャネル３１２が白色光内視鏡前面観察のために設けられる。チャネル３０８，３１０及び３１２のそれぞれの直径は、２．７ｍｍとすることができる。空気または水ノズルのための細チャネル３１４も設けられる。

【００９３】

本発明にしたがえば、断層観察内視鏡コヒーレント光顕微鏡（ＥＣＯＭ）３１６がＧＩ内視鏡３００に設けられる。断層観察ＥＣＯＭ３１６は（図１４及び１５には示されていない）ミラー１６を回転させるための駆動機構３１８を備える。先に述べたように、動径、並進またはヘリカル走査を用いることができる。さらに、先に述べたように、機械的駆動機構の代わりにＭＥＭＳ駆動機構を用いることができる。断層観察ＥＣＯＭ３１６は、境界３２０で設定される深度及び境界３２２で設定される角度範囲を有する、注目する組織領域３０６にわたって走査するように構成される。さらに、光透過窓３２４を断層観察ＥＣＯＭ３１６に設けることができる（図１５参照）。

【００９４】

前面観察白色光チャネル３１２は３０フレーム／秒のレートで更新される。断層観察ＥＣＯＭ３１６で得られる断層画像は４．４フレーム／秒で更新される。全ての画像チャネルが同時に表示される。ＧＩ内視鏡３００で生成され得る画像が図１６及び１７に示される。図１６は、断層観察ＥＣＯＭ３１６で達成できることが期待される空間分解能を組み入れた、ヒトの結腸上皮のシミュレーション画像である。図１７ａ及び１７ｂは、顕微鏡像と生体内ＯＣＴ画像との比較である。図１７ａには、それぞれがヒトの皮膚の汗腺管の顕微鏡像を示す、２枚の写真がある。図１７ｂには、それぞれがヒトの皮膚の汗腺管の生体内ＯＣＴ画像を示す、３枚の写真がある。生体内ＯＣＴ画像は波長１３００ｎｍで動作する光源により生成した。

【００９５】

内視鏡医によるＧＩ内視鏡３００の典型的な操作または使用には、以下の：

ａ） 一般的な内視鏡法の手順に続いて、従来の前面観察白色光チャネル３１２の案内の下にＧＩ内視鏡３００が挿入されるステップ；この操作は現時点で利用できるＧＩ内視鏡の操作と異なることはないはずである；

ｂ） 内視鏡医が顕微鏡検査を行う必要がある場合、彼／彼女がＧＩ内視鏡３００を押し込んで図１３に示されるように内腔壁に接触させるステップ；光学系は、ＧＩ内視鏡３００が組織に接触しているときに、光学系全体の正しい作動距離が得られるように設計される；ＧＩ内視鏡３００は壁に接触しているが、図１５に示されるように、顕微鏡検査下にある組織部分は接触しない；したがって、組織の表面構造が接触圧で変形することはない；しかし、このことはＧＩ内視鏡３００が接触モードでのみ動作し得ることを意味しない；実際上、ＧＩ内視鏡３００は、画像が形成される限り非接触モードで動作することができ、これは先に述べた動的トリガ印加アルゴリズムが空気－組織界面を見いだすか否かにより規定される；空気－組織界面がシステムの作動距離内にあれば、先に‘適応トリガ印加’法で説明したように、検出された光パターンに界面が明瞭なピークを生じさせるから、界面は明確かつ容易に検出されるはずである；

ｃ） 内視鏡医がステップ（ｂ）で画像化した領域に隣接する領域を検査する必要があれば、内視鏡医がＧＩ内視鏡３００をひねり、視野を回転させて新しい位置におくことができるステップ；

が取り入れられるであろう。

【００９６】

胃腸（ＧＩ）管の映像化のための使用に現時点で最良の手法には、内視鏡超音波検査法（ＥＵＳ）及び拡大内視鏡（ＭＥ）がある。ほぼ７０から１００ｍｍの高周波ＥＵＳの分解能は、組織の微細構造を擾乱する状況の多くの識別、とりわけＧＩ管の浅層（粘膜及び粘膜下組織）内に生じる潜行性病理変化の識別には不十分である。倍率が×１７０までのＭＥは微細な浅層粘膜パターンの優れた画像を提供するが、表面下構造及び病変期分類は決定できない。したがって、組織生検及び組織学が、現時点でも依然としてＧＩ管に関わる顕微的疾患の検出のための医療標準である。

【００９７】

本明細書に開示された断層観察ＥＣＯＭ３１６によれば、軸次元及び横断（横）次元のいずれにおいても５μｍの分解能でＧＩ壁の実時間２ｍｍ深度断層画像を得ることができる。参考のために、胃腸上皮細胞の大きさは平均して７から１０μｍであり、これは異形成

または新形成変化がおこるにつれてさらに増大する。ＧＩ管においては、２ｍｍの視深度であっても、粘膜起因疾患及びいかなる下層粘膜下組織への新形成浸潤のいずれの検出にも十分であり、このことは予後判定及び治療のために重要である。断層観察ＥＣＯＭ３１６の画像分解能は、×１００（総倍率）顕微鏡の下での無染色組織検査スライド観察に相当し得る。したがって、異形成（細胞性新形成変化）のような重要なエンティティーの多くあるいは粘膜固有層または粘膜筋板のような構造の新形成浸潤を、断層観察ＥＣＯＭ３１６により識別可能とすることができる。

【００９８】

本発明により、多様な顕微的粘膜病理及び病変期分類のその場診断が可能になり得る。基本的に、本“光生検”法は、標準的な生検及び組織学の方法の代わりになるか、最小限でも、手引きになり得る。これは、不必要な生検試料及び組織処理を減らし、患者のリスクを小さくし、サンプリングレート及び診判定率を高めて即時の診断フィードバックを医師にも患者にも提供し、（ある場合にはそれ自体が治療処置になり得る）生検を目標とすると言い直すことができる。少数の例を挙げれば、バレット食道、慢性潰瘍性大腸炎、初期扁平腺腫、または迷走結腸窩の病巣のような、前新形成ＧＩ状況には、断層観察ＥＣＯＭ３１６が適用可能であり得る。現時点では、上記状況内での新形成進行の検出及びサーベイランスは、それらの顕微的性質により、最善とは言えない。

【００９９】

第２に、断層観察ＥＣＯＭ３１６は、新形成及び非新形成の組織変化を時間を追って監視することを可能にする、機能性画像化システムとして役立ち得る。例えば、小さな腸絨毛の構造の回復及び炎症性細胞の減少を、グルテン過敏腸症、熱帯性スプルー及び腸インフェステーションのような、多様な腸の吸収不良性障害において、断層観察ＥＣＯＭ３１６で監視できる。顕微レベルにおける多くの粘膜疾患の自然発達も、侵襲性を最小限に抑えた態様で評価できる。時間とともに生体内で進行している構造的細胞変化を監視できる能力は、細胞機能に関する重要な生理学的情報及び細胞の病理学的トランスフォーメーションに関する洞察を提供できる。

【０１００】

第３に、断層観察ＥＣＯＭ３１６は予後治療組織監視に使用できる。ガン切除の外科切除限界またはその予後治療サーベイランス中の処置限界または粘膜の前新形成状況の光力学治療の妥当性の評価の、生体内顕微的標定は、いくつかの例に過ぎない。

【０１０１】

その他の医学専門分野における応用も可能である。皮膚科学、血液学、（薬物及び放射線）腫瘍学、眼科学、泌尿器科学、外科学、呼吸器科学及び胃腸病学のような非常に多くの医学専門分野に、本明細書に開示された多チャネルＯＣＴ装置が応用され得ることは、当業者には当然である。

【０１０２】

本明細書に開示された多チャネルＯＣＴ装置は、システム性能をさらに向上させるために改変することができる。例えば、なされ得る改善には、光源から発せられる光に対するコード化伝送の採用があろう。この手法により、ＳＮＲが劣悪なチャネルで得られる干渉パターンの光のＳＮＲを高めることで、画像分解能を高めることができる。

【０１０３】

本明細書に説明され図示された好ましい実施形態に、本発明を逸脱することなく様々な改変がなされ得ることは当然であり、本発明の範囲は特許請求の範囲で定められる。例えば、本明細書に開示された構成図のそれぞれにおいて、３ｄＢ結合器の代わりに他の光結合器を用いることもできる。

【図面の簡単な説明】

【図１ａ】

光路を示し、空気－組織界面の反射効果を無視する、本発明にしたがう装置のチップの平面図である

【図１ｂ】

光路を示し、空気－組織界面の反射効果を無視する、本発明にしたがう装置のチップの側面図である
【図１ｃ】
光路を示し、空気－組織界面の反射効果を無視する、本発明にしたがう装置のチップの端面図である
【図１ｄ】
光路を示し、空気－組織界面の反射効果を無視する、図１ａの装置のチップの別の実施形態である
【図２ａ】
図１のファイバ束チップを示す
【図２ｂ】
ファイバ束チップの拡大平断面図である
【図２ｃ】
ファイバ束チップの端面の拡大断面図である
【図３ａ】
図１のファイバ束チップの撮像ファイバの内の３本の焦点を示す
【図３ｂ】
相異なる深度にある焦点の詳細を示す図３ａの焦点の拡大図である
【図４ａ】
図１のファイバ束チップから光ビームを向ける様々な方向を示す略図である
【図４ｂ】
図４ａの方向Ａ及びＣにおける光ビームの平面図である
【図４ｃ】
図４ａの方向Ａ及びＣにおける光ビームの端面図である
【図４ｄ】
図４ａの方向Ｂ及びＤに向けられる光ビームの平面図である
【図４ｅ】
図４ａの方向Ｂ及びＤに向けられる光ビームの側面図である
【図４ｆ】
方向Ｂ及びＤにおける光ビームの斜視図を示す
【図５ａ】
多焦点域近傍の電場強度分布を示す、５チャネルファイバ束チップのビームスポット図である
【図５ｂ】
多焦点域近傍の電場強度分布を示す、１５チャネルファイバ束チップの中央５チャネルのビームスポット図である
【図５ｃ】
図５ａのファイバ束チップのビームスポット径対焦点域距離のグラフである
【図５ｄ】
図５ｂのファイバ束チップのビームスポット径対焦点域距離のグラフである
【図６】
本発明にしたがう装置の簡略なレイアウトである
【図７ａ】
本発明の装置に用いられる光遅延発生器の平面図である
【図７ｂ】
図７ａの光遅延発生器に用いられる走査ミラーの前面図である
【図８ａ】
ミラー及び図１ａのファイバ束チップの内の３本の撮像ファイバからの焦点の端面図である
【図８ｂ】

本発明の撮像ファイバの１本から放射された光に対する、結合された、Ａ－走査及び２次元輝度モード（Ｂ－モード）走査の経路を示す
【図９】
本発明の単一撮像ファイバの１本から放射されている光に対する、空気－組織界面による、コヒーレンスゲートと焦点との間の不一致を示す図である
【図１０】
図９に示される不一致を解消させるための、本発明の装置の適応トリガ印加を示す図である
【図１１ａ】
従来技術の単チャネル光コヒーレンス断層撮影装置の略図である
【図１１ｂ】
２チャネル光コヒーレンス断層撮影装置の略図である
【図１１ｃ】
Ｎチャネル光コヒーレンス断層撮影装置を構成するために用いられ得る光ネットワークの略図である
【図１２ａ】
光サーキュレータをもつ単チャネル光コヒーレンス断層撮影装置の略図である
【図１２ｂ】
光サーキュレータを採用する２チャネル光コヒーレンス断層撮影装置の略図である
【図１２ｃ】
光サーキュレータを採用するＮチャネル光コヒーレンス断層撮影装置を構成するために用いられ得る光ネットワークの略図である
【図１３ａ】
光チャネル共有コンポーネント間のクロストークを調べるために用いられた実験装置構成の略図である
【図１３ｂ】
図１３ａの構成で実施した実験による実験結果である
【図１３ｃ】
図１３ａの構成で実施した実験による別の実験結果である
【図１４】
本発明にしたがうＧＩ内視鏡コヒーレント光顕微鏡の端面図である
【図１５】
生検チャネルを示す図１４のＧＩ内視鏡コヒーレント光顕微鏡の破断側面図である
【図１６】
本発明の装置により得られると考えられるヒトの結腸上皮のシミュレーション画像である
【図１７ａ】
それぞれが人の皮膚の汗腺管の顕微鏡像を示す２枚の写真を示す
【図１７ｂ】
それぞれが人の皮膚の汗腺管の生体内ＯＣＴ像を示す３枚の写真を示す
【符号の説明】
１０　多束単一モードファイバ
１２　ファイバ束チップ
１４　集束レンズ
１６　ミラー
１８　表面
２０　軸
２１，２２，２３　ビーム
２１ａ，２２ａ，２３ａ　集束点
２４　画像化深度

【図１ａ】

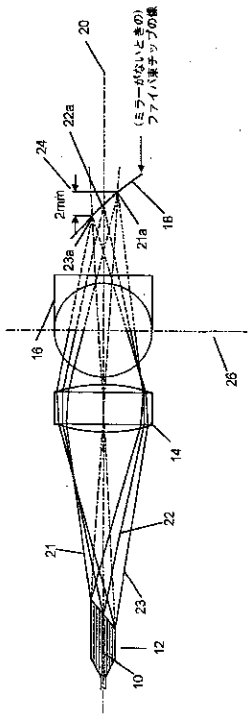

【図１ｂ】

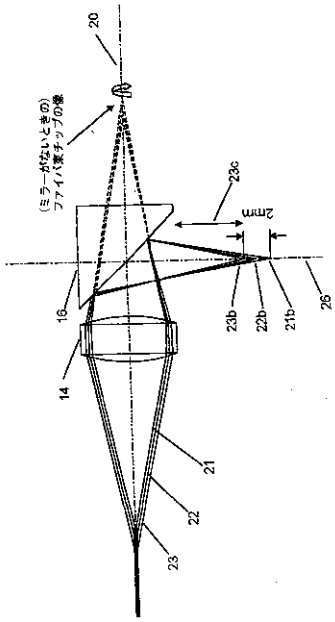

【図１ｄ】

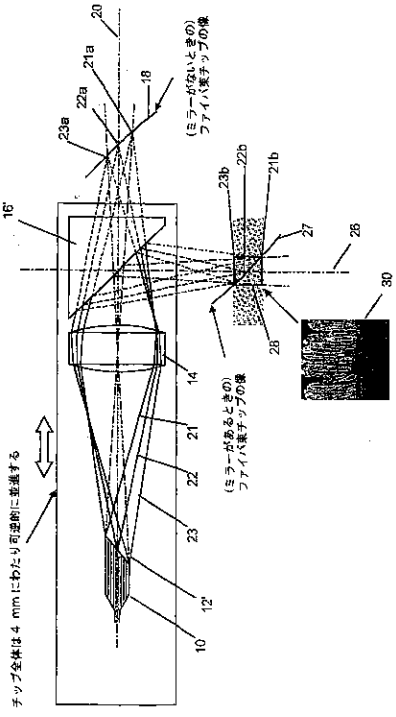

【図３】

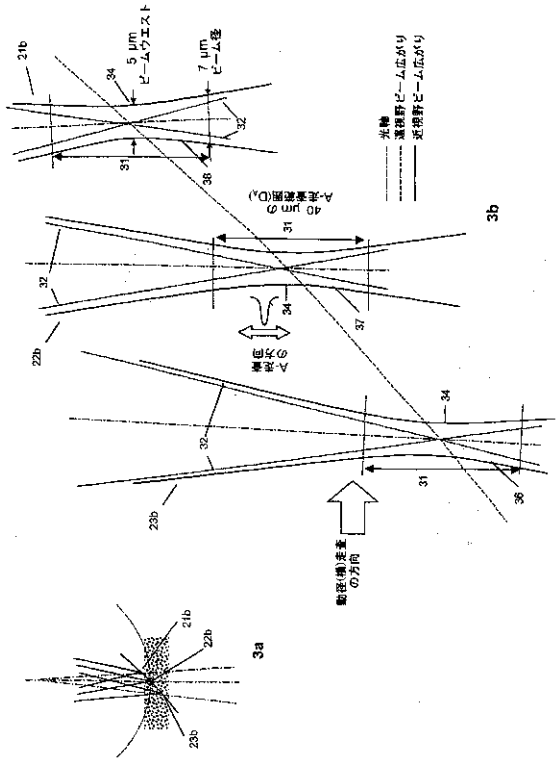

【図４】

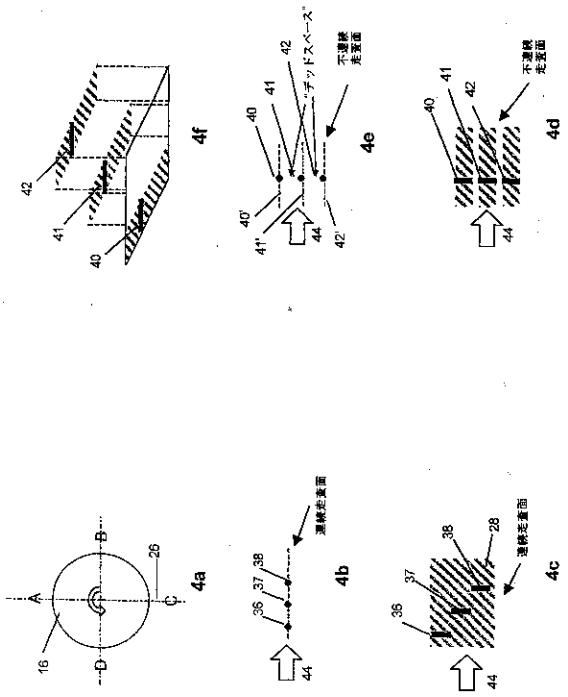

【図５ｃ】

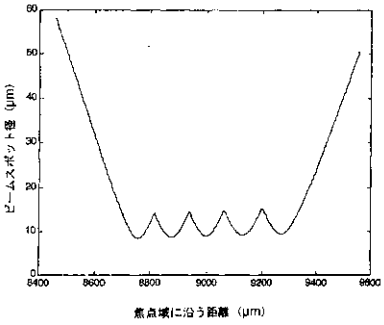

【図５ｄ】

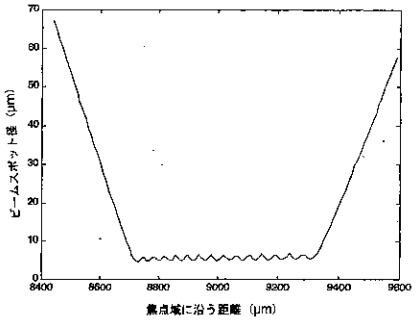

【図６】

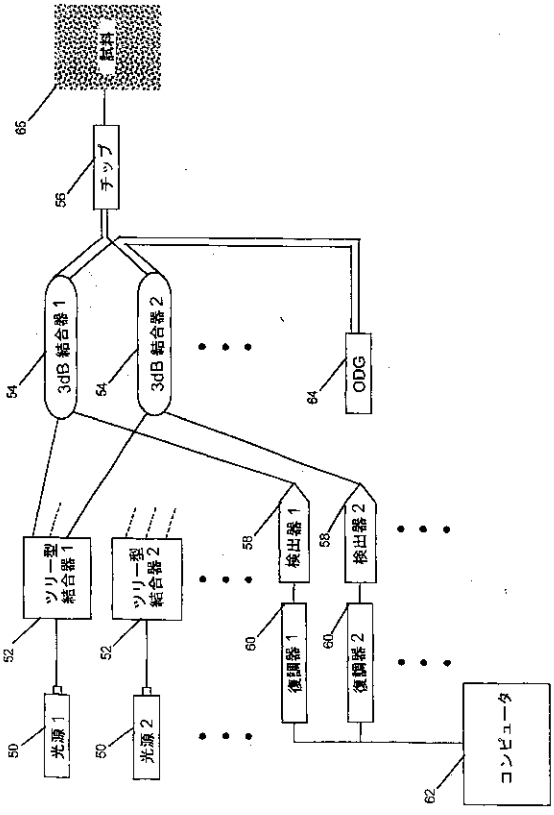

【図７】

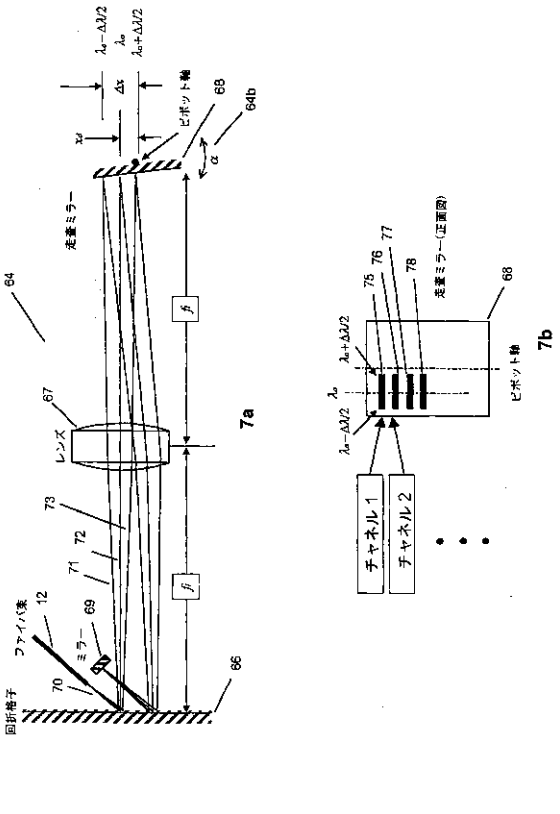

【図８】

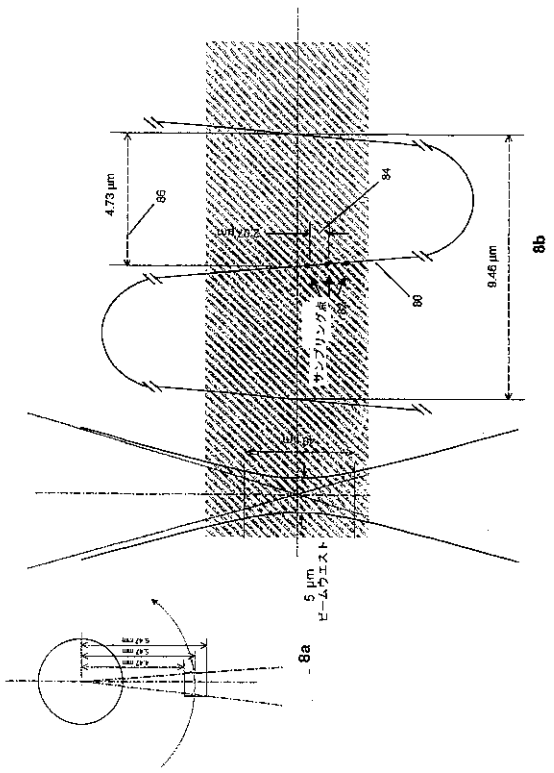

【図９】

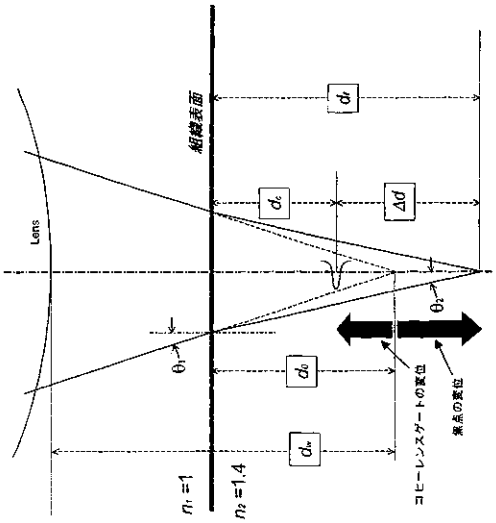

【図１０】

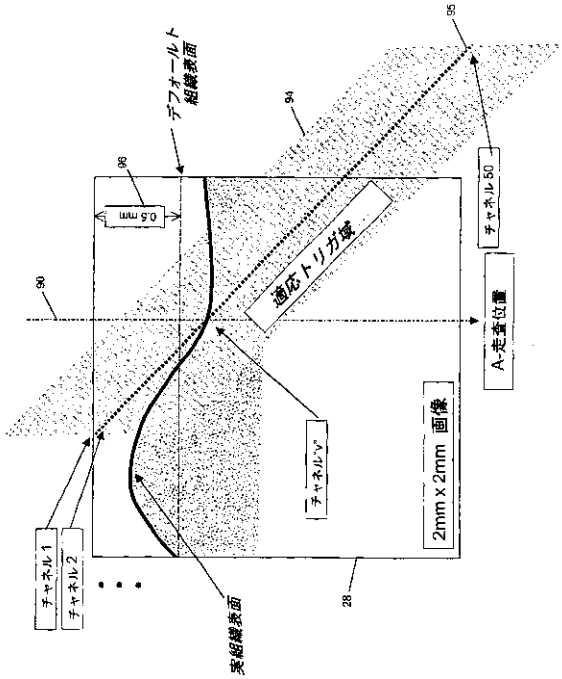

【図１１ａ】

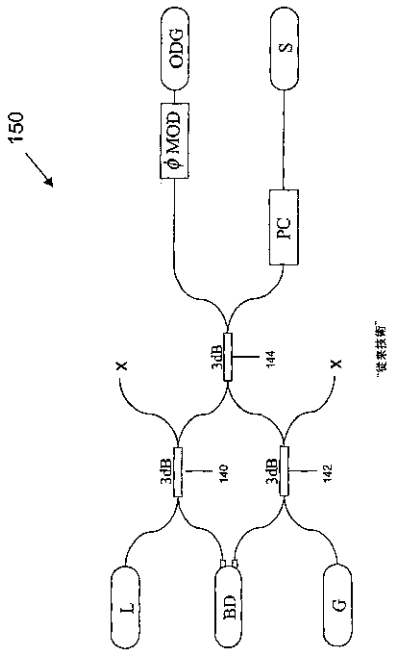

【図１１ｃ】

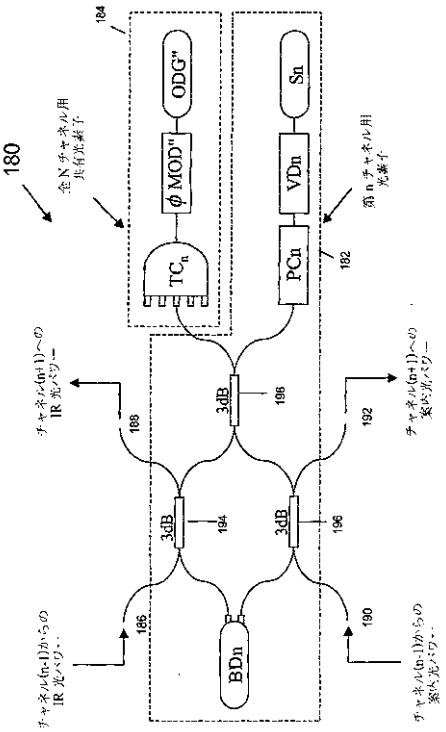

【図１２ａ】

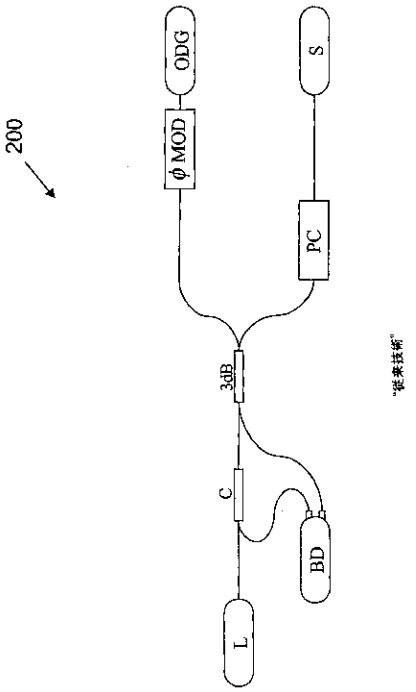

【図１２ｃ】

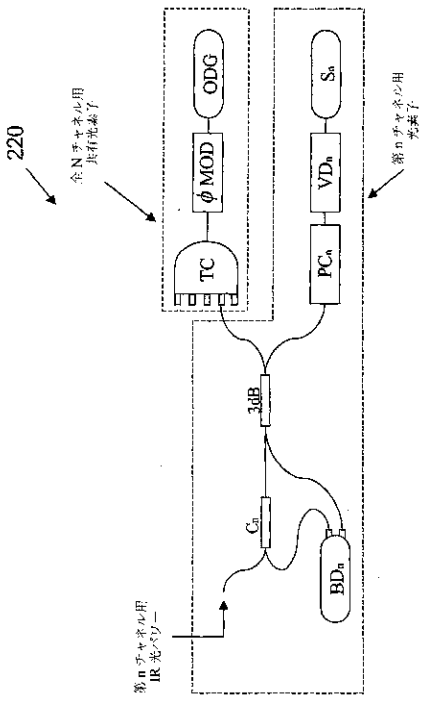

【図１４】

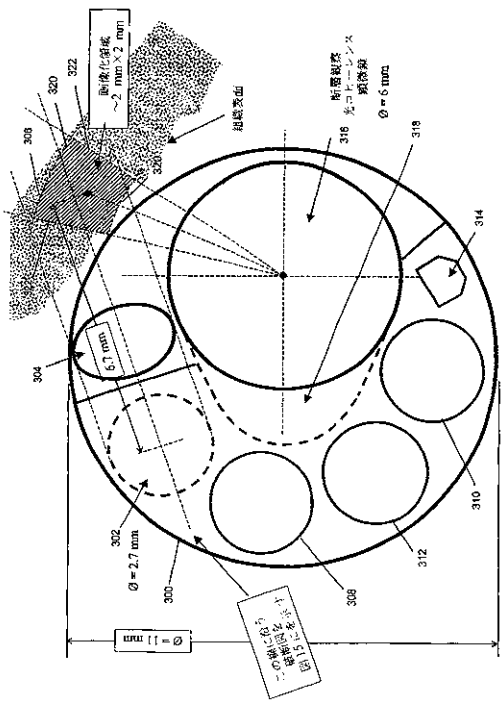

【図１５】

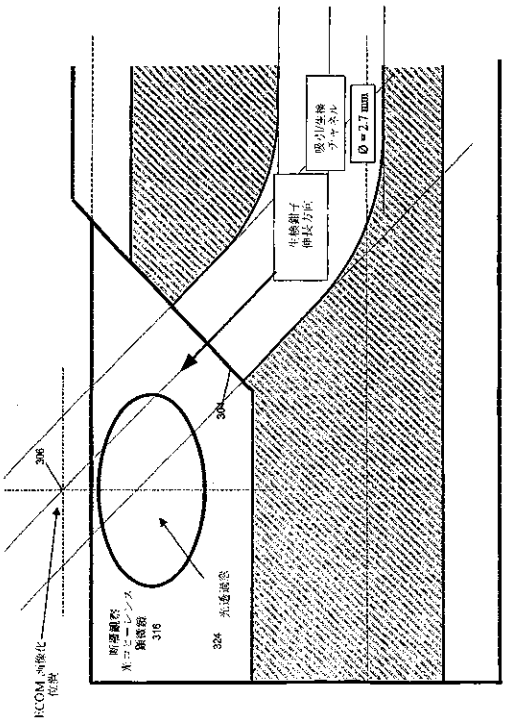

【図１７】

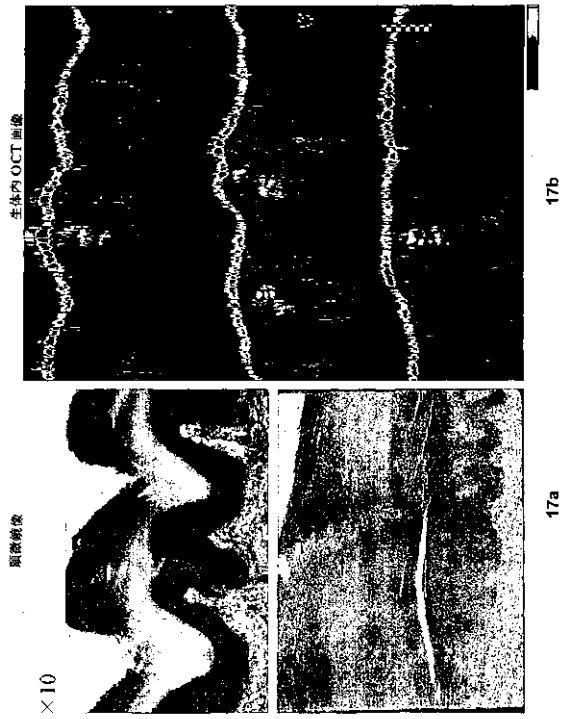

【国際公開パンフレット】

(12) INTERNATIONAL APPLICATION PUBLISHED UNDER THE PATENT COOPERATION TREATY (PCT)

(19) World Intellectual Property Organization
International Bureau

(43) International Publication Date
17 January 2002 (17.01.2002)

PCT

(10) International Publication Number
WO 02/04929 A2

(51) International Patent Classification⁷: G01N 21/47

(21) International Application Number: PCT/CA01/00992

(22) International Filing Date: 10 July 2001 (10.07.2001)

(25) Filing Language: English

(26) Publication Language: English

(30) Priority Data:
60/217,090 10 July 2000 (10.07.2000) US

(71) Applicant (*for all designated States except US*): **UNIVERSITY HEALTH NETWORK** [CA/CA]; Room 7-504, 610 University Avenue, Toronto, Ontario M2G 2M9 (CA).

(72) Inventors; and

(75) Inventors/Applicants (*for US only*): **YANG, Victor, Xiao, Dong** [CA/CA]; Unit - 936B, 60 Harbord Street, Toronto, Ontario M5S 3L1 (CA). **VITKIN, I., Alex** [CA/CA]; 130 Glenlake Avenue, Toronto, Ontario M6P 1E5 (CA). **WONGKEESONG, Louie** [CA/US]; Apartment 502, 211 2nd Street N.W., Rochester, MN 55901 (US). **KATZ, Sharon** [IL/CA]; 77 Winnifred Avenue, Toronto, Ontario M4M 2X2 (CA). **GORDON, Margaret, Leslie** [CA/CA]; 61 Dalewood Road, Toronto, Ontario M4P 2N4 (CA). **WILSON, Brian, C.** [GB/CA]; 85 Indian Grove, Toronto, Ontario M6R 2Y6 (CA). **MOK, Alvin, Ho, Kwan** [CA/CA]; 187 Spadina Road, Richmond Hill, Ontario L4B 3C5 (CA).

(74) Agent: **BERESKIN & PARR**; 40th floor, 40 King Street West, Toronto, Ontario M5H 3Y2 (CA).

(81) Designated States (*national*): AE, AG, AL, AM, AT, AU, AZ, BA, BB, BG, BR, BY, BZ, CA, CH, CN, CO, CR, CU, CZ, DE, DK, DM, DZ, EE, ES, FI, GB, GD, GE, GH, GM, HR, HU, ID, IL, IN, IS, JP, KE, KG, KP, KR, KZ, LC, LK, LR, LS, LT, LU, LV, MA, MD, MG, MK, MN, MW, MX, MZ, NO, NZ, PL, PT, RO, RU, SD, SE, SG, SI, SK, SL, TJ, TM, TR, TT, TZ, UA, UG, US, UZ, VN, YU, ZA, ZW.

(84) Designated States (*regional*): ARIPO patent (GH, GM, KE, LS, MW, MZ, SD, SL, SZ, TZ, UG, ZW), Eurasian patent (AM, AZ, BY, KG, KZ, MD, RU, TJ, TM), European patent (AT, BE, CH, CY, DE, DK, ES, FI, FR, GB, GR, IE, IT, LU, MC, NL, PT, SE, TR), OAPI patent (BF, BJ, CF, CG, CI, CM, GA, GN, GW, ML, MR, NE, SN, TD, TG).

Published:
— *without international search report and to be republished upon receipt of that report*

For two-letter codes and other abbreviations, refer to the "Guidance Notes on Codes and Abbreviations" appearing at the beginning of each regular issue of the PCT Gazette

WO 02/04929 A2

(54) **Title:** METHOD AND APPARATUS FOR HIGH RESOLUTION COHERENT OPTICAL IMAGING

(57) **Abstract:** A method and an apparatus for examining the sub-surface microstructure of a sample are provided. Radiation from a plurality of optical radiation sources travels along a first optical path. In the first optical path, a device focuses the optical radiation from each of the optical sources into a plurality of respective focal points along the first optical path to provide substantially continuous coverage of a selected portion of the first optical path. Then, a sample on the first optical path within the selected length extending into the sample is scanned along said selected portion of the first optical path.

Title: METHOD AND APPARATUS FOR HIGH RESOLUTION COHERENT OPTICAL IMAGING

FIELD OF THE INVENTION

This invention relates to both a method and an apparatus for high-resolution optical imaging. More particularly, this invention is concerned with providing high-resolution imaging suitable for incorporation into an endoscope.

BACKGROUND OF THE INVENTION

Modern medical imaging techniques have important applications in health care. Modalities such as X-ray computed tomography (CT), magnetic resonance imaging (MRI) and ultrasound imaging are the main tomographic techniques available in most modern medical centers. Visible-light endoscopy is another major imaging modality which is used extensively in procedures like bronchoscopy or colonoscopy. Each of these techniques employs different physical principles and measures different properties of the biological tissue under study with different resolution. Further, they can commonly be performed *in-vivo*. A third type of imaging, optical microscopy, is still utilized widely in clinical medicine. However, optical microscopy is currently limited to detailed examination of excised or resected specimens and is not used *in-vivo*. In many circumstances, the superior contrast and resolution afforded by optical microscopy is such that physical biopsy followed by optical microscopic histology is considered the gold standard for diagnosis.

Combinations of these techniques, such as using a low-resolution tomographic modality along with high-resolution imaging, biopsies or interventional procedures are constantly being studied and evaluated. Evaluation of these techniques is based on technological feasibility, clinical benefit and cost.

Optical Coherence Tomography (OCT) is a relatively new imaging technique based on the low-coherence property of electromagnetic radiation that enables high-resolution depth profilometry in a turbid, highly scattering

media such as biological tissue. Its use in biomedical imaging is currently being investigated in several research and industrial laboratories. The main advantage of OCT lies in its ability to localize the depth of reflection from a sub-surface site in tissue. This localization is essentially determined by the coherence properties of the light source used and can be as low as 2 to 20 μm for selected near-IR sources (e.g. lasers or amplified spontaneous emission devices). This gives a measure of the depth resolution attainable with OCT. Independently of the coherence characteristics, the lateral resolution is determined by the beam cross-section at the depth of imaging and by the lateral spacing of the acquired data. Typical values for lateral spacing in the literature are in the 5 to 30 μm range. The price to be paid for this remarkable cross-sectional imaging ability in intact turbid tissue is the limited imaging depth since, due to multiple scattering and absorption, both coherence and penetration of light are degraded resulting in OCT imaging depths of approximately 2 to 3 mm.

Most current implementations of OCT are based on Michelson interferometry with a 50/50 beam splitter directing the incident coherent light beam into a reference path containing a mirror (i.e. a reference arm) and a sample path containing the interrogated sample (i.e. a sample arm). Both free-space optic and fiber-optic implementations of this scheme are currently used. Reflected beams from the mirror in the reference arm and from the tissue in the sample arm are recombined in the same splitter and half of the resultant light energy impinges on a detector. Incoherent superposition of the two light fluxes typically occurs except when the optical path lengths of the two beams are matched to within the coherence length of the source. Within this limited distance, the coherent superposition of the two light fluxes yields an interference pattern with a fringe magnitude that is proportional to the reflectivity of the tissue at that particular depth. Depth profiling of the sample is then achieved by scanning the reference arm length or more correctly by scanning the optical path length of the reference arm by using a time delay in the reference arm (this is equivalent to lengthening the reference arm). Various detection methods to measure and quantify these faint amplitude

modulations amidst large background diffuse reflectance have been developed having a dynamic range of approximately 70 to 110 dB. Furthermore, lateral translation of the beam and axial motion of the reference mirror enables one to construct a two-dimensional reflectivity picture over a desired field of view. Means of improving the final image quality, such as performing image processing through de-convolution, have also been investigated.

The foregoing is a brief description of conventional reflectivity OCT imaging. Other variations include, for example, flow (Doppler) imaging and polarization imaging (albeit at the expense of additional complexity of the OCT optics and/or signal processing techniques). Images from these additional techniques are usually obtained in conjunction with images from conventional OCT so some image overlay or fusion is possible. Upon further technological development and/or clinical implementation, may add sufficient information content to increase the clinical utility of OCT in medicine.

However, many OCT designs and approaches that have been successfully implemented in tabletop research systems are not directly suitable for *in-vivo* imaging such as in gastroenterologic or bronchoscopic endoscopy. Instead, they may be more suitable for dermatological, ophthalmologic and dental applications. In contrast, *in-vivo* OCT imaging must address the issues of speed, resolution, contrast, penetration and instrument size. Images must be obtained sufficiently quickly to negate the effects of patient motion while still achieving suitable axial and lateral resolution, and maintaining an instrument size which is small enough to be endoscopically useful. Powerful near-IR sources, fast means of altering the reference arm length and custom-designed distal optical devices have been successfully developed to overcome the difficult challenges posed by *in-vivo* endoscopy.

The latest OCT technology employs a single-mode optical fiber with distal side-viewing optics introduced into the accessory channel of a conventional white-light endoscope. To build-up an image, the viewing direction of the OCT fiber is either linearly scanned to and fro over an approximate 2 mm distance, or is rotated via a flexible guide-wire or

interlocking gear mechanism at several revolutions per second. Simultaneous with this translation or rotation, the reference arm length outside the endoscope is rapidly varied via an optical phase delay to generate depth scans (i.e. A-scans). Currently, these OCT systems operate at frame rates up to conventional video rates but more typically at 4 to 8 frames per second, with a frame presenting a fully circumferential view to a depth of 2 to 3 mm. The resultant resolution values are approximately 5 to 25 μm in the depth (axial) direction and approximately 20 to 40 μm in the lateral direction. As well, the lateral resolution generally degrades with an increase in distance from the fiber tip of the OCT device due to geometric divergence. These OCT systems have a dynamic range which is somewhat lower than that of corresponding *ex-vivo* systems due to increased noise levels and faster imaging speeds.

Based on the latest OCT technology, it is questionable whether coherent *in-vivo* OCT systems are adequate for successful clinical imaging. The images are certainly useful, but substantial improvement is required if the elusive goal of "optical biopsy" is to be realized. For example axial and lateral resolution can be improved. While the improvement in the former usually involves the use of better low-coherence sources (i.e. CW and pulsed sources), the issue of sub-optimal and depth-varying lateral resolution is more difficult to address. In *ex-vivo* systems, with its relaxed constraints of speed and physical size, lateral resolution is improved by focusing the beam to a few microns with a high-NA (numerical aperture) objective lens. In contrast to conventional OCT scanning, the imaging can now be performed in the lateral (*en face*) direction with a pre-selected depth with small oscillations in path length difference, followed by a small depth increment as necessary. The high-NA objective lens is often coupled to tissue via a refractive-index matching liquid. The general approach of using OCT with a high-NA distal optic lens is known as Optical Coherence Microscopy (OCM). However, the improved lateral resolution at the beam waist location comes at the expense of lateral blurring at other depths because the highly focused beam has a very shallow depth of field. Thus,

the lens-to-surface distance must be varied to focus to different depths. In addition, a dynamic tracking scheme is needed to keep the location of the coherence gate (within which coherent interference between the optical beams from the sample arm and the reference arm is possible) and the beam waist at the same depth. These techniques for lateral resolution improvement have not been attempted during *in-vivo* endoscopy because of size and speed requirements.

SUMMARY OF THE INVENTION

The present invention is based on the concept of providing an endoscopic optical coherence tomography (OCT) device with microscopic resolution which will hereinafter be referred to as an endomicroscope. After reviewing possible clinical applications of the endomicroscope, the following parameters and features were identified since it is difficult to achieve these parameters and features simultaneously with current *in vivo* OCT systems.

1. High Resolution

In order to achieve cellular and sub-cellular resolution, an endomicroscope should preferably resolve features smaller than 5 μm both in the axial and lateral directions. In contrast to most existing *in vivo* OCT systems, the lateral resolution must not degrade substantially with the depth of the tissue being imaged due to geometric divergence.

2. Large field of view

An appropriate field of view of the endomicroscope is approximately 2 x 2 mm in the axial and lateral directions of the optical axis. This field of view is considered to be adequate for clinical applications. In order to achieve a 5 μm resolution in both the axial and lateral directions throughout the entire image, more than 800 A-scans (i.e. depth scans) have to be performed for each frame. The resultant image will contain more than 640,000 pixels. This is several orders of magnitude higher than existing *in vivo* OCT systems.

3. Small size of endoscope tip

Most of the existing *in vivo* OCT systems are designed around the constraints of the instrument channel of existing endoscopes. As a result, the outer diameter of these systems is restricted to approximately 2 to 3 mm which limits the numerical aperture of the imaging system. This makes it difficult to obtain high lateral resolution under *in vivo* conditions. These constraints may be technically unnecessary and limit one from fully exploiting the benefit of OCT/OCM in the clinical applications under consideration. Accordingly, a larger outer diameter, such as 3 mm or more, for example, may be used for the endoscope as well as a length of less than 20 mm for the rigid tip.

4. High imaging speed

Since the endomicroscope will be used to image a large area at high resolution under *in vivo* conditions, motion artifacts must be considered because of tissue motion due to physiological motion. These motion artifacts should be eliminated to ensure good image quality. Accordingly, the endomicroscope should preferably be able to acquire a single frame image within 12.6 ms given a typical physiological motion speed of 5 mm/s. This results in 63,000 A-scans per second. This imaging speed is more than one order of magnitude higher than that of current *in vivo* OCT systems.

5. Integration with currently available endoscopic imaging procedures

In order to improve clinical usefulness, conventional white light imaging should preferably be integrated into the endomicroscope. In addition, instrument channels should be preferably designed so that an excisional biopsy could be performed under the guidance of the endomicroscope. As well, instrument channels for water and air delivery may be preferably made available.

The advanced requirements for an endomicroscope outlined above are not compatible with existing OCT/OCM designs. For instance, if

an outer diameter of 6 mm is allowed for the endomicroscope and a distal optical design is used based on a single rotating fiber as described by Tearney, G.J., Brezinski, M.E., Bouma, B.E., Boppart, S.A., Pitris, C., Southern, J.F., and Fujimoto, J.G. ("In vivo Endoscopic Optical Biopsy with Optical Coherence Tomography", Science, **276**: 2037-2039, 27 June 1997), then although the 5 µm lateral resolution can be achieved at a single specific depth within the tissue in any one scan, such lateral resolution will degrade due to beam divergence at other depths. In addition, since a high NA system will be required to produce the requisite small beam waist size, the coherence gate and the focal point will not stay together in depth over a substantial (e.g. 2 mm) distance unless some dynamic compensation is implemented as described by Schmitt, J.M., Lee, S.L., and Yung, K.M ("An Optical Coherence Microscope with Enhanced Resolving Power in Thick Tissue", Optics Communications, **142**: 203-207, 1997). Therefore, in order to achieve some of the aforementioned requirements of the endomicroscope, dynamic focusing (changing the probe/tissue distance) and dynamic compensation (changing the path length difference) must be used. However, these focusing and compensation techniques complicate the practical realization of the device and may make it more difficult to satisfy the high imaging speed requirement. If one tries to first satisfy the imaging speed, as described by Rollins, A.M., Kulkarni, M.D., Yazdanfar, S., Ung-arunyawee, R., and Izatt, J.A. ("In vivo Video Rate Optical Coherence Tomography", Optics Express, **Vol. 3 No. 6**: 219-229, 14 September 1998), then image resolution, particularly lateral resolution, is degraded to an extent that the clinical utility of the device is compromised.

The present invention provides an endomicroscope with multiple fibers (i.e. channels) employing OCT to allow for different parts of the image to be scanned in parallel, instead of in series as is currently implemented in existing *in vivo* or *ex vivo* OCT/OCM systems. Using multiple parallel channels focused to different depths in the tissue, with each channel collecting high-resolution OCT data only across a very small axial range allows for a series of tight focal points to be achieved throughout the entire

field of view without dynamic focusing or dynamic compensation. This greatly simplifies the design of the device which may now use mostly fixed optical components, and may facilitate high-speed operation. In addition, the intrinsically miniature dimension of the fiber optic based OCT technique makes the multichannel concept possible to implement in a flexible endoscopic device while the proximal part of the endoscope, which is outside of the patient, allows room for sources, detectors, and other equipment.

In accordance with a first aspect of the present invention, there is an apparatus for optical examination of a sample, the apparatus comprising:

an optical source means for providing a plurality of separate optical radiation sources;

a first optical path extending from the source means; and,

a focusing means in the first optical path for focusing optical radiation from the optical radiation sources into a plurality of respective focal points located on a surface within the first optical path to provide substantially continuous coverage of a selected portion of the first optical path, whereby, in use, a sample can be located at least partially within the selected portion, thereby permitting simultaneous scanning of a plurality of points within the sample.

In accordance with a second aspect of the present invention, an N channel apparatus for optical examination of a sample, wherein the N channel apparatus comprises a plurality of optical networks and a reference arm, each optical network providing one channel for the N channel apparatus and sharing the reference arm.

In accordance with another aspect of the present invention, there is provided a method for optical examination of a sample, the method comprising:

(a) providing radiation from a plurality of separate optical radiation sources, along a first optical path;

(b) providing focusing means in the first optical path;

(c) focusing the optical radiation from the optical sources into a plurality of respective focal points along a surface within the first optical

path to provide substantially continuous coverage of a selected portion of the first optical path; and

(d) providing a sample located at least partially within the first optical path; and,

(e) simultaneously scanning a plurality of points within the sample.

It is to be appreciated that a sample, for use with the present invention, may comprise any biological tissue or other suitable material.

Further objects and advantages of the invention will appear from the following description, taken together with the accompanying drawings.

BRIEF DESCRIPTION OF THE DRAWINGS

For a better understanding of the present invention and to demonstrate how it may be carried into effect, reference will now be made, by way of example, to the accompanying drawings which show a preferred embodiment of the present invention and in which:

Figure 1a is a top view of the tip of an apparatus in accordance with the present invention showing optical paths and ignoring the refraction effects of an air-tissue interface;

Figure 1b is a side view of the tip of an apparatus in accordance with the present invention showing optical paths and ignoring the refraction effects of an air-tissue interface;

Figure 1c is an end view of the tip of an apparatus in accordance with the present invention showing optical paths and ignoring the refraction effects of an air-tissue interface;

Figure 1d is an alternate embodiment of the tip of the apparatus of Figure 1a showing optical paths and ignoring the refraction effects of an air-tissue interface;

Figure 2a shows the fiber bundle tip of Figure 1;

Figure 2b is a top view of an enlarged section of the fiber bundle tip;

Figure 2c is an end view of an enlarged section of the fiber bundle tip;

Figure 3a illustrates the focal points of three of the imaging fibers of the fiber bundle tip of Figure 1;

Figure 3b is a magnified view of the focal points of Figure 3a showing details of the focal points at different depths;

Figure 4a is a schematic indicating different directions for directing the optical beams from the fiber bundle tip of Figure 1;

Figures 4b and 4c are top and end views of optical beams in directions A and C of Figure 4a;

Figures 4d and 4e are top and side views of optical beams directed in directions B and D of Figure 4a;

Figure 4f shows a perspective view of the optical beams in the directions B and D;

Figure 5a is a beam spot diagram of a 5 channel fiber bundle tip showing electric field strength distribution near multiple focal zones;

Figure 5b is a beam spot diagram of 5 central channels of a 15 channel fiber bundle tip showing electric field strength distribution near multiple focal zones;

Figure 5c is a graph of beam spot diameter versus focal zone distance for the fiber bundle tip of Figure 5a;

Figure 5d is a graph of beam spot diameter versus focal zone distance for the fiber bundle tip of Figure 5b;

Figure 6 is a schematic layout of an apparatus in accordance with the present invention;

Figures 7a is a top view of an optical delay generator used in the apparatus of the present invention;

Figure 7b is a front view of a scanning mirror used in the optical delay generator of Figure 7a.

Figure 8a is an end view of the mirror and the focal points from three of the imaging fibers of the fiber bundle tip of Figure 1a;

Figure 8b shows a combined A-scan and a two-dimensional brightness-mode (B-mode) scan path for light radiated from a single imaging fiber of the present invention;

Figure 9 is a diagram illustrating mismatch between the coherence gate and the focal point due to the air-tissue interface for light radiating from a single imaging fiber of the present invention;

Figure 10 is a diagram illustrating flexible triggering of the apparatus of the present invention to accommodate the mismatch shown in Figure 9;

Figure 11a is a schematic diagram of a Prior Art single channel Optical Coherence Tomography device;

Figure 11b is a schematic diagram of a two channel Optical Coherence Tomography device;

Figure 11c is a schematic diagram of an optical network that could be used to construct an N-channel Optical Coherence Tomography device;

Figure 12a is a schematic diagram of a single channel Optical Coherence Tomography device with an optical circulator;

Figure 12b is a schematic diagram of a two channel Optical Coherence Tomography device employing optical circulators;

Figure 12c is a schematic diagram of an optical network that could be used to construct an N channel Optical Coherence Tomography device employing an optical circulator;

Figure 13a is a schematic of an experimental setup used to investigate cross-talk between optical channels sharing components;

Figure 13b is an experimental result from experimentation on the setup of Figure 13a;

Figure 13c is another experimental result from experimentation on the setup of Figure 13a;

Figure 14 is an end view of a GI endoscopic coherent optical microscope in accordance with the present invention;

Figure 15 is a cutaway side view of the GI endoscopic coherent optical microscope of Figure 14 showing a biopsy channel;

Figure 16 is a simulated image of a human colon epithelium that is expected to be obtained with the apparatus of the present invention;

Figure 17a has two panels which each show a microscopy image of sweat ducts in the human skin; and,

Figure 17 b has three panels which each show an *in vivo* OCT image of sweat ducts in the human skin.

DETAILED DESCRIPTION OF THE INVENTION

In the following description, various specific dimensions and other parameters are mentioned such as the wavelength used by the imaging source and the physical dimensions of the optical components used in the apparatus. It is to be appreciated that this is for exemplary purposes only and does not limit this invention. Specific parameters, dimensions and the like may be chosen depending on an intended application of the invention.

Referring to Figure 1, the present invention provides an apparatus comprising an endoscopic coherent optical microscope having multiple single mode fibers **10**, a fiber bundle tip **12**, a focusing lens **14** and a mirror **16**. The multiple single mode fibers **10** and the focusing lens **14** are stationary while the mirror **16** is rotatable. Accordingly, the mirror **16** is mounted for rotation in known manner. Details of the rotating mechanism for the mirror **16** are not described further and can be conventional. Multiple single mode fibers **10** (of which there may be approximately 50 fibers) form an array at the fiber bundle tip **12**. This array is cleaved and arranged in a "staircase" pattern as shown in Figure 2. Radiated light from the fiber bundle tip **12** is focused by the focusing lens **14** and reflected by the mirror **16**. The focusing lens **14** may have a diameter of 5 mm (i.e. ϕ = 5 mm) and a focal length of 5 mm (i.e. f = 5 mm). The mirror **16** may have a diameter of 5 mm and a front face that is cleaved at 45°. A magnified image of the focal points of the fiber bundle tip **12** is shown in Figure 3.

Figure 1a shows three beams **21**, **22** and **23** from three exemplary fibers arbitrarily chosen from the multiple single mode fibers **10**. Due to the staggered or staircase nature of the multiple single mode fibers **10** (see Figure 2), each of the beams **21**, **22** and **23** originates from a different point and consequently is brought into focus, by the focusing lens

14, at a different point **21a**, **22a** and **23a** on a surface **18** when the mirror **16** is not used. It will be appreciated that a similar effect is achieved for all of the multiple single mode fibers **10** of the fiber bundle tip **12** to produce beams focused to different points on the surface **18**. As indicated at **24** (and as shown in Figure 3), if the multiple single mode fibers **10** comprise 50 optical fibers, each being focused within a short range of approximately 40 microns and having their ends staggered to space the focal points apart by 40 microns (as measured along axis **20** of the focusing lens **14**), a total range or depth of 2 mm is covered. The axis **20** for the focusing lens **14** is part of a first optical path.

With the mirror **16** present, the optical beams **21**, **22** and **23** are focused as shown in Figures 1b and 1c. Thus, three focal points **21b**, **22b** and **23b** are spaced apart in a vertical or depth direction along axis **26** which forms an extension of the first optical path. As the view of Figure 1c shows, the three focal points **21b**, **22b** and **23b** are also spaced apart in the circumferential direction (i.e. they are spaced apart laterally) relative to the motion of the mirror **16**. The three focal points **21b**, **22b** and **23b** fall on a surface **27** to facilitate imaging of a selected portion of the first optical path. The surface **27** may be a complex surface or a planar surface. If multiple single mode fibers **10** comprises 50 individual fibers, then the focal points of all the individual fibers from the fiber bundle tip **12** would be spaced apart correspondingly. . Alternatively, the reflected focal points **21b**, **22b** and **23b** do not necessarily have to be perpendicular to the axis **20** but may be at a large angle to the axis **20**.

Rotation of the mirror **16** results in motion of the surface **27**. This enables a two-dimensional B-scan image **30** to be obtained, as shown in Figure 1c, covering a scan area **28** which has a square shape with preferable dimensions of 2 mm x 2 mm. The B-scan image **30** indicates an exemplary view that may be obtained for the scan area **28**.

Redesigning the multiple single mode fibers **10**, for example, by changing the diameter of the core and cladding of the multiple single mode fibers **10**, results in variations on the surface **27**. Furthermore, optical wave

guide wafers may also be used in the place of the multiple single mode fibers **10**.

In an alternative embodiment, the mirror **16** may be replaced by a mirror **16'** that moves linearly in combination with the focusing lens **14** and the fiber bundle tip **12** as shown in Figure 1d. The linear translation may preferably incorporate a reciprocal motion. In terms of mechanics, the fiber bundle tip **12**, depicted in Figure 1a, utilizes a radial scanning motion. The radial scanning motion is well suited for scanning organs having larger diameters, such as the esophagus or the large intestine. However, due to the complex driving mechanism needed for radial scanning, the diameter of the fiber bundle tip **12** will not allow for endomicroscopy in organs having small inner diameters such as blood vessels. Therefore, the alternative embodiment shown in Figure 1d may be used which comprises a similar fiber bundle tip **12'** that is adapted to perform linear translational scanning instead of radial scanning.

As shown in Figure 1d, the main differences between the two methods of scanning are that the mirror **16'** will not be rotating and the entire fiber bundle tip **12'** needs to be translated along its horizontal axis in preferably a reciprocal motion over a range of 4 mm for example. Mechanically, the linear translational scanning motion is less complicated than the radial scanning motion. In addition, linear translational scanning is better suited for endomicroscopy in organs having a small inner diameter such as blood vessels. However, for some larger organs, such as the large intestine, linear translational scanning is not as well suited due to positioning difficulties.

In a further alternative embodiment, both of the scanning motions may be combined to produce an endomicroscopy device having helical scanning. The helical scanning motion would comprise the rotational movement of the mirror **16** in combination with the linear translation of the mirror **16**, the focusing lens **14** and the fiber bundle tip **16**. Such an endomicroscopy device may be more suitable for imaging certain types of organs such as the human large intestine. The helical scanning

endomicroscopy device may be implemented by linearly translating the apparatus shown in Figure 1a.

In yet another alternative embodiment, the fiber bundle tip **12** may be altered to employ a Micromachined Electro-Mechanical System (MEMS) driving mechanism. Since the aforementioned embodiments require some form of motion for the mirror **16**, all embodiments require mechanical driving mechanisms. Accordingly, a motor is situated outside of the endoscope and a mechanical drive-train mechanism or wire is placed along the entire length of the endoscope. However, the multi-channel fiber optical design is not restricted to such mechanical driving means. In fact, due to the extremely small spatial resolutions realizable by the multi-channel system, adverse effects, such as vibration induced polarization dependence, from the mechanical drive means, may limit the full potential of the present invention if a mechanical drive means is utilized. Therefore, a MEMS electrical driving mechanism may be employed where electrically-driven, micro-mechanical optical devices are used to facilitate the scanning. This implementation may potentially circumvent the adverse effects that may be caused by a mechanical driving mechanism since the MEMS implementation reduces vibrations along the axis of the device except in the vicinity of the object which is being translated such as the mirror **16**. The MEMS implementation may also offer advantages in terms of miniaturization and performance.

In a further alternative embodiment, the fiber bundle tip may not require the mirror **16**. The combination of the fiber bundle tip **12** and the focusing lens **14** may be pivotally attached. Accordingly, through a pivoting motion, the combination of the fiber bundle tip **12** and the focusing lens **14** may be adapted to direct a plurality of focusing points along portions of a plurality of surfaces extending into the sample to construct the B-scan image **30** of the scan area **28**.

In yet another embodiment, the mirror **16** may be a surface of a prism. The rest of the apparatus would follow as previously described and shown in Figures 1a to 1d.

It should further be understood that the optical path can be straight, bent or curved. Furthermore, the optical path may be a 3 dimensional path having a length, width and height. Depending on the scanning motion (i.e. radial, linear or helical), the orientation of the surface, upon which the focal points reside, may also vary. Furthermore, the optical path may comprise optical radiation from one optical radiation source or a plurality of optical radiation sources (i.e. a plurality of light sources or a plurality of fibers each transmitting optical radiation).

Referring now to Figures 2b and 2c, a magnified view of the fiber bundle tip **12** comprising the multiple single mode fibers **10** is shown. Each of the multiple single mode fibers **10** comprises a cladding **10a** around a core **10b** having diameters of, for example, 40 μm and 5 μm respectively. The ends of the multiple single mode fibers **10** may be stepped by 40 μm so that the focal points of the optical radiation through each of these fibers are spaced apart. However, a step spacing other than 40 μm may also be used.

Referring now to Figure 3, A-scans for each of the multiple single mode fibers **10**, in the fiber bundle tip **12**, are acquired over approximately the entire 2 mm imaging depth, but retained only over a short axial range of approximately 40 μm near the focal point of each fiber where the beam diameter is close to a minimum (indicated at **34**) and does not vary substantially with axial position. This range of 40 μm, in this exemplary design, is indicated at **31**. The A-scans are performed simultaneously by each of the multiple single mode fibers **10** within the fiber bundle tip **12**. Effectively, the multiple A-scans cover the entire depth of 2 mm in the sample tissue at different radial directions, but for each of the multiple single mode fibers **10**, only sections of the respective A-scan in a corresponding 40 μm depth-of-focus **31** are used to build up the image. As shown in the focal zone **31**, each of the beams **21b**, **22b** and **23b** show a distinct "hourglass" shape for the focal points **38**, **37** and **36**, in known manner. For each of the beams **21b**, **22b** and **23b**, the far field beam spread is indicated by lines **32** and the near field beam spread is indicated by lines **34**.

The purpose of rotating the mirror **16** is to create radial (i.e. lateral) scans in a direction that is perpendicular to the A-scan direction to create a B-scan image, i.e. the scan area **28** of Figure 1. The resultant radial scan pattern of the focal points of the individual fibers from the multiple single mode fibers **10** is illustrated in Figure 4. It is worth noting that a continuous scan surface is only present when the cleaved face of the mirror **16** is faced substantially in the direction of locations "A" and "C", where B-scan images should be taken. At other locations on the radial scan pattern, a "dead space" between the individual A-scans is too large to allow for sufficient sampling of the tissue. Therefore, the present invention comprises a sector-scan imaging device, to scan a sector substantially in the "A" or "C" locations, with a sector angle of about 20°, within which a 2 mm by 2 mm image is obtained. In this example, with the given geometry, a larger sector angle will produce "dead spaces" which are too large to form a suitable cross-sectional image.

Figures 4b and 4c show beam focal points **36**, **37** and **38** from both a top view and an end view respectively. As shown, and corresponding to earlier figures, the individual focal points **36**, **37** and **38** are spaced apart in the radial plane perpendicular to the axis **20**. As Figure 4c shows, in an end view along the axis **26**, the focal points **36**, **37** and **38** are spaced apart in terms of depth but overlap to create a continuous scanning surface or scan area **28**.

If, the cleaved face of the mirror **16** is faced substantially in the direction of the locations indicated at "B" and "D", in Figure 4a, which is perpendicular to the scanning surface or scan area **28**, then the patterns shown in Figure 4d (a top view of the pattern) and Figure 4e (a side view of the pattern) are obtained. Here, the focal points are indicated at **40**, **41** and **42**. As shown in Figure 4d, the focal points **40**, **41** and **42** are each in an individual plane **40'**, **41'** and **42'** which are spaced apart corresponding to the spacing of the fibers in the fiber bundle tip **12**. The planes **40'**, **41'** and **42'** are perpendicular to the axis **20**. In Figures 4b to 4e, arrows **44** indicate the direction of the radial scan.

For the linearly translated system shown in Figure 1d, there are no "dead spaces" and thus linear translation can produce images suitable images approximately 2 mm by 2 mm in size.

In the exemplary design of the endomicroscopic system, the maximal speed of tissue motion, due to physiological motion, was chosen as 5 mm/s for *in vivo* imaging. A near diffraction-limited focusing lens (i.e. a lens which approximates an ideal lens by providing very small focal points) was chosen as the focusing lens **14**. The near diffraction-limited focusing lens was supplied by Melles Griot Inc. In addition, each single mode fiber, from the plurality of single mode fibers **10**, had a core diameter of 5 microns (i.e. $\varnothing_c \approx 5$ μm) and was operated at a wavelength of 0.86 μm. Furthermore, the design incorporates an approximate core index of $n_c = 1.447$ and a difference in the refractive index between the core and the cladding of $\Delta n = 0.005$. Using these values, the NA of the fiber is then given by:

$$NA \approx n_c(2\Delta n)^{1/2} = 0.145 \quad (1)$$

and the acceptance angle, θ_a, of the fiber is given by:

$$\theta_a = \sin^{-1}(NA) = 8.32° = 0.145 \text{ rad} \quad (2)$$

The design further incorporates the concept of an ideal lens which is used to focus optical radiation, from the plurality of single mode fibers **10**, at a magnification of 1 to 1 and that the far field beam divergence angle is similar to θ_{a1}. Then, for light beam radiation with a center wavelength λ_0, the beam diameter at the focal point is given by:

$$\varnothing_f = 2w_0 = 2\frac{\lambda_0}{\pi\theta_a} = 3.95\mu m \approx \varnothing_c \quad (3)$$

The spot diameter $\varnothing_f$ is approximately equal to the core diameter ($\varnothing_c$=5μm) which results in efficient optical coupling. The depth of focus is $2\frac{\pi w_0^2}{\lambda_0} = 27.2$ mm and the beam diameter at the ends of the focal zones for focal points **36**, **37** and **38** is given by:

$$\varnothing_f' = 2\sqrt{2}\, w_0 = 5.59 \text{ mm} \quad (4)$$

Since the $\varnothing_f$ and $\varnothing_f'$ parameters are defined in terms of amplitudes, within 40 μm of the focal point in the axial direction, the beam diameter based on

light intensity (i.e. the square of the light amplitude) may actually be smaller than 5 μm.

The above calculation is based on ideal optics operating on the principle optical axis. Using an off-the-shelf lens system with ∅ = 5 mm, f = 5 mm, and a working distance of 8.2 mm, it has been found that the off-axis angle required to cover a 2 by 2 mm image is about 5° using commercial ray-tracing software. At approximately an 80% fill factor of the focusing lens **14**, the ray-tracing results show the on-axis RMS focal point to be 5.3 μm in radius, and the 5° off-axis RMS focal point to be 10.3 μm in radius. A custom designed lens system should have better performance.

As illustrated in Figure 1, the working distance of the entire optical system, i.e. the distance from the focusing lens **14** to the focal point of the apparatus is determined by the focal length of the lens system, the diameter of the focusing lens **14** and the gap between the focusing lens **14** and the mirror **16**. Using the off-the-shelf lens system discussed above, the working distance is about 2.35 mm. The distance from the center of the image to the rotational axis of the mirror **16** is about 5.47 mm. To obtain a 2 mm scan in the radial direction, the sector scanning angle should be approximately ±10.4°, or about 20° in total, as determined by the geometry of the optical system.

Currently existing *in vivo* OCT systems perform radial scans at 4 to 8 revolutions per second (RPS) to yield a biologically acceptable 4 to 8 frames per second. For the design of the present embodiment, 4.4 RPS is chosen as the rotational speed. The rotational speed depends on the repetition rate of the A-scans and the number of A-scans required to obtain a 5 μm lateral resolution. Therefore, the imaging speed of the apparatus of the present invention is 4.4 frames/s while other imaging speeds may be chosen based on different end-user applications. The imaging time for each individual frame is 12.6 ms, as determined by the rotation speed and the sector scanning angle. Therefore, for a given frame, the system is acquiring signals for 12.6 ms and the time between frames is about 215 ms during which data processing is performed. These parameters are dependent on

the performance of the optical delay generator (which is described later) that is used in the system.

While the above calculations were made based on a light source operating at a light wavelength of 860 nm and custom made single mode fibers, implementation using a light source operating at other wavelengths, such as 1300 nm, and off-the-shelf fiber may also be possible. Figure 5a shows a beam spot diagram for a 5 channel fiber bundle tip operating at a wavelength of 1300 nm and using off-the-shelf fibers (Corning SMF-28). The fiber bundle tip has a fiber step size of 125 μm. The light beams from these fibers, focused by a lens having a 5 mm diameter and a 4.5 mm focal length, cover a focal zone of approximately 0.65 mm. The resulting lateral imaging resolution is approximately 10 μm. Figure 5b shows a beam spot diagram for a 15 channel fiber bundle tip operating at a wavelength of 890 nm and using custom designed fibers having a core diameter of 5 μm and a cladding diameter of 40 μm. This fiber bundle tip has a fiber step size of 40 μm. The beams spots of only the central 5 channels are shown. The resulting lateral imaging resolution is approximately 5 μm over a focal zone of approximately 0.65 mm.

Figure 5c shows beam spot diameter versus distance along the focal zone for the 5 channel fiber bundle tip of Figure 5a. Figure 5c shows that the beam spot diameter is consistently less than 15 μm over the entire 0.65 mm focal zone. Figure 5d shows beam spot diameter versus distance along the focal zone for the 15 channel fiber bundle tip of Figure 5b. Figure 5d shows that the beam spot diameter is approximately 5 μm over the entire 0.65 mm focal zone.

Referring now to Figure 6, the overall general layout of the basic optical elements of the apparatus of the present invention comprises a plurality of optical sources **50**, a plurality of tree couplers **52**, a plurality of 3 dB couplers **54**, a fiber bundle tip **56**, a plurality of detectors **58**, a plurality of demodulators **60** and an optical delay generator **64**. The plurality of optical sources **50**, which may be lasers, are connected to the plurality of tree couplers **52**. More than one laser may be needed to ensure that

adequate optical radiation is provided to each of the fibers (i.e. channels) in the tip **56**. Each tree coupler **52** couples a respective optical source **50** to a subset of the plurality of 3 dB couplers **54**. The plurality of 3 dB couplers **54** are connected to the fiber bundle tip **56** for onward transmission of approximately half of the light radiation from the plurality of optical sources **50**. The fiber bundle tip **56** includes fiber bundle tip **12** and the other optical elements of Figure 1 (i.e. the focusing lens **14** and the mirror **16**). The other half of the radiation from the plurality of optical sources **50** is reflected back to detectors **58** which in turn are connected through the demodulators **60** to a computer **62** which functions to process the sampled data to generate the B-scan image **30**. The optical delay generator **64** is used by the 3 dB couplers **54** to provide a delayed reflected signal to the detectors **58**. The sample being investigated by the tip **56** is indicated at **65**.

In the layout shown in Figure 6, 1 dB or 10 dB optical couplers and the like may be used in place of the 3 dB couplers **54**. Furthermore, the intensity of the optical radiation transmitted to each of the 3 dB couplers **54**, and consequently each fiber, by the tree couplers **52** need not be the same and in fact is chosen depending on whether the 3 dB coupler provides optical radiation to a fiber (*i.e.* channel) that facilitates a deep or shallow scan into the tissue. High intensity optical radiation is needed to scan deeply into the tissue. Accordingly, tree couplers **52** and 3 dB couplers **54** that feed optical radiation to fibers that scan deeply into the tissue are adapted to provide larger amounts of optical radiation.

Figures 7a and 7b show the optical delay generator **64** in greater detail. The optical delay generator **64**, similar to those in existing *in vivo* OCT systems, is used to perform the A-scans using the coherence envelope of each individual fiber. The optical delay generator **64** comprises a grating **66**, a lens **67**, a scanning mirror **68** and a mirror **70**. Rapid depth scanning can be achieved with the optical delay generator **64** by dispersing quasi-monochromatic light from the multiple single mode fibers **10** in the fiber bundle tip **12** onto the diffraction grating **66** and focusing the dispersed light onto the oscillating mirror **69**. This has the effect of applying a linear ramp in the frequency or Fourier domain as described by G. J. Tearney,

B.E. Bouma and J. G. Fujimoto ("High-speed phase and group delay scanning with a grating based phase control line" Nature Medicine **4**(7), 861-865 (1998)). With recombination of the reflected wavelengths at the diffraction grating **66**, a real space-time delay is created. The angle of the scanning mirror **68** is rapidly oscillated through several degrees of rotation creating a rapidly varying time delay in the reference arm which allows for fast, repeated depth scanning of a sample.

The optical radiation **70** from one fiber from the multiple single mode fibers **10** is shown in Figure 7a. The optical radiation **70** is dispersed into spectral components represented by spectral components **71**, **72** and **73** by the grating **66**. Spectral component **71** represents the lowest wavelength in the optical radiation **70**; spectral component **73** represents the highest wavelength in the optical radiation **70**; and spectral component **72** represents the center wavelength in the optical radiation **70**. These spectral components of the optical radiation **70** are vertically aligned in the optical delay generator **64**. In a similar fashion, optical radiation from other fibers from the multiple single mode fibers **10** are dispersed and vertically aligned, with a vertical spacing between the dispersed optical radiation from the different fibers. The offset of the center wavelength of the dispersed optical radiation from the pivot axis of the scanning mirror **68**, for a given fiber, is represented by x_d which facilitates phase modulation of the dispersed optical radiation from each of the multiple single mode fibers **10**. Alternatively, if x_d were zero then a phase modulator would be needed, for each of the single mode fibers **10**, to phase modulate the optical radiation from each of the single mode fibers **10**. This has the advantage of allowing for a reduction in size of the scanning mirror **68** which in turn allows for a higher frame rate to be used. Furthermore, the phase modulator is electrically controlled which allows for very stable signals are generated

Referring now to Figure 7b, the multiple single mode fibers **10** are aligned in the fiber bundle tip **12**, such that dispersed optical radiation from each of the multiple single mode fibers **10** is vertically aligned on the scanning mirror **68** as rows **75**, **76**, **77** and **78**. Alternatively, other ordered arrangements may also be used for the spectral components of the optical

radiation from each fiber from the multiple single mode fibers **10** such as columns.

As illustrated in Figure 6, a single optical delay generator may be used to introduce delay in multiple fibers. The limiting factor in determining the number of channels that may be coupled to a single optical delay generator is the physical size of the scanning mirror which is in turn limited by the resonance frequency of the optical delay generator. Commercially available resonance optical scanners can operate up to 16 kHz. Accordingly, a size of 4 mm by 5 mm may be used for the scanning mirror **68**. Since the fiber bundle array is about 2 mm in size, it is possible to fit the entire array onto one optical delay generator. Therefore, for the embodiment of the present invention, a single optical delay generator is used having an optical scanner operating at f_r = 16 kHz with an optical scan angle α of $\pm$ 2°. The embodiment also incorporates a grating pitch of p = 3.33 µm, a center wavelength of λ_0 = 0.86 µm and a focal length of f_l = 21 mm. Accordingly, the free space group path length difference Δl_g is given by (from Rollins et al. 1998):

$$\Delta l_g = 4\alpha(f_l \frac{\lambda_0}{p} - x_d) = 0.618 \text{ mm} \quad (5)$$

which is also 1.24 mm peak to peak. In equation 5, x_d = 1 mm is the displacement between the λ_0 spectral line and the pivoting axis on the resonance mirror. The peak A-scan speed is given by:

$$V_{Amax} = 2\pi\Delta l_g f_r = 62.1 \text{ m/s} \quad (6)$$

and the A-scan speed varies according to equation 7.

$$V_A = V_{Amax}\cos(2\pi f_r t) \quad (7)$$

Choosing a source with a coherence length l_c of 5 µm and a Gaussian emission spectrum, the equivalent emission bandwidth is given by:

$$\Delta\lambda = \beta\frac{\lambda_0^2}{l_c} = 98 \text{ nm} \quad (8)$$

where b = 0.66 for a Gaussian envelope.

The size of the resonant mirror is determined next. For an optical delay generator with a grating having a first order diffraction, the diffraction angle is given by:

$$\theta(\lambda) = \sin^{-1}(\lambda/p) \quad (9)$$

The spread of the spectrum from $(\lambda_0 - \Delta\lambda/2)$ to $(\lambda_0 + \Delta\lambda/2)$ at the Fourier plane of the lens is given by:

$$\Delta x = 2f_1\left[\theta(\lambda_0 + \Delta\lambda/2) - \theta(\lambda_0 - \Delta\lambda/2)\right] = 1.3 \text{ mm} \quad (10)$$

Since the mirror width is 4 mm, one can fit the spectrum on one side of the resonant mirror with the displacement x_d having a value of approximately 1 mm. This is illustrated in Figures 7a and 7b. The carrier frequency of an individual channel of the system is given by (Rollins et al. 1998):

$$f_c = (4x_d\alpha 2\pi f_r/\lambda_0)\cos(2\pi f_r t) \quad (11)$$

which is 16.3 MHz at the maximum.

The bandwidth of the interferogram (i.e. the interference fringe pattern) is given by:

$$\Delta f = \frac{\Delta\lambda}{\lambda_0^2} 4\pi\alpha f_r 2(f_1\lambda_0/p - x_d)\cos(2\pi f_r t) \quad (12)$$

which is 8.4 MHz at the maximum.

Since $f_c(t) > \Delta f(t)$, proper demodulation can be performed by conventional rectifying and low-pass filtering, although a sharp frequency cut-off is needed. It is preferable to set up the individual channels of the system such that D_A = 40 µm (the depth of the A-scan performed by a single channel) coincides with the maximum carrier frequency, so that the variation in carrier frequency over D_A is minimized. The carrier frequency varies sinusoidally in time given by:

$$\Delta f_c = f_c\{1 - \cos[\sin^{-1}(D_A/\Delta l_0)]\} = 34 \text{ kHz} \quad (13)$$

which is about 0.2% of f_c.

At other locations, the signal can still be properly demodulated, but the variation in carrier frequency will be larger. The demodulators **60** may incorporate an analog high-speed rectifier and a 10-pole low-pass filter to demodulate the signal. Effectively, the signal is frequency down-shifted

such that the signal is centered at DC and has a bandwidth of Δf. The demodulated envelope signal is then digitized at an appropriate sampling rate. Current existing data acquisition (DAQ) cards operate at 30 MegaSamples per second (MS/s) with an SNR of about 60 dB. Choosing a Gaussian shape for the interferogram spectrum with Δf = 8.4 MHz, the 60 dB point is at about 14.5 MHz. Accordingly, the Nyquist rate for digitizing such a signal is approximately 29 MS/s. Therefore, current existing DAQ cards will be able to digitize the envelope signal without aliasing.

Given a sampling rate of 30 MS/s for digitizing the envelope signal at the maximum carrier frequency, the spatial sampling interval in the axial direction is: $\Delta_{axial} = V_{A,max}/S$ = 2.07 μm. As shown in Figure 8, a scan path **80** is indicated showing A-scans alternately going up and down through the sample. Sampling points are indicated at **82**. The axial spacing of 2.07 μm is indicated at **84**. The spatial sampling interval in the lateral direction is determined by the lateral or B-scan velocity and the resonant frequency of the optical scanner in the optical delay generator **64**. At the center of the image, where the radial distance r is 5.47 mm from the rotational axis of the mirror, the radial sampling interval is given by:

$$\Delta_{radial} = V_{radial}/2f_r = 2\pi\Omega r/2f_r = 4.73\ \mu m \qquad (14)$$

This interval is indicated at **86** in Figure 8. For the fiber scanning the shallowest depth, the spatial lateral sampling interval is 3.86 μm and for the deepest channel it is 5.59 μm. Therefore, the pixel size at the center of the image is 2.07 by 4.73 μm in the axial and lateral direction respectively. The lateral pixel size varies across the depth of the image from 3.86 to 5.59 μm. By varying the rotational speed of the mirror **16**, the lateral sampling interval can be changed, at the expense of frame rate. If a higher resonance frequency optical scanner is used, the sampling interval may also be reduced.

For a pulsed optical source (e.g. a 15 to 20 fs pulsed laser emitting light with a wavelength of 860 nm), the coherence length will be approximately 4.5 to 6 μm. Since the spatial sampling interval in the axial

direction is about 2 μm, which is smaller than half of the coherence length, the image is reasonably sampled in the axial direction. Using a near diffraction-limited focusing lens as the focusing lens **14**, the beam spot size should be about 5 μm. Since the spatial sampling interval in the lateral direction varies from 3.86 to 5.59 μm, the image is slightly under sampled, given that the beam waist size is about 5 μm. However, the spatial sampling interval is not equivalent to the final image resolution, which is also influenced by local contrast and noise levels. Local contrast is the difference in reflectivity between two points in the sample that show up as adjacent pixels in the image. If the two points have similar reflectivity, i.e. low local contrast, it will be difficult to resolve these points.

Imaging speed should be fast enough to reduce motion blurring. Given that the target speed (i.e. tissue motion) is typically 5 mm/sec, then within a frame time (an elapsed time of 12.6 ms), the target can move up to 63 μm in a particular direction which is much larger than the designed 5 μm resolution. In the present embodiment, the A-scan is performed simultaneously in all channels such that one line of the image is formed within 0.6 μs which is the time required to scan the coherence gate through a 40 μm distance. The time between two consecutive A-scans is about 16 μs, which is determined by the rotational speed of the mirror **16** of the system and the number of A-scans per image. Thus, the resultant image should be crisp since the motion during 16 μs is 0.08 μm which is much less than the resolution. Accordingly, there should be no motion blurring in the image but a motion artifact may still exist. The resultant motion artifact may be a geometric deformation of the features being imaged that may be as large as 63 μm depending on the size of the feature and the target velocity. This motion artifact is due to the effect that the air-tissue interface has on the optical radiation from the plurality of optical sources **50**.

As illustrated in Figure 9, the focal point of an individual fiber of the apparatus, inside the tissue being imaged, can vary depending on the distance d_0 of the location of the focal point in the tissue, whether the tissue surface had a refractive index of 1, and the actual refractive index of the

tissue (which is typically approximately 1.4). Accordingly, the actual focal point is at a distance d_f below the tissue surface given by:

$$d_f = d_0 \frac{\tan\theta_1}{\tan\theta_2} = d_0 \frac{\tan\theta_a}{\tan\left[\sin^{-1}\left(\frac{n_1}{n_2}\sin\theta_a\right)\right]} \quad (15)$$

where θ_1 is assumed to be equal to θ_a, the acceptance angle of the individual fibers and θ_2 will be determined by the refractive index $n_1 = 1$ (i.e. air) outside the tissue and $n_2 = 1.4$ inside the tissue.

The coherence gate location varies according to:

$$d_o = \frac{n_1}{n_2} d_0 \quad (16)$$

Accordingly, due to the fact that optical radiation travels more slowly in a medium with a larger refractive index there is an optical path mismatch between the focal point and the coherence gate of an optical beam which is matched in a medium with $n_1 = 1$ (i.e., with no tissue present). This mismatch is:

$$\Delta d = n_2(d_f - d_o) = \frac{n_2 d_0 \tan\theta_a}{\tan\left[\sin^{-1}\left(\frac{\sin\theta_a}{n_2}\right)\right]} - d_0 \quad (17)$$

A tissue refractive index of $n_2 = 1.4$ yields $\Delta d = 0.97\, d_o$. This mismatch problem is common for all high-NA OCM systems and many existing high-NA OCM systems use some form of dynamic compensation, i.e., changing the reference path length dynamically to compensate for Δd, however, such dynamic compensation is difficult with a high imaging speed. Accordingly, one aspect of the embodiment of the present invention is to use 'flexible triggering' of the detected interferogram signal.

As shown above, the free space group path length difference is $2\Delta l_g = 1.24$ mm peak to peak, which is much larger than the useful A-scan range of only 40 µm. This leaves room for dealing with the mismatch since one then can trigger to obtain the interferogram only when the coherence gate is passing through the focal point.

As shown in Figure 9, the working distance for each fiber channel, d_w, varies with n_2, which is approximately constant Therefore, if one knows

where the tissue surface is, d_0 can be determined and in turn Δd can be determined.

Referring to Figure 10, showing a perspective view of a tissue surface and an arbitrary axial line **90**, channel 1, which is designated to scan the surface of the tissue, is the first to pass through the axial line **90**, in the scan area **28**. The focal points of channels 1 and 2 are indicated at **91** and **92** in a schematic representation **94** of the optical radiation from the multiple single mode fibers **10** (i.e. channels) passing through the axial line **90**. The focal point of the last channel, i.e. channel 50 in this example, is indicated at **95** and is designated to scan the deepest layer of the tissue in the image. The overall profile of the representation **94** defines a flexible trigger zone, within which the coherence gate and the focal length can be matched. One of the 50 channels, i.e. channel "v", will experience a large and distinctive specular reflection since the air-tissue interface approximates a mirror and reflects incident light. Underneath the tissue surface, the tissue acts as a turbid media which scatters and absorbs incident optical radiation. Thus, channel "v" will determine d_0 for this particular axial line **90** since all of the channels before channel "v" will return a signal that is at noise level. Accordingly, the "flexible triggering" method comprises comparing the detected reflected optical radiation for adjacent channels to locate the tissue surface by identifying the channel in which there is a large increase in reflectance compared to its 'neighboring' channels. This information is then passed on to each of the subsequent channels and the trigger point for each channel is set accordingly to reduce mismatch between the focal point and the coherence gate.

As an example, if channel "v" is channel 13 then the apparatus is calibrated such that channels 1 to 12 are set to scan free space above the tissue surface, channel 13 to scan the tissue surface, and subsequent channels are set to scan deeper tissue, with no mismatch between the focal point and the coherence gate of the optical beam of each channel. During imaging, a tolerance of $\Delta d_0 = \pm 0.5$ mm of the location of the tissue surface can be allowed as indicated at **96** in Figure 10. This tolerance is related to

the A-scan performance and the frequency response of the envelope detector as will now be explained.

Given Δd_o = 0.5 mm, the mismatch that needs to be compensated for is given by:

$$\Delta d' = 0.693 \times 0.5 \approx 0.347 \text{ mm} \quad (18)$$

This means that instead of triggering the interferogram signal at the maximum carrier frequency, the actual carrier frequency needs to be:

$$f_c' = f_{cmax} \cos(\sin^{-1}(\Delta d'/\Delta l_g)) = 13.5 \text{ MHz} \quad (19)$$

which is about 83% of the maximum carrier frequency with the interferogram signal bandwidth changing accordingly. Although the envelope detector's frequency response can be tuned dynamically, it is simpler and faster for the envelope detector to have a fixed response but it was designed for a 17% tolerance of the cut-off frequencies. In this way, the entire flexible triggering scheme contains only fixed components and all of the compensation is performed electronically to satisfy the high imaging speed requirement.

The optical components shown in Figure 6 can be chosen as follows. Based on Boppart, S.A., Bouma, B.E., Pitris, C., Southern, J.F., Brezinski, M.E., and Fujimoto, J.G. (*In vivo Cellular Optical Coherence Tomography Imaging*, Nature Medicine, **Vol. 4 No.7**:861-865, July 1998), an SNR of greater than 100 dB can be achieved in a non-endoscopic OCT system using 2 mW of incident power on the tissue to allow for imaging to a depth of approximately 2 to 3 mm. The optical source used was a Kerr-lens mode-locked solid-state Cr^{4+}: forsterite laser operating at a 1280 nm center wavelength with a coherence length of 5.1 µm. However, the embodiment of the present invention is not limited to this type or any other particular type of source, such as a broadband superluminescent diode. For instance, another possibility is a white-light emission Cr:LISAF optical source with a bandwidth of approximately 100 nm centered at 860 nm which will provide a coherence length of approximately 4.5 to 6 µm. This diode-pumped, solid-state, mode-locked laser should operate with a pulse-repetition rate of about 100 MHz and an average power of 30 mW when operated at 860 nm.

The pulse energy variation should be less than 1%. Several (e.g., 2 or 4) of these lasers as indicated at **50** in Figure 6 are needed to provide the total power requirement of the 50 channels. The channels scanning the deeper portion of the tissue will need about approximately 1 to 2 mW of incident power per channel and the channels scanning the shallower portion will need less. The tree couplers **52** can be configured to split the source power to match these requirements. Since the maximum carrier frequency is 16.3 MHz, each interference fringe will contain at least 6 laser pulses. Therefore the fringe pattern should be adequately sampled.

For each channel, a separate photo receiver or detector **58** may be used to detect the interference fringes. The maximum detector bandwidth is 125 MHz, although in the apparatus of the present invention, a detector bandwidth of 30.8 MHz may be sufficient, as determined by the carrier frequency and the bandwidth of the interferogram.

An alternate embodiment of the present invention involves the concept of sharing optical components to reduce device complexity and cost. Referring to Figure 11a, a typical single channel interferometer **150** with balanced detection in which the AC component of the interferogram is separated from the DC component of the interferogram and only the AC component is amplified is shown. The single channel interferometer **150** comprises an IR broadband light source **L**, a visible wavelength guide light **G**, a balanced detector **BD**, a polarization controller **PC**, a phase modulator **ϕMOD** and an optical delay generator **ODG** which are connected through a network of optical fibers and 3 dB couplers **140**, **142** and **144**. The "x" denotes a dead end in the fiber network. The visible wavelength guide light **G** may be a green laser which indicates the direction in which the single channel interferometer **150** is pointing (i.e. it indicates what will be imaged). The single channel interferometer **150** is connected to a sample **S**.

The design of Figure 11a can be extended to construct a two channel interferometer **160** as shown in Figure 11b. The subscripts denote the components that are in the two channels. A component without subscripts indicates that the component is used in both channels. The two

channel interferometer **160** comprises a laser **L'**, a visible wavelength guide laser **G'**, a 2 to 1 tree coupler **TC1**, polarization controllers PC_1, PC_2 and phase modulator **ϕMOD'**, variable delay elements VD_1 and VD_2, an optical delay generator **ODG'**, detectors BD_1 and BD_2 and 3 dB couplers **162**, **164**, **166**, **168**, **170** and **172**. The variable delay elements VD_1 and VD_2 are introduced to adjust the coherence gate positions for each channel. The two channels are coupled to samples S_1 and S_2 which may be two points at different locations in a tissue sample. The light source **L'** is shared between the two channels in this case, with the optical power in channel 1 being twice that in channel 2. Therefore, channel 1 should be used to scan a deeper region of tissue than channel 2. The 1 to 2 tree coupler **TC1** is used so that both channels can share the same reference arm (comprising the phase modulator **ϕMOD'** and the optical delay generator **ODG'**). The ability to share the same reference arm allows one phase modulator to be used to phase modulate the optical radiation from the multiple single mode fibers **10** (i.e. all the channels). Note that the two channels are combined into one fiber by the tree coupler **TC1** and then fed to the same phase modulator **ϕMOD'**. Accordingly, cost and complexity of the two channel interferometer **160** is reduced.

Based on Figure 11b, it is conceivable that a general optical network can be used to construct an N channel OCT system such as optical network **180** shown in Figure 11c. The optical network **180** comprises an optical network for an n^{th} channel **182** and a reference arm **184** that is shared by all n channels. The optical network for the n^{th} channel **182** comprises a detector BD_n, 3 dB couplers **194**, **196** and **198** and a sample arm comprising a polarization controller PC_n and a variable delay element VD_n connected to a sample S_n. The optical network for the n^{th} channel **182** receives optical source radiation **186** from the $n\text{-}1^{th}$ channel and transmits optical source radiation **188** to the $n+1^{th}$ channel via 3 dB coupler **194**. The optical network for the n^{th} channel **182** receives guide light power **190** from the $n\text{-}1^{th}$ channel and sends guide light power **192** to the $n+1^{th}$ channel via 3 dB coupler **196**. In this embodiment, a light source (not shown) may be

shared between each of the N channels with a power distribution that follows a geometric series or another suitable power partition scheme. The reference arm **184**, comprising an N to 1 tree coupler **TCn**, a phase modulator **ϕMOD"** and an optical delay generator **ODG"**, is shared between each of the N channels.

Each of the schematics shown in Figures 11a, 11b and 11c, suffer from the fact that a portion of the optical radiation of the interference pattern, from the interference between the reflected optical radiation from the sample and reference arms, which is sent from the 3 dB coupler connected to the detector is lost. In this case 50% of the optical radiation of the interference pattern is lost since a 3 dB coupler is used. For instance in Figure 11a, only 50% of the optical radiation of the interference pattern is sent from 3 dB couplers **140** and **142** to the detector **BD**. This makes if more difficult to detect the interference pattern especially for interference patterns with low intensities. To address this, a non-reciprocal optical device, such as an optical circulator may be used to send, to a detector, the portion of the optical radiation that would have been lost if only a 3 dB coupler were used.

Referring to Figures 12a, 12b and 12c, alternate embodiments of a single channel OCT device **200**, a two channel OCT device **210** and an optical network for an N channel OCT device **220** are shown comprising optical circulators. In Figures 12a, 12b and 12c, the optical circulators **C**, $\mathbf{C_1}$, $\mathbf{C_2}$ and $\mathbf{C_n}$ are used to salvage and direct the optical radiation of the interference pattern to the detectors **BD**, $\mathbf{BD_1}$, $\mathbf{BD_2}$ and $\mathbf{BD_n}$ respectively to provide a larger intensity interference signal for detection. The rest of the components in these embodiments are similar to those in the of the single channel OCT device **150**, the two channel OCT device **160** and the optical network for the N channel OCT device **180** shown in Figures 11a to 11c. The concept of using optical circulators to salvage optical radiation and provide the salvaged optical radiation to a detector may also be applied to the apparatus of Figure 6 in which optical circulators could be placed between the 3 dB couplers and the detectors.

The schematic shown in Figure 11c and 12c leads to an elegant design, however, parallel interferometers that share components (i.e. a phase modulator) may produce prohibitive amounts of channel cross talk which may consequently lead to image degradation. However, with fiber length mismatching between channels, cross talk may be effectively handled. Electronic cross-talk can be handled using standard shielding and grounding techniques. The following describes the optical cross-talk.

Referring now to Figure 13a, a two channel OCT system **230** was assembled to investigate channel cross talk. The two channel OCT system **230** comprises a laser L_E, detectors D_1 and D_2, beam splitters BS_1 and BS_2, a 1 to 2 tree coupler TC_E, a phase modulator PM_E, an optical delay generator ODG_E, beam collimators BC_1 and BC_2 and two mirrors S_{1E} and S_{2E} which simulate samples. In the two channel OCT system **230**, the desired imaging signals come from the channel 1 and channel 2 optical paths. The desired imaging signal for channel 1 occurs when light from the optical pathway:

$$L_E \rightarrow BS_1 \rightarrow S_1 \rightarrow BS_1 \rightarrow D_1 \quad (20)$$

interferes coherently with light from the optical pathway:

$$L_E \rightarrow BS_1 \rightarrow ODG_E \rightarrow BS_1 \rightarrow D_1 \quad (21)$$

and is detected by the detector D_1. The desired imaging signal for channel 2 occurs when light from the optical pathway:

$$L_E \rightarrow BS_2 \rightarrow S_2 \rightarrow BS_2 \rightarrow D_2 \quad (22)$$

interferes coherently with light from the optical pathway:

$$L_E \rightarrow BS_2 \rightarrow ODG_E \rightarrow BS_2 \rightarrow D_2 \quad (23)$$

and is detected by the detector D_2. Furthermore, OCT imaging in the two channels occurs only when the optical distance $BS_1 \rightarrow S_1$ is equal to the optical distance $BS_1 \rightarrow ODG_E$ and when the optical distance $BS_2 \rightarrow S_2$ is equal to the optical distance $BS_2 \rightarrow ODG_E$. Otherwise, image degradation could occur from constructive interference of light reflected from two (or more) different paths that are not the desired imaging paths stated above.

Based on the optical network shown in Figure 13a, there may be two major classes of potential cross talk. The primary source of cross talk may be coherent light that is reflected (from a mirror or the sample) from

one channel's beam splitter into the other channel's beam splitter and detector. Such cross talk would have intensities equal to the imaging signal intensities and could potentially cause significant image degradation. Reflection from one channel to the other could occur at the optical delay generator ODG_E or at the samples S_1 or S_2. Therefore, light from the optical pathway:

$$L_E \rightarrow BS_1 \rightarrow S_1 \rightarrow BS_1 \rightarrow D_1 \quad (20)$$

may interfere with light from the optical pathway:

$$L_E \rightarrow BS_2 \rightarrow ODG_E \rightarrow BS_1 \rightarrow D_1 \quad (24)$$

Alternatively, light from the optical pathway:

$$L_E \rightarrow BS_2 \rightarrow S_2 \rightarrow BS_2 \rightarrow D_2 \quad (22)$$

may interfere with light from the optical pathway:

$$L_E \rightarrow BS_1 \rightarrow ODG_E \rightarrow BS_2 \rightarrow D_2 \quad (25)$$

Sample arms 1 and 2 would not normally be separated as they are in Figure 13a because the sample arms would be aimed at different points (i.e. different depths) on a tissue sample. When the samples are not separate, reflection could occur from channel 1 into channel 2 and vice-versa. In such a case, light from the optical pathway:

$$L_E \rightarrow BS_2 \rightarrow S_2 \rightarrow BS_1 \rightarrow D_1 \quad (26)$$

may interfere with light from the optical pathway:

$$L_E \rightarrow BS_1 \rightarrow ODG_E \rightarrow BS_1 \rightarrow D_1 \quad (21)$$

Alternatively, light from the optical pathway:

$$L_E \rightarrow BS_1 \rightarrow S_1 \rightarrow BS_2 \rightarrow D_2 \quad (27)$$

may interfere with light from the optical pathway:

$$L_E \rightarrow BS_2 \rightarrow ODG_E \rightarrow BS_2 \rightarrow D_2 \quad (23)$$

It should be recalled that reflection may also occur at undesirable locations such as beam splitters and connector insertion points. Conceivably, such reflections may contribute to image noise if the light from these pathways produced interference fringes having a significant intensity. However, this kind of noise may be secondary to the channel cross talk previously described because of its lower intensity.

Analysis of the system revealed that the worst-case scenario for interference of such back-reflections involves one reflection from a connector. For example, light from the following optical path:

$$L_E \rightarrow BS_1 \rightarrow S_1 \rightarrow BS_1 \rightarrow D_1 \quad (20)$$

may interfere with light from the optical pathway:

$$L_E \rightarrow BS_2 \rightarrow ODG_E \rightarrow PM_E \rightarrow ODG_E \rightarrow BS_1 \rightarrow D_1 \quad (28)$$

There are four possible outcomes for the interference of light from any two pathways and the outcome depends on path length difference. Firstly, if the path lengths are identical, then the intensity of the interference fringes at the detector will be greater than the true signal intensity based solely on the sample reflectivity. This sort of image noise would not be detectable as noise and would alter the measured sample intensity throughout the image. Fortunately, the probability of the path lengths matching exactly is remote. A second possibility is that the path lengths could match to within the coherence length of the light source. This situation would result in an increase in the width of the interference fringe envelope and consequently degradation in axial resolution. This situation is unlikely, but it may be detected by measuring the full-width-half-maximum of the mirror surface depth profile. A third possibility involves the path lengths differing by a distance greater than the coherence length of the source L_E and less than the scanning depth of the optical delay generator ODG_E. This situation may manifest as two separate coherence envelopes within one depth sweep by the optical delay generator ODG_E. The final and most likely possibility is that the path lengths differ by more than the scanning depth of the optical delay generator ODG_E and no noise or extraneous interference fringes will be detected by the system.

The primary type of channel cross talk should be unlikely because of fiber optic manufacturing. Optical path lengths $BS_1 \rightarrow ODG_E$ and $BS_2 \rightarrow ODG_E$ are essentially predetermined by the lengths of the fiber pigtails coming from beam splitters BS_1 and BS_2. Optical path lengths $BS_1 \rightarrow S_1$ and $BS_2 \rightarrow S_2$ are deliberately matched to the predetermined corresponding reference arm lengths. Typically manufactured fiber lengths differed by several tens of millimeters which is at least one order of magnitude greater

than the scanning depth of the optical delay generator ODG_E. Therefore, this type of cross talk should not be a problem in a dual channel system.

In the case of insertion point reflections, if the optical distance $PM_E \rightarrow ODG_E$ matched the path length difference between optical paths $BS_1 \rightarrow S_1$ and $BS_2 \rightarrow ODG_E$, then interference fringes and image degradation may occur. Again, this sort of secondary noise should be unlikely because the fiber lengths are about 300 mm while the optical delay generator ODG_E scans through only a couple of millimeters. Furthermore, the intensity of such interference fringes would be lost in the system noise. Secondly, the equipment used has a maximum 0.6 dB insertion loss (in other words a maximum of reflection of 0.6 dB) and therefore such a signal is below the detection limits used in the setup of Figure 13a.

To demonstrate that two channels can use the same fiber and optical components, the OCT system **230** was evaluated. The sample arm mirrors S_1 and S_2 were placed such that the sample arm optical path length and the optical delay generator ODG_E reference arm optical path length matched for each channel and a set of interference fringes were seen at each of the detectors D_1 and D_2. The sample arms for samples S_1 and S_2 were kept separate for alignment purposes and to eliminate the possibility of light from channel 1 reflecting into the fiber containing channel 2 and vice-versa. Although an optical delay generator could be used to produce both phase modulation and group delay (Tearney et al. 1997), with the setup shown in Figure 13a, the optical delay generator ODG_E was used for group delay (i.e. depth scanning) while the phase modulator PM_E in the reference arm was used to produce phase delay.

In the experimental setup of Figure 12a, the light source L_E comprised a 1310 nm, 9 mW light source (model BBS1310) made by AFC Technologies Inc. The central wavelength of the light source L_E was 1310 nm with a measured spectral spread of ± 40 nm. The measured coherence length of the light source L_E was 10 µm. The detectors D_1 and D_2 were 155 Mbps Perkin Elmer InGaAs photodiode receivers with a detection band centered at 1310 nm having a bandwidth greater than or equal to 100 nm.

The phase modulator PM_E was a JDS Uniphase 43 MHz phase modulator. The beam splitters BS_1 and BS_2 were made by MetroTek. OZ Optics manufactured the beam collimators BC_1 and BC_2. Alternate suitable components may be used from these or other suppliers.

The optical delay generator ODG_E dispersed the collimated light using a 150 line/mm diffraction grating blazed for 1310 nm which was made by CVI Spectral Products. A Melles Griot glass doublet lens with a 30 mm diameter and 100 mm focal length was used to focus light onto the oscillating mirror. EOPC (Electro-Optical Products Corporation) manufactured the resonant scanner that operated at 8 kHz and scanned through a ± 1° mechanical or a ± 2° optical angle. This angular setting corresponded to a depth scan of about 1 mm in the sample arms for the samples S_1 and S_2. Scanning depth is an important consideration in terms of mismatching the optical lengths of the two channels. For instance, if the optical path lengths differ by more than 1 mm then cross talk between the two channels should be minimal and proper shielding and grounding techniques should address electronic cross-talk as well.

Figures 13b and 13c show results from experiments conducted on the setup shown in Figure 13a. Figure 13b shows the oscilloscope trace from the detectors D_1 and D_2 in channel 1 and channel 2. Figure 13b shows that the interference fringes occur at different points in the cycle of the optical delay generator ODG_E which reflects the slightly different positioning of the two channels within the cycle of the optical delay generator ODG_E, i.e. the sample arm mirrors S_1 and S_2 were deliberately offset by a small amount to simulate imaging at different depths. Figure 13b shows that there is a strong imaging signal in each of the channels and no evidence of any cross talk. The arrows **232** and **234** indicate reflection from two different sample points which could correspond to two different points in a tissue sample. Furthermore, the full-width-half-maximum of the envelope of each detected pulse corresponded to the coherence length of the light source L_E which indicates that the light signal in each channel originated from the light source L_E. Figure 13b shows the experimental results when one of the

sample points was moved relative to the other sample point. In this case, cross-talk was also not observed.

In another embodiment of the invention, the fiber optic network, previously disclosed herein, is incorporated into an endoscope so that the multi-channel OCT methodology may be used clinically. Due to the size of the fiber bundle tip **12** of the apparatus, the fiber bundle tip **12** will not fit into the working channel of a conventional diagnostic endoscope (although it may be incorporated into the larger-diameter therapeutic endoscopes). Therefore, an alternate design approach was taken. Instead of designing the fiber bundle tip **12** to accommodate the working channel of a conventional diagnostic endoscope, all of the functionality of a conventional diagnostic endoscope was designed around the fiber bundle tip **12**. As shown in Figure 14, one embodiment of a GI endoscope **300** (corresponding to the tip **56** of Figure 6) incorporating the endomicroscope of the present invention is approximately 11 mm in diameter. This is slightly larger than the conventional diagnostic endoscope which is 8 - 9 mm in diameter. The GI endoscope **300** has the endomicroscopy capability disclosed above in addition to conventional forward-viewing white light imaging. Therefore, a user of the GI endoscope **300** should be able to obtain a 2 by 2 mm cross-sectional image as illustrated in Figure 16.

The GI endoscope **300** includes a 2.7 mm diameter suction/biopsy channel **302**. The end of the suction/biopsy channel **302** is bent so as to present an opening **304** directed towards the tissue area of interest **306**. The axis of the suction/biopsy channel **302** may be on the order of 6.7 mm from the center of the tissue area of interest **306**. Two channels **308** and **310** are provided for white light illumination and a channel **312** is provided for white light endoscope forward viewing. Each of the channels **308**, **310** and **312** may have a diameter of 2.7 mm. A small channel **314** is also provided for an air or water nozzle.

In accordance with the present invention, a side-viewing Endoscopic Coherent Optical Microscope (ECOM) **316** is provided in the GI endoscope **300**. The side-viewing ECOM **316** includes a drive mechanism **318** for rotating the mirror **16** (not shown in Figures 14 and 15). As

mentioned previously, radial, translational or helical scanning may be employed. Furthermore, as previously mentioned, a MEMS drive mechanism may be used instead of a mechanical drive mechanism. The side-viewing ECOM **316** is configured to scan through the tissue area of interest **306** having the depth set by the boundaries **320** and the angular extent set by the boundaries **322**. Additionally an optical window **324** may be provided for the side-viewing ECOM **316** (see Figure 14).

The forward-viewing white light channel **312** is updated at a rate of 30 frames/sec. The cross-sectional images obtained by the side-viewing ECOM **316** are updated at 4.4 frames/sec. All imaging channels are displayed simultaneously. The images that may be generated by the GI endoscope **300** are illustrated in Figures 16 and 17. Figure 16 shows a simulated image of a human colon epithelium incorporating the expected spatial resolution which may achievable with the side-viewing ECOM **316**. Figures 17a and 17b are a comparison of microscopy imaging versus *in vivo* OCT imaging. Figure 17a has two panels which each show a microscopy image of sweat ducts in the human skin. Figure 17b has three panels which each show an *in vivo* OCT image of sweat ducts in the human skin. The *in vivo* OCT images were generated with a light source operating at a wavelength of 1300 nm.

Typical maneuvers or use of the GI endoscope **300** by an endoscopist will incorporate the following steps:

a) Following the steps of a general endoscopy procedure, the GI endoscope **300** is inserted under the guidance of the conventional forward-viewing white light channel **312**. This maneuver should be no different from that of currently available GI endoscopes.

b) When the endoscopist needs to make microscopic examinations, he/she first pushes the GI endoscope **300** into contact with the wall of the lumen as shown in Figure 13. The optics are designed such that when the GI endoscope **300** is in contact with the tissue, the correct working distance of the entire optical system is obtained. Although the GI endoscope **300** is in contact with the

wall, the part of the tissue under microscopic examination is not, as illustrated in Figure 15. Therefore, the surface features of the tissue are not distorted by contact pressure. However, this does not imply that the GI endoscope **300** can only be operated in a contact mode. In fact, the GI endoscope **300** may be operated in a non-contact mode, as long as images are formed, which is dictated by whether the previously described dynamic triggering algorithm has found an air-tissue interface. If the air-tissue interface lies within the working distance of the system then the interface should be specific and easily detected since the interface produces clear peaks in the detected light pattern as previously described in the 'flexible triggering' method.

c) if the endoscopist needs to examine a region adjacent to the area imaged in step (b), then the endoscopist can torque the GI endoscope **300** and rotate the field of view to a new location.

The best techniques currently in use for visualization of the gastrointestinal (GI) tract include endoscopic ultrasonography (EUS) and magnification endoscopy (ME). The resolution of high-frequency EUS, approximately 70 to 100 mm, is insufficient for the identification of many conditions that perturb tissue microstructure, most notably subtle pathologic changes arising within the superficial layers of the GI tract (mucosa and submucosa). ME, with a magnification of up to 170X, provides excellent images of fine superficial mucosal patterns but subsurface structures and lesion staging cannot be determined. Accordingly, tissue biopsy and histology currently remain the standard of care for detecting microscopic diseases involving the GI tract.

The side-viewing ECOM **316** disclosed herein may achieve real-time, 2 mm deep cross-sectional images of the GI wall at a resolution of 5 µm in both axial and transverse (lateral) dimensions. For reference, gastrointestinal epithelial cells average 7 to 10 µm in size which increases further as dysplastic or neoplastic transformation ensues. In the GI tract, a depth of view at 2 mm is nevertheless sufficient to detect mucosally-based

diseases as well as any neoplastic invasion into the underlying submucosa, which is of important for prognostic and therapeutic purposes. The image resolution of the side-viewing ECOM **316** may correspond to observing an *unstained* histology slide under a 100X (total magnification) microscope. Accordingly, many important entities such as dysplasia (cellular neoplastic alterations) or neoplastic violation of structures such as the lamina propria or muscularis mucosae may be discernible with the side-viewing ECOM **316**.

The present invention may allow for *in-situ* diagnosis of diverse *microscopic* mucosal pathologies and lesion staging. In essence, this "optical biopsy" technique may replace, or at the very least, guide the standard biopsy and histology method. This may translate into reducing unnecessary biopsy samples and tissue processing, decreasing patient risk and increasing sampling rate and diagnostic yield thus providing immediate diagnostic feedback both to the physician and the patient and targeting biopsies (which in itself may become a therapeutic maneuver in some cases). Pre-neoplastic GI conditions such as Barrett's esophagus, chronic ulcerative colitis, early flat adenomas, or foci of aberrant colonic crypts, to name a few, may be applicable to the side-viewing ECOM **316**. Currently, detection and surveillance of neoplastic progression within these conditions are suboptimal due to their microscopic nature.

Secondly, the side-viewing ECOM **316** may serve as a functional imaging system permitting monitoring of neoplastic and non-neoplastic tissue alterations over time. For instance, the recovery of the structure of small intestinal villi and reduction in inflammatory cells may be monitored by the side-viewing ECOM **316** in diverse malabsorptive disorders of the gut such as gluten-sensitive enteropathy, tropical sprue and intestinal infestation. The natural history of many mucosal diseases at the microscopic level may also be assessed in a minimally invasive manner. The ability to monitor structural cellular changes that are occurring *in vivo* with time may provide important physiologic information on cellular function and insight into cellular pathologic transformation.

Thirdly, the side-viewing ECOM **316** may be used in the monitoring of tissue post therapy. *In vivo* microscopic evaluation of surgical resection margins or treatment margins during post-therapeutic surveillance of cancer resection or assessment of the adequacy of photodynamic therapy of mucosal preneoplastic conditions are only some examples.

Applications in other medical specialties may also be possible. It should be understood by those skilled in this art that the multichannel OCT apparatus disclosed herein may have application in a large number of medical specialties such as dermatology, hematology, oncology (medical and radiation), ophthalmology, urology, surgery, respirology and gastroenterology.

The multichannel OCT system disclosed herein may be altered to further improve system performance. For instance a modification that may be made would be to employ coded transmission for the optical radiation which is radiated from the optical sources. This technique may increase the image resolution by increasing the SNR of the optical radiation of the interference pattern obtained in channels which suffer from poor SNR.

It should be understood that various modifications can be made to the preferred embodiments described and illustrated herein, without departing from the present invention, the scope of which is defined in the appended claims. For instance, in each of the schematics, herein disclosed, other optical couplers may also be used in place of the 3 dB couplers.

CLAIMS:

1. An apparatus for optical examination of a sample, the apparatus comprising:

an optical source means for providing a plurality of separate optical radiation sources;

a first optical path extending from the source means;

a focusing means in the first optical path for focusing optical radiation from the optical radiation sources into a plurality of respective focal points located on a surface within the first optical path to provide substantially continuous coverage of a selected portion of the first optical path, whereby, in use, a sample can be located at least partially within said selected portion, thereby permitting simultaneous scanning of a plurality of points within the sample.

2. An apparatus as claimed in claim 1, wherein the optical source means comprises a primary optical source and optical coupling means connecting the primary optical source to the optical radiation sources and comprising a plurality of optical fibers.

3. An apparatus as claimed in claim 2, wherein the plurality of optical fibers terminate in a fiber bundle tip, wherein ends of the optical fibers in the fiber bundle tip are stepped relative to one another along the first optical path and wherein optical radiation from each optical fiber is focused to a different focal point.

4. An apparatus as claimed in claim 1, 2 or 3, which includes a rotatable mirror in the first optical path, for deflecting radiation from the optical radiation sources to permit rotational movement of the surface.

5. An apparatus as claimed in claim 1, 2 or 3, which includes a mirror in the first optical path and wherein the optical source means, the

focusing means and the mirror, in combination, may be linearly translated to permit linear movement of the surface.

6. An apparatus as claimed in claim 1, 2 or 3, which includes a rotatable mirror in the first optical path and wherein the optical source means, the focusing means and the rotatable mirror, in combination, may be linearly translated to permit helical movement of the surface.

7. An apparatus as claimed in claim 4, 5 or 6, wherein the surface is a complex surface.

8. An apparatus as claimed in claims 4, 5 or 6, wherein the mirror is a surface of a prism.

9. An apparatus as claimed in claims 4 or 6, including a micromachined electro-mechanical system coupled to the mirror for rotating the mirror.

10. An apparatus as claimed in claim 5 or 6, including a micromachined electro-mechanical system for linearly translating the optical source means, the focusing means and the mirror.

11. An apparatus as claimed in claim 2, 3 or 4, which further includes a plurality of optical couplers between the primary optical source and the optical fibers, an optical delay generator coupled to the optical couplers and detector means coupled to the optical couplers, wherein the optical couplers transmit a portion of the radiation from the primary optical source along the first optical path and a portion of the radiation from the primary optical source to the optical delay generator, the optical delay generator providing a second optical path, wherein an interference effect occurs between radiation returned along the first and second optical paths to the optical couplers and the optical couplers transmit the radiation returned along the first and second optical paths to the detector means.

12. An apparatus as claimed in claim 11, which includes a plurality of primary optical sources and a plurality of tree couplers, each tree coupler being associated with one primary optical source and coupling said one primary optical source to at least one of the optical couplers.

13. An apparatus as claimed in claim 12, which includes a plurality of optical circulators, placed between the optical couplers and the detectors for providing salvaged optical radiation to the detectors.

14. An apparatus as claimed in claim 11, wherein a plurality of optical fibers couple the optical couplers to the optical delay generator, the optical delay generator having a grating and a scanning mirror, the scanning mirror having an axis, wherein the grating separates optical radiation from each optical fiber into spectral components linearly oriented on the scanning mirror, wherein the midpoint of said spectral components is offset from the axis of the scanning mirror by a distance x_d to phase modulate said spectral components.

15. An apparatus as claimed in claim 11, which includes a first plurality of optical fibers for coupling each optical coupler to a phase modulator and a second plurality of optical fibers for coupling each phase modulator to the optical delay generator, the optical delay generator having a grating and a scanning mirror, the scanning mirror having an axis, wherein for each optical fiber, the phase modulator phase modulates the optical radiation and said grating separates said phase modulated optical radiation into spectral components which are linearly oriented on said scanning mirror, the midpoint of said spectral components being centered on the axis of said scanning mirror and wherein the spectral components from each optical fiber is spaced apart from the spectral components of the optical radiation from the other optical fibers.

16. An apparatus as claimed in claim 11, which includes a plurality of optical fibers coupling each optical coupler to a tree coupler for combining optical radiation from each of the optical fibers into a first optical fiber, said first optical fiber connected to a phase modulator for phase modulating said combined optical radiation and including a second optical fiber for coupling said phase modulator and said optical delay generator.

17. An apparatus as claimed in claims 4, 5 or 6, wherein the apparatus is configured as an endoscope for internal examination of a body, wherein the first optical path, the focusing means and the mirror are provided in the endoscope, and wherein the endoscope includes at least one of: at least one channel for white light illumination; a channel for white light endoscope forward viewing; a channel for one of an air nozzle and a water nozzle; and a suction/biopsy channel.

18. An apparatus as claimed in claim 17, wherein the endoscope is adapted to perform radial, translational or helical scanning.

19. An apparatus as claimed in claim 18, wherein the endoscope further includes a micromachined electro-mechanical system as a drive mechanism.

20. An N channel apparatus for optical examination of a sample, wherein the N channel apparatus comprises a plurality of optical networks and a reference arm, each optical network providing one channel for the N channel apparatus and sharing the reference arm.

21. An N channel apparatus as claimed in claim 20, wherein the optical network comprises a detector, an optical coupling means and a sample arm, wherein the optical coupling means is configured to receive optical radiation from a previous optical network and to transmit optical radiation to a next optical network.

22. An N channel apparatus as claimed in claim 21, wherein the sample arm comprises a polarization control means, a variable delay element and a sample.

23. An N channel apparatus as claimed in claim 20, wherein the reference arm comprises a tree coupling means, a phase modulating means and an optical delay means.

24. A two channel apparatus, for optical examination of a sample, said two channel apparatus comprising two optical networks as claimed in claim 20, 21, 22, 23, an optical source and a visible light source for guiding the orientation of the two channel apparatus.

25. A method for optical examination of a sample, the method comprising:

(a) providing radiation from a plurality of separate optical radiation sources, along a first optical path;

(b) providing focusing means in the first optical path;

(c) focusing the optical radiation from the optical sources into a plurality of respective focal points along a surface within the first optical path to provide substantially continuous coverage of a selected portion of the first optical path; and

(d) providing a sample located at least partially within the first optical path; and,

(e) simultaneously scanning a plurality of points within the sample.

26. A method as claimed in claim 25, which includes providing radiation from a primary optical source and transmitting the radiation along a plurality of optical fibers to a plurality of separate optical radiation sources.

27. A method as claimed in claim 26, which includes terminating the plurality of optical fibers in a fiber bundle tip, providing the ends of the

optical fibers in the fiber bundle tip in a common plane and stepping the ends of the optical fibers relative to one another, along the first optical path, and focusing radiation from the optical fibers through a common lens.

28. A method as claimed in claim 27, which includes:
(a) providing a rotatable mirror in the first optical path;
(b) deflecting the first optical path;
(c) causing the plurality of focal points to be located on a surface;
(d) performing an axial scan;
(e) rotating the mirror to move the surface; and,
(f) repeating step (d) at least two times and performing step (e) between each repetition.

29. A method as claimed in claim 27, which includes:
(a) providing a mirror in the first optical path;
(b) deflecting the first optical path;
(c) causing the plurality of focal points to be located on a surface;
(d) performing an axial scan;
(e) linearly translating, in combination, the focusing means, the plurality of optical radiation sources and the mirror to move the surface; and,
(f) repeating step (d) at least two times and performing step (e) between each repetition.

30. A method as claimed in claim 27, which includes:
(a) providing a mirror in the first optical path;
(b) deflecting the first optical path;
(c) causing the plurality of focal points to be located on a surface;
(d) performing an axial scan;
(e) simultaneously rotating the mirror and linearly translating, in combination, the focusing means, the plurality of optical radiation sources and the mirror to move the surface; and,
(f) repeating step (d) at least two times and performing step (e) between each repetition.

31. A method as claimed in claims 28, 29 or 30, which includes providing a surface of a prism as the mirror.

32. A method as claimed in claims 28, 29 or 30, which includes supplying radiation from the primary optical source through a plurality of couplers to the optical fibers, providing an optical delay generator connected to the optical couplers and providing a second optical path, permitting radiation to be transmitted back along the first and second optical paths to the couplers, for forming interference, and transmitting radiation received from the first and second optical paths at the optical couplers to detection means for detection of the interference pattern.

33. A method as claimed in claim 32, which includes providing a plurality of primary optical sources and, for each primary optical source, a respective tree coupler, and coupling each primary optical source through said respective tree coupler to each of the optical couplers.

34. A method as claimed in claim 32, which includes providing optical circulator means between the optical couplers and the detection means for providing salvaged optical radiation to the detection means.

35. A method as claimed in claim 33, which includes providing the apparatus as an endoscope adapted for examining an internal cavity of the body, including at least one of: at least one channel for white light illumination, a white light endoscope forward viewing channel, a suction/biopsy channel and a channel for one of an air nozzle and a water nozzle.

36. A method as claimed in claims 30, 31 or 32, wherein there is a change in refractive index between a medium containing the optical radiation sources and the sample and for each focal point, a distance mismatch due to the change in refractive index between the coherence gate

of each optical radiation source and the focal point in the sample due is obtained according to the steps of:

(a) scanning optical radiation from the plurality of optical radiation sources in said first optical path such that the focal points of the optical radiation sources are aligned along a path extending from the medium containing the optical radiation sources into the sample;

(b) detecting the reflected optical radiation for each focal point; and,

(c) locating the focal point for which there is a large change in reflected optical radiation compared to neighboring focal points,

whereby, the focal point located in step (c) indicates the location of the interface between the sample and the medium containing the optical radiation sources.

37. A method as claimed in claim 36, wherein the method further comprises repeating steps (a) to (c) for each axial scan to obtain proper spatial resolution for the selected scan zone.

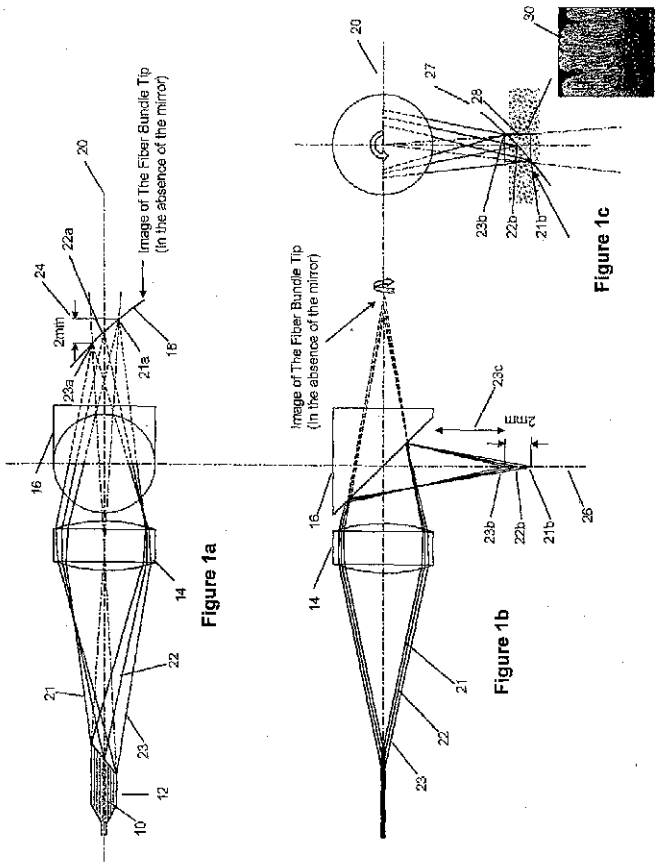
Image of The Fiber Bundle Tip
(In the absence of the mirror)
20
22a
24
2min
18'
21a
22a
16
14
22
21
23
12
10
Figure 1a
Image of The Fiber Bundle Tip
(In the absence of the mirror)
20
16
14
23c
2mm
23b
22b
21b
25
21
22
23
Figure 1b
30
27
28
23b
22b
21b
Figure 1c

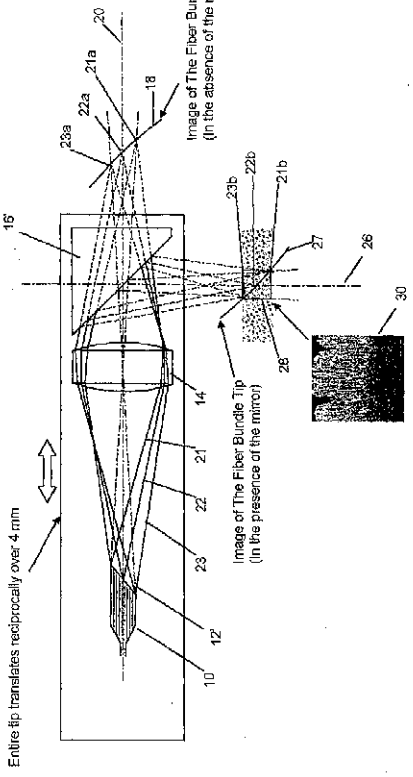
Image of The Fiber Bundle Tip
(In the absence of the mirror)
20
21a
18
22a
23a
16'
23b
22b
21b
27
26
30
28
14'
21'
22'
23'
12'
10'
Image of The Fiber Bundle Tip
(In the presence of the mirror)
Entire tip translates reciprocally over 4 mm

Figure 1d

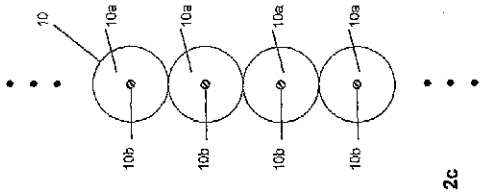

Figure 2c

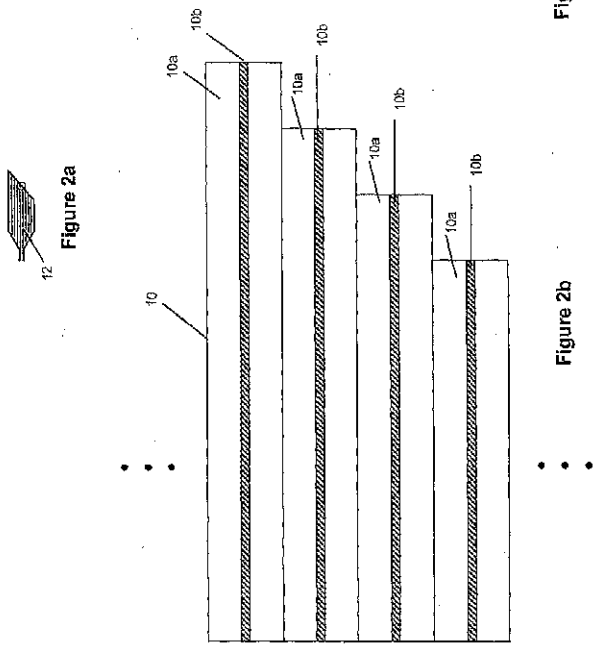

Figure 2a

Figure 2b

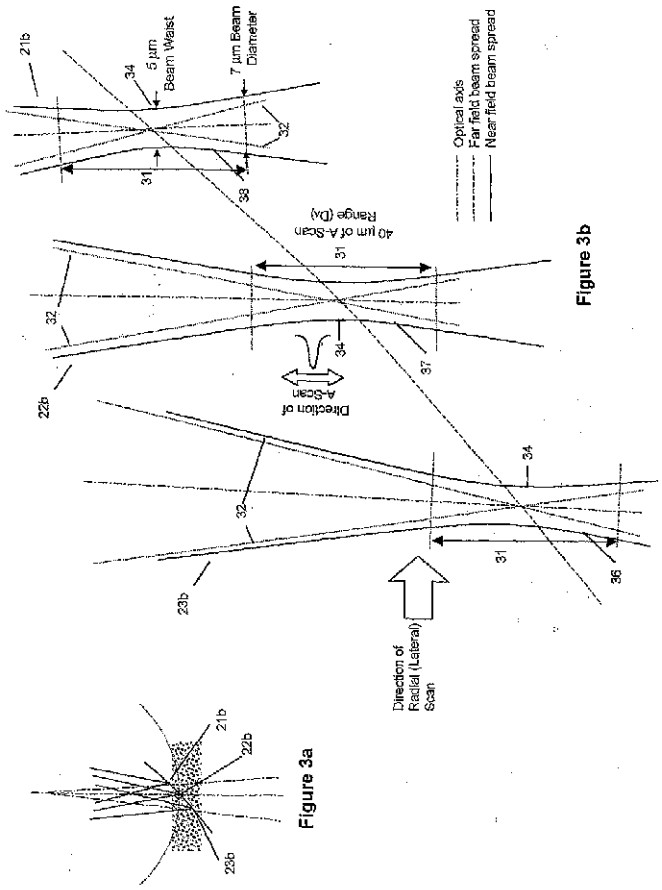

Figure 3b

Figure 3a

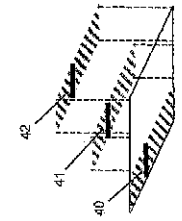

Figure 4f

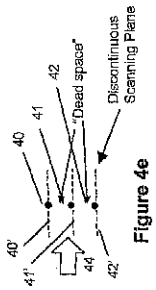

Figure 4e

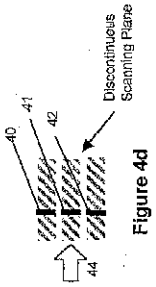

Figure 4d

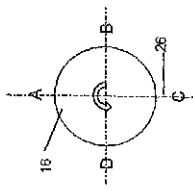

Figure 4a

Figure 4b

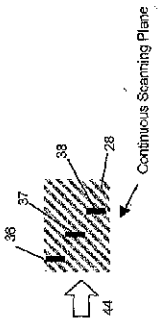

Figure 4c

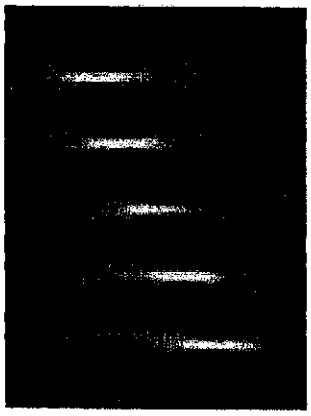

Figure 5b

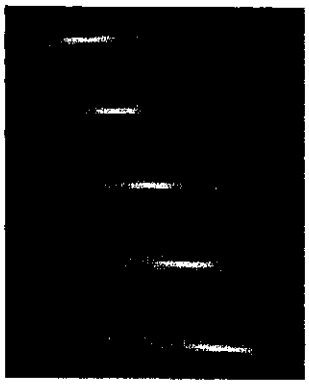

Figure 5a

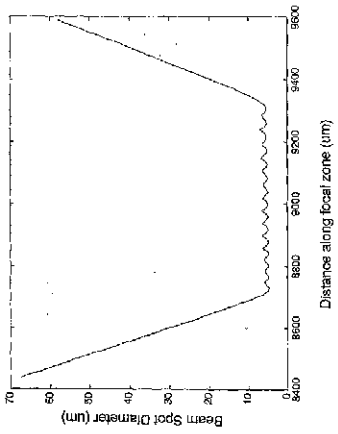

Figure 5d

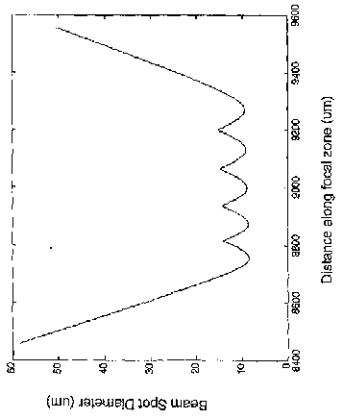

Figure 5c

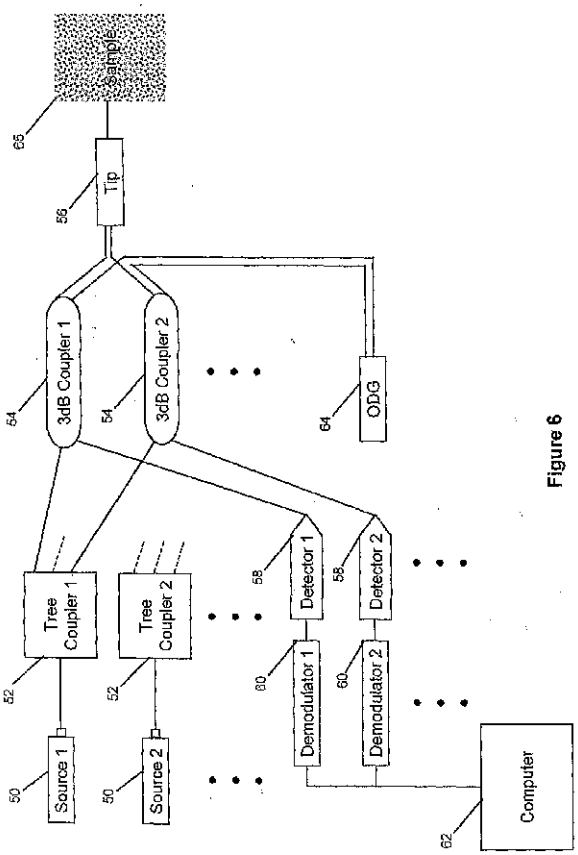
Sample
65
Tip
66
3dB Coupler 1
54
3dB Coupler 2
54
ODG
64
Tree Coupler 1
52
Tree Coupler 2
52
Detector 1
58
Detector 2
58
Demodulator 1
60
Demodulator 2
60
Source 1
50
Source 2
50
Computer
62

Figure 6

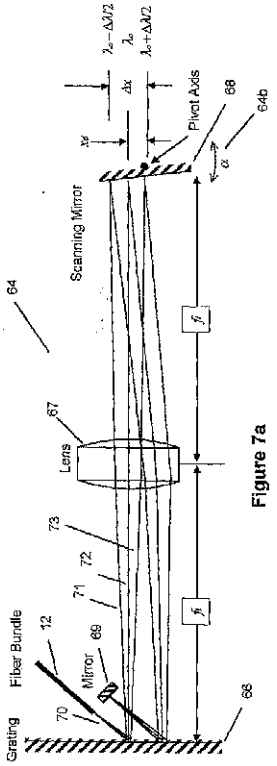

Figure 7a

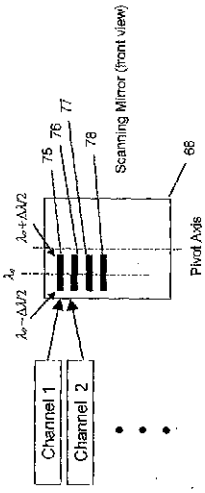

Figure 7b

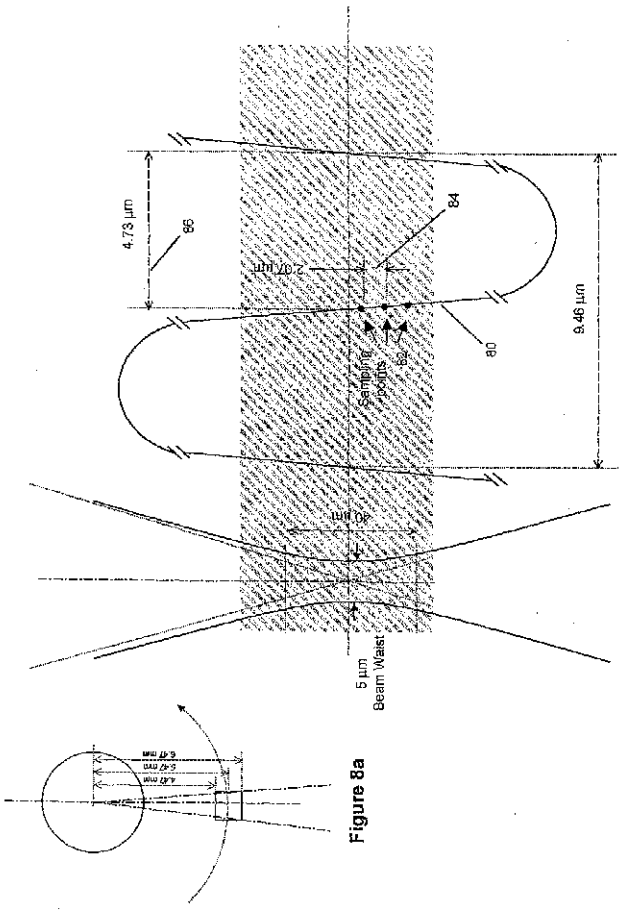

Figure 8b

Figure 8a

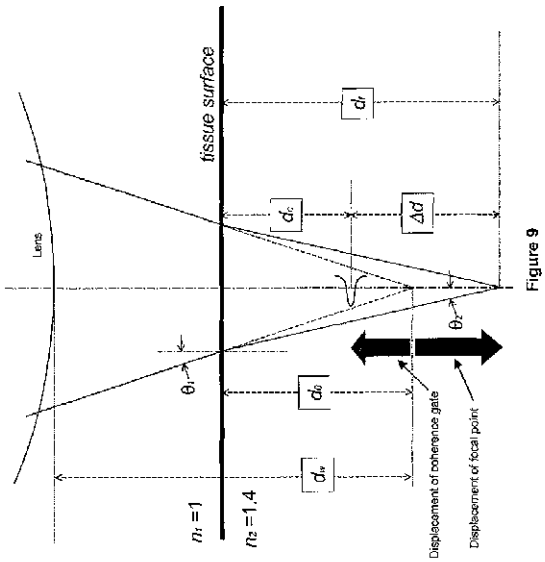
tissue surface
Lens
d_f
d_c
Δd
θ_1
θ_2
d_o
d_w
$n_1 = 1$
$n_2 = 1.4$
Displacement of coherence gate
Displacement of focal point

Figure 9

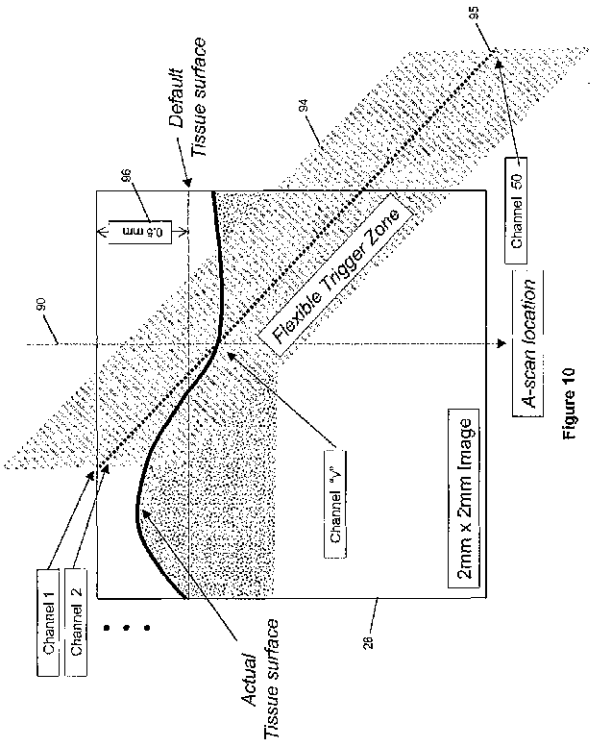
Default Tissue surface
95
94
96
0.8 mm
Channel 50
Flexible Trigger Zone
90
A-scan location
Channel "y"
2mm x 2mm Image
Channel 1
Channel 2
26
Actual Tissue surface

Figure 10

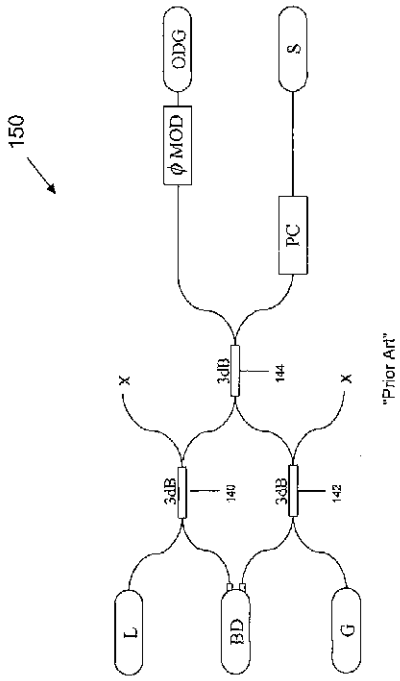

"Prior Art"

Figure 11a

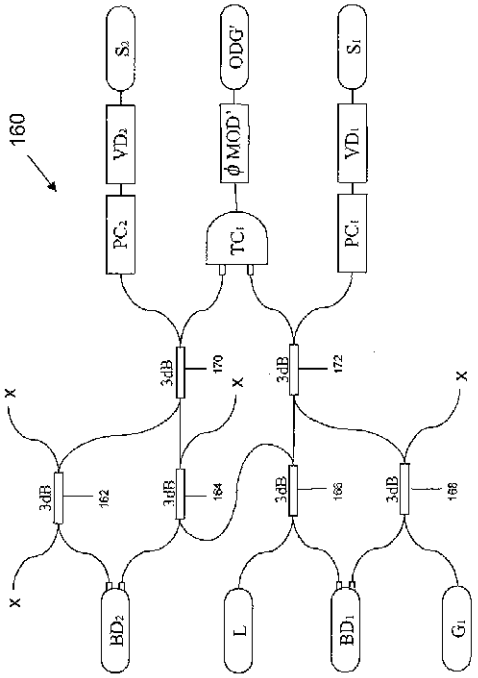
160
S0
VD2
PC2
ODG'
ϕ MOD'
TC1
S1
VD1
PC1
3dB
170
3dB
172
3dB
162
3dB
164
3dB
166
3dB
168
X
BD2
L
BD1
G1

Figure 11b

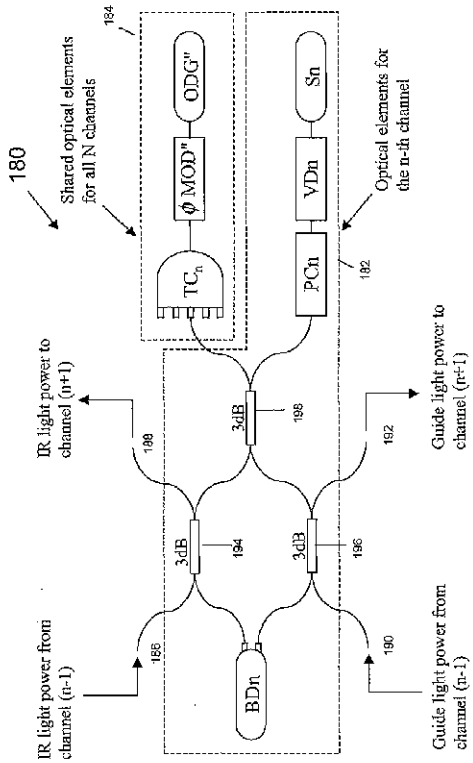
180
Shared optical elements for all N channels
184
ODG"
ϕ MOD"
TCn
Sn
VDn
PCn
Optical elements for the n-th channel
182
IR light power to channel (n+1)
188
3dB
198
192
Guide light power to channel (n+1)
3dB
194
3dB
196
IR light power from channel (n-1)
186
BDn
190
Guide light power from channel (n-1)

Figure 11c

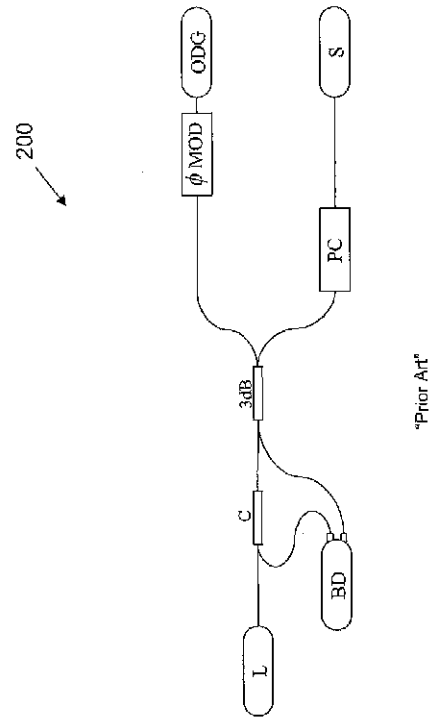

"Prior Art"

Figure 12a

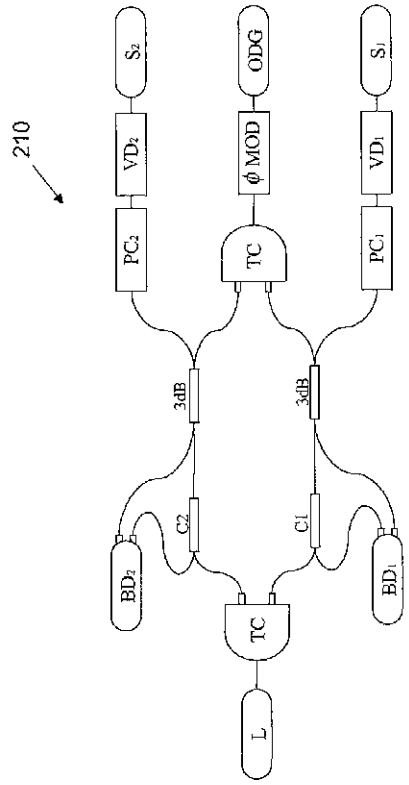

Figure 12b

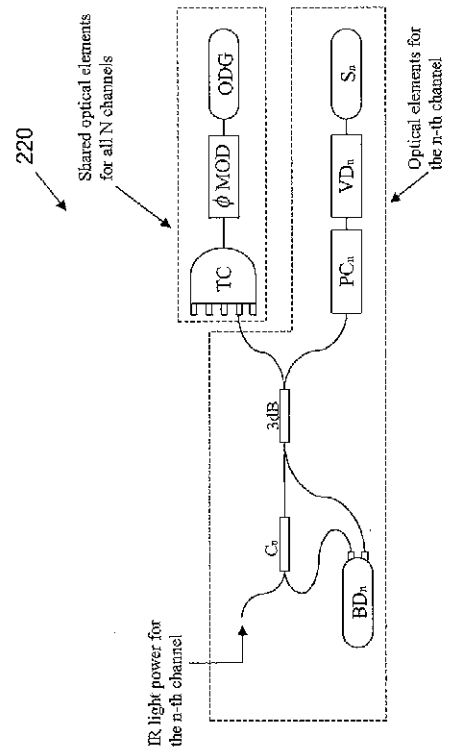
220
Shared optical elements for all N channels
Optical elements for the n-th channel
ODG
ϕ MOD
TC
S_n
VD_n
PC_n
3dB
C_n
BD_n
IR light power for the n-th channel

Figure 12c

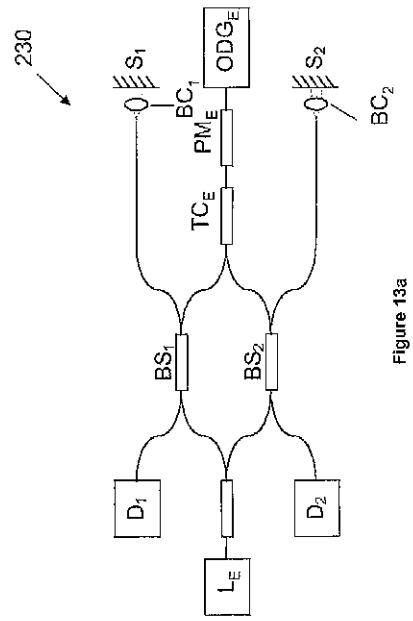

Figure 13a

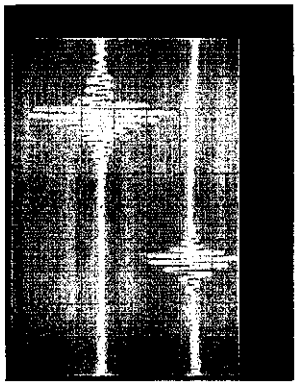

Figure 13c

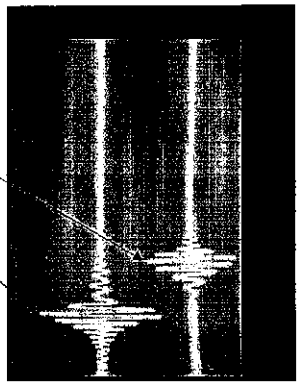

Figure 13b

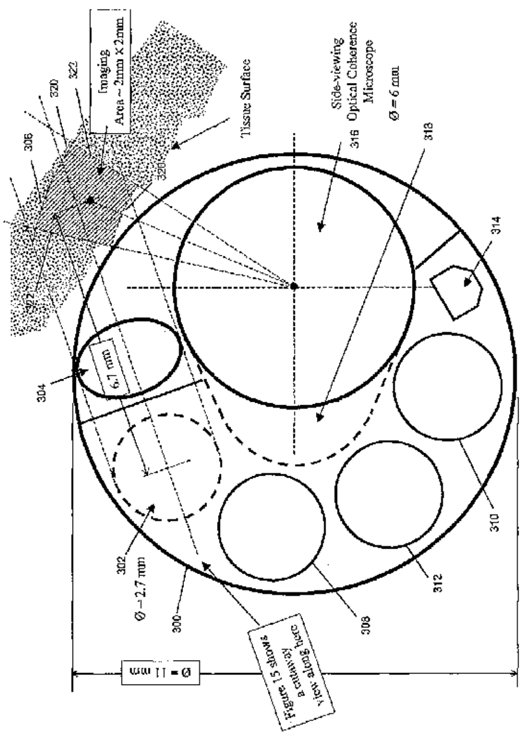
Imaging
Area ~ 2mm x 2mm
Tissue Surface
Side-viewing
Optical Coherence
Microscope
Ø = 6 mm
306
320
322
326
316
318
314
304
6.7 mm
302
Ø ~2.7 mm
300
308
312
310
Figure 15 shows
a cutaway
view along here
Ø = 11 mm

Figure 14

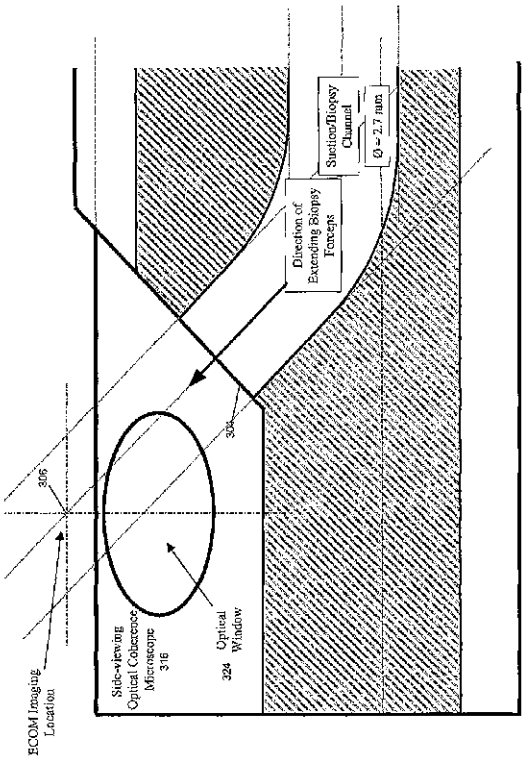
Suction/Biopsy Channel
Ø ~ 2.7 mm
Direction of Extending Biopsy Forceps
306
304
306
Side-viewing Optical Coherence Microscope 316
Optical Window 224
ECOM Imaging Location

Figure 15

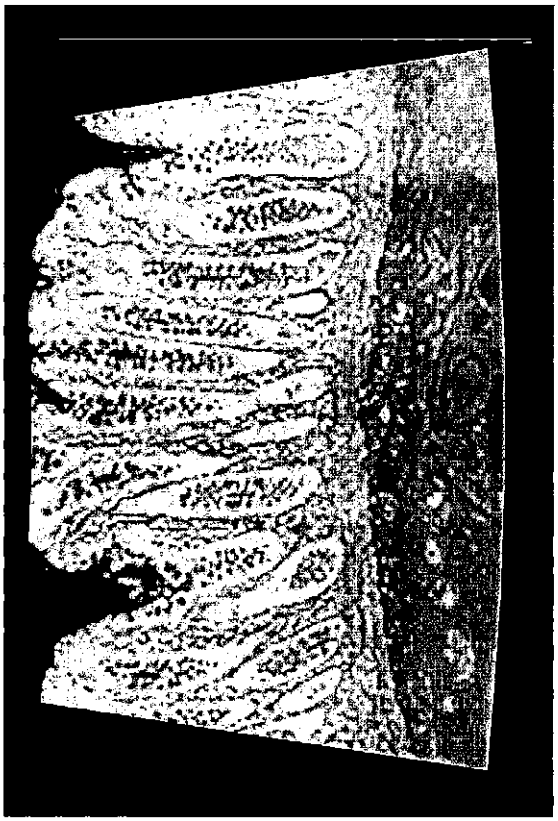

Figure 16

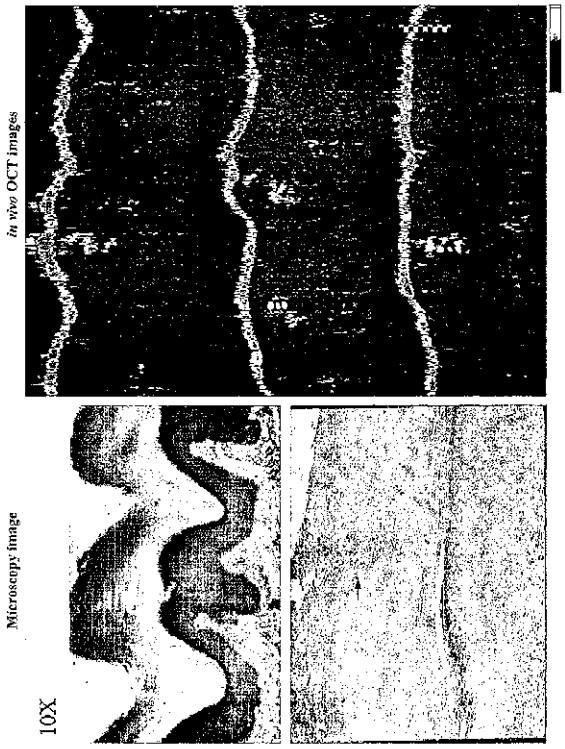

Figure 17b

Figure 17a

【国際公開パンフレット（コレクトバージョン）】

(12) INTERNATIONAL APPLICATION PUBLISHED UNDER THE PATENT COOPERATION TREATY (PCT)

(19) World Intellectual Property Organization
International Bureau

(43) International Publication Date
17 January 2002 (17.01.2002)

PCT

(10) International Publication Number
WO 02/004929 A3

(51) International Patent Classification⁷: G01N 21/47

(21) International Application Number: PCT/CA01/00992

(22) International Filing Date: 10 July 2001 (10.07.2001)

(25) Filing Language: English

(26) Publication Language: English

(30) Priority Data:
60/217,090 10 July 2000 (10.07.2000) US

(71) Applicant (*for all designated States except US*): UNIVERSITY HEALTH NETWORK [CA/CA]; Room 7-504, 610 University Avenue, Toronto, Ontario M2G 2M9 (CA).

(72) Inventors; and

(75) Inventors/Applicants (*for US only*): YANG, Victor, Xiao, Dong [CA/CA]; Unit - 936B, 60 Harbord Street, Toronto, Ontario M5S 3L1 (CA). VITKIN, I., Alex [CA/CA]; 130 Glenlake Avenue, Toronto, Ontario M6P 1E5 (CA). WONGKEESONG, Louie [CA/US]; Apartment 502, 211 2nd Street N.W., Rochester, MN 55901 (US). KATZ, Sharon [IL/CA]; 77 Winnifred Avenue, Toronto, Ontario M4M 2X2 (CA). GORDON, Margaret, Leslie [CA/CA]; 61 Dalewood Road, Toronto, Ontario M4P 2N4 (CA). WILSON, Brian, C. [GB/CA]; 85 Indian Grove, Toronto, Ontario M6R 2Y6 (CA). MOK, Alvin, Ho, Kwan [CA/CA]; 187 Spadina Road, Richmond Hill, Ontario L4B 3C5 (CA).

(74) Agent: BERESKIN & PARR; 40th floor, 40 King Street West, Toronto, Ontario M5H 3Y2 (CA).

(81) Designated States (*national*): AE, AG, AL, AM, AT, AU, AZ, BA, BB, BG, BR, BY, BZ, CA, CH, CN, CO, CR, CU, CZ, DE, DK, DM, DZ, EE, ES, FI, GB, GD, GE, GH, GM, HR, HU, ID, IL, IN, IS, JP, KE, KG, KP, KR, KZ, LC, LK, LR, LS, LT, LU, LV, MA, MD, MG, MK, MN, MW, MX, MZ, NO, NZ, PL, PT, RO, RU, SD, SE, SG, SI, SK, SL, TJ, TM, TR, TT, TZ, UA, UG, US, UZ, VN, YU, ZA, ZW.

(84) Designated States (*regional*): ARIPO patent (GH, GM, KE, LS, MW, MZ, SD, SL, SZ, TZ, UG, ZW), Eurasian patent (AM, AZ, BY, KG, KZ, MD, RU, TJ, TM), European patent (AT, BE, CH, CY, DE, DK, ES, FI, FR, GB, GR, IE, IT, LU, MC, NL, PT, SE, TR), OAPI patent (BF, BJ, CF, CG, CI, CM, GA, GN, GW, ML, MR, NE, SN, TD, TG).

Published:
— *with international search report*

(88) Date of publication of the international search report:
26 September 2002

For two-letter codes and other abbreviations, refer to the "Guidance Notes on Codes and Abbreviations" appearing at the beginning of each regular issue of the PCT Gazette.

(54) Title: METHOD AND APPARATUS FOR HIGH RESOLUTION COHERENT OPTICAL IMAGING

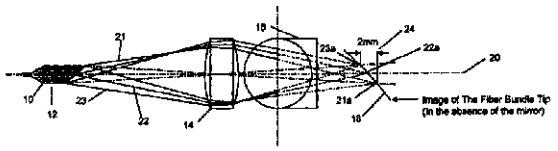

(57) Abstract: A method and an apparatus for examining the sub-surface microstructure of a sample are provided. Radiation from a plurality of optical radiation sources travels along a first optical path. In the first optical path, a device focuses the optical radiation from each of the optical sources into a plurality of respective focal points along the first optical path to provide substantially continuous coverage of a selected portion of the first optical path. Then, a sample on the first optical path within the selected length extending into the sample is scanned along said selected portion of the first optical path.

WO 02/004929 A3

【国際公開パンフレット（コレクトバージョン）】

(12) INTERNATIONAL APPLICATION PUBLISHED UNDER THE PATENT COOPERATION TREATY (PCT)

CORRECTED VERSION

(19) World Intellectual Property Organization
International Bureau

(43) International Publication Date
17 January 2002 (17.01.2002)

PCT

(10) International Publication Number
WO 02/004929 A3

(51) International Patent Classification⁷: G01N 21/47

(21) International Application Number: PCT/CA01/00993

(22) International Filing Date: 10 July 2001 (10.07.2001)

(25) Filing Language: English

(26) Publication Language: English

(30) Priority Data:
60/217,090 10 July 2000 (10.07.2000) US

(71) Applicant (*for all designated States except US*): UNIVERSITY HEALTH NETWORK [CA/CA], Room 7-504, 610 University Avenue, Toronto, Ontario M5G 2M9 (CA).

(72) Inventors; and

(75) Inventors/Applicants (*for US only*): YANG, Victor, Xiao, Dong [CA/CA]; Unit - 936B, 140 Harbord Street, Toronto, Ontario M5S 3L1 (CA). VITKIN, I., Alex [CA/CA]; 130 Glenlake Avenue, Toronto, Ontario M6P 1B5 (CA). WONG,KEESONG, Louie [CA/US]; Apartment 502, 311 2nd Street N.W., Rochester, MN 55901 (US). KATZ, Sharon [IL/CA]; 77 Winnifred Avenue, Toronto, Ontario M6M 2X2 (CA). GORDON, Margaret, Leslie [CA/CA]; 61 Dalewood Road, Toronto, Ontario M4P 2N4 (CA). WILSON, Brian, C. [GB/CA]; 85 Indian Grove, Toronto, Ontario M6R 2Y6 (CA). MOK, Alvin, Ho, Kwan [CA/CA]; 187 Spadina Road, Richmond Hill, Ontario L4B 3E5 (CA).

(74) Agent: BERESKIN & PARR; 40th floor, 40 King Street West, Toronto, Ontario M5H 3Y2 (CA).

(81) Designated States (*national*): AE, AG, AL, AM, AT, AU, AZ, BA, BB, BG, BR, BY, BZ, CA, CH, CN, CO, CR, CU, CZ, DE, DK, DM, DZ, EE, ES, FI, GB, GD, GE, GH, GM, HR, HU, ID, IL, IN, IS, JP, KE, KG, KP, KR, KZ, LC, LK, LR, LS, LT, LU, LV, MA, MD, MG, MK, MN, MW, MX, MZ, NO, NZ, PL, PT, RO, RU, SD, SE, SG, SI, SK, SL, TJ, TM, TR, TT, TZ, UA, UG, US, UZ, VN, YU, ZA, ZW.

(84) Designated States (*regional*): ARIPO patent (GH, GM, KE, LS, MW, MZ, SD, SL, SZ, TZ, UG, ZW), Eurasian patent (AM, AZ, BY, KG, KZ, MD, RU, TJ, TM), European patent (AT, BE, CH, CY, DE, DK, ES, FI, FR, GB, GR, IE, IT, LU, MC, NL, PT, SE, TR), OAPI patent (BF, BJ, CF, CG, CI, CM, GA, GN, GW, ML, MR, NE, SN, TD, TG).

Published:
with international search report

(88) Date of publication of the international search report:
26 September 2002

(48) Date of publication of this corrected version:
7 November 2002

(15) Information about Correction:
see PCT Gazette No. 45/2002 of 7 November 2002, Section II

For two-letter codes and other abbreviations, refer to the "Guidance Notes on Codes and Abbreviations" appearing at the beginning of each regular issue of the PCT Gazette.

(54) Title: METHOD AND APPARATUS FOR HIGH RESOLUTION COHERENT OPTICAL IMAGING

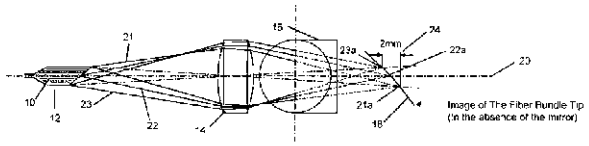

(57) Abstract: A method and an apparatus for examining the sub-surface microstructure of a sample are provided. Radiation from a plurality of optical radiation sources travels along a first optical path. In the first optical path, a device focuses the optical radiation from each of the optical sources into a plurality of respective focal points along the first optical path to provide substantially continuous coverage of a selected portion of the first optical path. Then, a sample on the first optical path within the selected length extending into the sample is scanned along said selected portion of the first optical path.

WO 02/004929 A3

Title: METHOD AND APPARATUS FOR HIGH RESOLUTION COHERENT OPTICAL IMAGING

FIELD OF THE INVENTION

This invention relates to both a method and an apparatus for high-resolution optical imaging. More particularly, this invention is concerned with providing high-resolution imaging suitable for incorporation into an endoscope.

BACKGROUND OF THE INVENTION

Modern medical imaging techniques have important applications in health care. Modalities such as X-ray computed tomography (CT), magnetic resonance imaging (MRI) and ultrasound imaging are the main tomographic techniques available in most modern medical centers. Visible-light endoscopy is another major imaging modality which is used extensively in procedures like bronchoscopy or colonoscopy. Each of these techniques employs different physical principles and measures different properties of the biological tissue under study with different resolution. Further, they can commonly be performed *in-vivo*. A third type of imaging, optical microscopy, is still utilized widely in clinical medicine. However, optical microscopy is currently limited to detailed examination of excised or resected specimens and is not used *in-vivo*. In many circumstances, the superior contrast and resolution afforded by optical microscopy is such that physical biopsy followed by optical microscopic histology is considered the gold standard for diagnosis.

Combinations of these techniques, such as using a low-resolution tomographic modality along with high-resolution imaging, biopsies or interventional procedures are constantly being studied and evaluated. Evaluation of these techniques is based on technological feasibility, clinical benefit and cost.

Optical Coherence Tomography (OCT) is a relatively new imaging technique based on the low-coherence property of electromagnetic radiation that enables high-resolution depth profilometry in a turbid, highly scattering

media such as biological tissue. Its use in biomedical imaging is currently being investigated in several research and industrial laboratories. The main advantage of OCT lies in its ability to localize the depth of reflection from a sub-surface site in tissue. This localization is essentially determined by the coherence properties of the light source used and can be as low as 2 to 20 μm for selected near-IR sources (e.g. lasers or amplified spontaneous emission devices). This gives a measure of the depth resolution attainable with OCT. Independently of the coherence characteristics, the lateral resolution is determined by the beam cross-section at the depth of imaging and by the lateral spacing of the acquired data. Typical values for lateral spacing in the literature are in the 5 to 30 μm range. The price to be paid for this remarkable cross-sectional imaging ability in intact turbid tissue is the limited imaging depth since, due to multiple scattering and absorption, both coherence and penetration of light are degraded resulting in OCT imaging depths of approximately 2 to 3 mm.

Most current implementations of OCT are based on Michelson interferometry with a 50/50 beam splitter directing the incident coherent light beam into a reference path containing a mirror (i.e. a reference arm) and a sample path containing the interrogated sample (i.e. a sample arm). Both free-space optic and fiber-optic implementations of this scheme are currently used. Reflected beams from the mirror in the reference arm and from the tissue in the sample arm are recombined in the same splitter and half of the resultant light energy impinges on a detector. Incoherent superposition of the two light fluxes typically occurs except when the optical path lengths of the two beams are matched to within the coherence length of the source. Within this limited distance, the coherent superposition of the two light fluxes yields an interference pattern with a fringe magnitude that is proportional to the reflectivity of the tissue at that particular depth. Depth profiling of the sample is then achieved by scanning the reference arm length or more correctly by scanning the optical path length of the reference arm by using a time delay in the reference arm (this is equivalent to lengthening the reference arm). Various detection methods to measure and quantify these faint amplitude

modulations amidst large background diffuse reflectance have been developed having a dynamic range of approximately 70 to 110 dB. Furthermore, lateral translation of the beam and axial motion of the reference mirror enables one to construct a two-dimensional reflectivity picture over a desired field of view. Means of improving the final image quality, such as performing image processing through de-convolution, have also been investigated.

The foregoing is a brief description of conventional reflectivity OCT imaging. Other variations include, for example, flow (Doppler) imaging and polarization imaging (albeit at the expense of additional complexity of the OCT optics and/or signal processing techniques). Images from these additional techniques are usually obtained in conjunction with images from conventional OCT so some image overlay or fusion is possible. Upon further technological development and/or clinical implementation, may add sufficient information content to increase the clinical utility of OCT in medicine.

However, many OCT designs and approaches that have been successfully implemented in tabletop research systems are not directly suitable for *in-vivo* imaging such as in gastroenterologic or bronchoscopic endoscopy. Instead, they may be more suitable for dermatological, ophthalmologic and dental applications. In contrast, *in-vivo* OCT imaging must address the issues of speed, resolution, contrast, penetration and instrument size. Images must be obtained sufficiently quickly to negate the effects of patient motion while still achieving suitable axial and lateral resolution, and maintaining an instrument size which is small enough to be endoscopically useful. Powerful near-IR sources, fast means of altering the reference arm length and custom-designed distal optical devices have been successfully developed to overcome the difficult challenges posed by *in-vivo* endoscopy.

The latest OCT technology employs a single-mode optical fiber with distal side-viewing optics introduced into the accessory channel of a conventional white-light endoscope. To build-up an image, the viewing direction of the OCT fiber is either linearly scanned to and fro over an approximate 2 mm distance, or is rotated via a flexible guide-wire or

interlocking gear mechanism at several revolutions per second. Simultaneous with this translation or rotation, the reference arm length outside the endoscope is rapidly varied via an optical phase delay to generate depth scans (i.e. A-scans). Currently, these OCT systems operate at frame rates up to conventional video rates but more typically at 4 to 8 frames per second, with a frame presenting a fully circumferential view to a depth of 2 to 3 mm. The resultant resolution values are approximately 5 to 25 μm in the depth (axial) direction and approximately 20 to 40 μm in the lateral direction. As well, the lateral resolution generally degrades with an increase in distance from the fiber tip of the OCT device due to geometric divergence. These OCT systems have a dynamic range which is somewhat lower than that of corresponding *ex-vivo* systems due to increased noise levels and faster imaging speeds.

Based on the latest OCT technology, it is questionable whether coherent *in-vivo* OCT systems are adequate for successful clinical imaging. The images are certainly useful, but substantial improvement is required if the elusive goal of "optical biopsy" is to be realized. For example axial and lateral resolution can be improved. While the improvement in the former usually involves the use of better low-coherence sources (i.e. CW and pulsed sources), the issue of sub-optimal and depth-varying lateral resolution is more difficult to address. In *ex-vivo* systems, with its relaxed constraints of speed and physical size, lateral resolution is improved by focusing the beam to a few microns with a high-NA (numerical aperture) objective lens. In contrast to conventional OCT scanning, the imaging can now be performed in the lateral (*en face*) direction with a pre-selected depth with small oscillations in path length difference, followed by a small depth increment as necessary. The high-NA objective lens is often coupled to tissue via a refractive-index matching liquid. The general approach of using OCT with a high-NA distal optic lens is known as Optical Coherence Microscopy (OCM). However, the improved lateral resolution at the beam waist location comes at the expense of lateral blurring at other depths because the highly focused beam has a very shallow depth of field. Thus,

the lens-to-surface distance must be varied to focus to different depths. In addition, a dynamic tracking scheme is needed to keep the location of the coherence gate (within which coherent interference between the optical beams from the sample arm and the reference arm is possible) and the beam waist at the same depth. These techniques for lateral resolution improvement have not been attempted during *in-vivo* endoscopy because of size and speed requirements.

SUMMARY OF THE INVENTION

The present invention is based on the concept of providing an endoscopic optical coherence tomography (OCT) device with microscopic resolution which will hereinafter be referred to as an endomicroscope. After reviewing possible clinical applications of the endomicroscope, the following parameters and features were identified since it is difficult to achieve these parameters and features simultaneously with current *in vivo* OCT systems.

1. High Resolution

In order to achieve cellular and sub-cellular resolution, an endomicroscope should preferably resolve features smaller than 5 μm both in the axial and lateral directions. In contrast to most existing *in vivo* OCT systems, the lateral resolution must not degrade substantially with the depth of the tissue being imaged due to geometric divergence.

2. Large field of view

An appropriate field of view of the endomicroscope is approximately 2 x 2 mm in the axial and lateral directions of the optical axis. This field of view is considered to be adequate for clinical applications. In order to achieve a 5 μm resolution in both the axial and lateral directions throughout the entire image, more than 800 A-scans (i.e. depth scans) have to be performed for each frame. The resultant image will contain more than 640,000 pixels. This is several orders of magnitude higher than existing *in vivo* OCT systems.

3. Small size of endoscope tip

Most of the existing *in vivo* OCT systems are designed around the constraints of the instrument channel of existing endoscopes. As a result, the outer diameter of these systems is restricted to approximately 2 to 3 mm which limits the numerical aperture of the imaging system. This makes it difficult to obtain high lateral resolution under *in vivo* conditions. These constraints may be technically unnecessary and limit one from fully exploiting the benefit of OCT/OCM in the clinical applications under consideration. Accordingly, a larger outer diameter, such as 3 mm or more, for example, may be used for the endoscope as well as a length of less than 20 mm for the rigid tip.

4. High imaging speed

Since the endomicroscope will be used to image a large area at high resolution under *in vivo* conditions, motion artifacts must be considered because of tissue motion due to physiological motion. These motion artifacts should be eliminated to ensure good image quality. Accordingly, the endomicroscope should preferably be able to acquire a single frame image within 12.6 ms given a typical physiological motion speed of 5 mm/s. This results in 63,000 A-scans per second. This imaging speed is more than one order of magnitude higher than that of current *in vivo* OCT systems.

5. Integration with currently available endoscopic imaging procedures

In order to improve clinical usefulness, conventional white light imaging should preferably be integrated into the endomicroscope. In addition, instrument channels should be preferably designed so that an excisional biopsy could be performed under the guidance of the endomicroscope. As well, instrument channels for water and air delivery may be preferably made available.

The advanced requirements for an endomicroscope outlined above are not compatible with existing OCT/OCM designs. For instance, if

an outer diameter of 6 mm is allowed for the endomicroscope and a distal optical design is used based on a single rotating fiber as described by Tearney, G.J., Brezinski, M.E., Bouma, B.E., Boppart, S.A., Pitris, C., Southern, J.F., and Fujimoto, J.G. ("In vivo Endoscopic Optical Biopsy with Optical Coherence Tomography", Science, **276**: 2037-2039, 27 June 1997), then although the 5 μm lateral resolution can be achieved at a single specific depth within the tissue in any one scan, such lateral resolution will degrade due to beam divergence at other depths. In addition, since a high NA system will be required to produce the requisite small beam waist size, the coherence gate and the focal point will not stay together in depth over a substantial (e.g. 2 mm) distance unless some dynamic compensation is implemented as described by Schmitt, J.M., Lee, S.L., and Yung, K.M ("An Optical Coherence Microscope with Enhanced Resolving Power in Thick Tissue", Optics Communications, **142**: 203-207, 1997). Therefore, in order to achieve some of the aforementioned requirements of the endomicroscope, dynamic focusing (changing the probe/tissue distance) and dynamic compensation (changing the path length difference) must be used. However, these focusing and compensation techniques complicate the practical realization of the device and may make it more difficult to satisfy the high imaging speed requirement. If one tries to first satisfy the imaging speed, as described by Rollins, A.M., Kulkarni, M.D., Yazdanfar, S., Ung-arunyawee, R., and Izatt, J.A. ("In vivo Video Rate Optical Coherence Tomography", Optics Express, **Vol. 3 No. 6**: 219-229, 14 September 1998), then image resolution, particularly lateral resolution, is degraded to an extent that the clinical utility of the device is compromised.

The present invention provides an endomicroscope with multiple fibers (i.e. channels) employing OCT to allow for different parts of the image to be scanned in parallel, instead of in series as is currently implemented in existing *in vivo* or *ex vivo* OCT/OCM systems. Using multiple parallel channels focused to different depths in the tissue, with each channel collecting high-resolution OCT data only across a very small axial range allows for a series of tight focal points to be achieved throughout the entire

field of view without dynamic focusing or dynamic compensation. This greatly simplifies the design of the device which may now use mostly fixed optical components, and may facilitate high-speed operation. In addition, the intrinsically miniature dimension of the fiber optic based OCT technique makes the multichannel concept possible to implement in a flexible endoscopic device while the proximal part of the endoscope, which is outside of the patient, allows room for sources, detectors, and other equipment.

In accordance with a first aspect of the present invention, there is an apparatus for optical examination of a sample, the apparatus comprising:

an optical source means for providing a plurality of separate optical radiation sources;

a first optical path extending from the source means; and,

a focusing means in the first optical path for focusing optical radiation from the optical radiation sources into a plurality of respective focal points located on a surface within the first optical path to provide substantially continuous coverage of a selected portion of the first optical path, whereby, in use, a sample can be located at least partially within the selected portion, thereby permitting simultaneous scanning of a plurality of points within the sample.

In accordance with a second aspect of the present invention, an N channel apparatus for optical examination of a sample, wherein the N channel apparatus comprises a plurality of optical networks and a reference arm, each optical network providing one channel for the N channel apparatus and sharing the reference arm.

In accordance with another aspect of the present invention, there is provided a method for optical examination of a sample, the method comprising:

(a) providing radiation from a plurality of separate optical radiation sources, along a first optical path;

(b) providing focusing means in the first optical path;

(c) focusing the optical radiation from the optical sources into a plurality of respective focal points along a surface within the first optical

path to provide substantially continuous coverage of a selected portion of the first optical path; and

(d) providing a sample located at least partially within the first optical path; and,

(e) simultaneously scanning a plurality of points within the sample.

It is to be appreciated that a sample, for use with the present invention, may comprise any biological tissue or other suitable material.

Further objects and advantages of the invention will appear from the following description, taken together with the accompanying drawings.

BRIEF DESCRIPTION OF THE DRAWINGS

For a better understanding of the present invention and to demonstrate how it may be carried into effect, reference will now be made, by way of example, to the accompanying drawings which show a preferred embodiment of the present invention and in which:

Figure 1a is a top view of the tip of an apparatus in accordance with the present invention showing optical paths and ignoring the refraction effects of an air-tissue interface;

Figure 1b is a side view of the tip of an apparatus in accordance with the present invention showing optical paths and ignoring the refraction effects of an air-tissue interface;

Figure 1c is an end view of the tip of an apparatus in accordance with the present invention showing optical paths and ignoring the refraction effects of an air-tissue interface;

Figure 1d is an alternate embodiment of the tip of the apparatus of Figure 1a showing optical paths and ignoring the refraction effects of an air-tissue interface;

Figure 2a shows the fiber bundle tip of Figure 1;

Figure 2b is a top view of an enlarged section of the fiber bundle tip;

Figure 2c is an end view of an enlarged section of the fiber bundle tip;

Figure 3a illustrates the focal points of three of the imaging fibers of the fiber bundle tip of Figure 1;

Figure 3b is a magnified view of the focal points of Figure 3a showing details of the focal points at different depths;

Figure 4a is a schematic indicating different directions for directing the optical beams from the fiber bundle tip of Figure 1;

Figures 4b and 4c are top and end views of optical beams in directions A and C of Figure 4a;

Figures 4d and 4e are top and side views of optical beams directed in directions B and D of Figure 4a;

Figure 4f shows a perspective view of the optical beams in the directions B and D;

Figure 5a is a beam spot diagram of a 5 channel fiber bundle tip showing electric field strength distribution near multiple focal zones;

Figure 5b is a beam spot diagram of 5 central channels of a 15 channel fiber bundle tip showing electric field strength distribution near multiple focal zones;

Figure 5c is a graph of beam spot diameter versus focal zone distance for the fiber bundle tip of Figure 5a;

Figure 5d is a graph of beam spot diameter versus focal zone distance for the fiber bundle tip of Figure 5b;

Figure 6 is a schematic layout of an apparatus in accordance with the present invention;

Figures 7a is a top view of an optical delay generator used in the apparatus of the present invention;

Figure 7b is a front view of a scanning mirror used in the optical delay generator of Figure 7a.

Figure 8a is an end view of the mirror and the focal points from three of the imaging fibers of the fiber bundle tip of Figure 1a;

Figure 8b shows a combined A-scan and a two-dimensional brightness-mode (B-mode) scan path for light radiated from a single imaging fiber of the present invention;

Figure 9 is a diagram illustrating mismatch between the coherence gate and the focal point due to the air-tissue interface for light radiating from a single imaging fiber of the present invention;

Figure 10 is a diagram illustrating flexible triggering of the apparatus of the present invention to accommodate the mismatch shown in Figure 9;

Figure 11a is a schematic diagram of a Prior Art single channel Optical Coherence Tomography device;

Figure 11b is a schematic diagram of a two channel Optical Coherence Tomography device;

Figure 11c is a schematic diagram of an optical network that could be used to construct an N-channel Optical Coherence Tomography device;

Figure 12a is a schematic diagram of a single channel Optical Coherence Tomography device with an optical circulator;

Figure 12b is a schematic diagram of a two channel Optical Coherence Tomography device employing optical circulators;

Figure 12c is a schematic diagram of an optical network that could be used to construct an N channel Optical Coherence Tomography device employing an optical circulator;

Figure 13a is a schematic of an experimental setup used to investigate cross-talk between optical channels sharing components;

Figure 13b is an experimental result from experimentation on the setup of Figure 13a;

Figure 13c is another experimental result from experimentation on the setup of Figure 13a;

Figure 14 is an end view of a GI endoscopic coherent optical microscope in accordance with the present invention;

Figure 15 is a cutaway side view of the GI endoscopic coherent optical microscope of Figure 14 showing a biopsy channel;

Figure 16 is a simulated image of a human colon epithelium that is expected to be obtained with the apparatus of the present invention;

Figure 17a has two panels which each show a microscopy image of sweat ducts in the human skin; and,

Figure 17 b has three panels which each show an *in vivo* OCT image of sweat ducts in the human skin.

DETAILED DESCRIPTION OF THE INVENTION

In the following description, various specific dimensions and other parameters are mentioned such as the wavelength used by the imaging source and the physical dimensions of the optical components used in the apparatus. It is to be appreciated that this is for exemplary purposes only and does not limit this invention. Specific parameters, dimensions and the like may be chosen depending on an intended application of the invention.

Referring to Figure 1, the present invention provides an apparatus comprising an endoscopic coherent optical microscope having multiple single mode fibers **10**, a fiber bundle tip **12**, a focusing lens **14** and a mirror **16**. The multiple single mode fibers **10** and the focusing lens **14** are stationary while the mirror **16** is rotatable. Accordingly, the mirror **16** is mounted for rotation in known manner. Details of the rotating mechanism for the mirror **16** are not described further and can be conventional. Multiple single mode fibers **10** (of which there may be approximately 50 fibers) form an array at the fiber bundle tip **12**. This array is cleaved and arranged in a "staircase" pattern as shown in Figure 2. Radiated light from the fiber bundle tip **12** is focused by the focusing lens **14** and reflected by the mirror **16**. The focusing lens **14** may have a diameter of 5 mm (i.e. ϕ = 5 mm) and a focal length of 5 mm (i.e. f = 5 mm). The mirror **16** may have a diameter of 5 mm and a front face that is cleaved at 45°. A magnified image of the focal points of the fiber bundle tip **12** is shown in Figure 3.

Figure 1a shows three beams **21**, **22** and **23** from three exemplary fibers arbitrarily chosen from the multiple single mode fibers **10**. Due to the staggered or staircase nature of the multiple single mode fibers **10** (see Figure 2), each of the beams **21**, **22** and **23** originates from a different point and consequently is brought into focus, by the focusing lens

14, at a different point **21a**, **22a** and **23a** on a surface **18** when the mirror **16** is not used. It will be appreciated that a similar effect is achieved for all of the multiple single mode fibers **10** of the fiber bundle tip **12** to produce beams focused to different points on the surface **18**. As indicated at **24** (and as shown in Figure 3), if the multiple single mode fibers **10** comprise 50 optical fibers, each being focused within a short range of approximately 40 microns and having their ends staggered to space the focal points apart by 40 microns (as measured along axis **20** of the focusing lens **14**), a total range or depth of 2 mm is covered. The axis **20** for the focusing lens **14** is part of a first optical path.

With the mirror **16** present, the optical beams **21**, **22** and **23** are focused as shown in Figures 1b and 1c. Thus, three focal points **21b**, **22b** and **23b** are spaced apart in a vertical or depth direction along axis **26** which forms an extension of the first optical path. As the view of Figure 1c shows, the three focal points **21b**, **22b** and **23b** are also spaced apart in the circumferential direction (i.e. they are spaced apart laterally) relative to the motion of the mirror **16**. The three focal points **21b**, **22b** and **23b** fall on a surface **27** to facilitate imaging of a selected portion of the first optical path. The surface **27** may be a complex surface or a planar surface. If multiple single mode fibers **10** comprises 50 individual fibers, then the focal points of all the individual fibers from the fiber bundle tip **12** would be spaced apart correspondingly. . Alternatively, the reflected focal points **21b**, **22b** and **23b** do not necessarily have to be perpendicular to the axis **20** but may be at a large angle to the axis **20**.

Rotation of the mirror **16** results in motion of the surface **27**. This enables a two-dimensional B-scan image **30** to be obtained, as shown in Figure 1c, covering a scan area **28** which has a square shape with preferable dimensions of 2 mm x 2 mm. The B-scan image **30** indicates an exemplary view that may be obtained for the scan area **28**.

Redesigning the multiple single mode fibers **10**, for example, by changing the diameter of the core and cladding of the multiple single mode fibers **10**, results in variations on the surface **27**. Furthermore, optical wave

guide wafers may also be used in the place of the multiple single mode fibers **10**.

In an alternative embodiment, the mirror **16** may be replaced by a mirror **16'** that moves linearly in combination with the focusing lens **14** and the fiber bundle tip **12** as shown in Figure 1d. The linear translation may preferably incorporate a reciprocal motion. In terms of mechanics, the fiber bundle tip **12**, depicted in Figure 1a, utilizes a radial scanning motion. The radial scanning motion is well suited for scanning organs having larger diameters, such as the esophagus or the large intestine. However, due to the complex driving mechanism needed for radial scanning, the diameter of the fiber bundle tip **12** will not allow for endomicroscopy in organs having small inner diameters such as blood vessels. Therefore, the alternative embodiment shown in Figure 1d may be used which comprises a similar fiber bundle tip **12'** that is adapted to perform linear translational scanning instead of radial scanning.

As shown in Figure 1d, the main differences between the two methods of scanning are that the mirror **16'** will not be rotating and the entire fiber bundle tip **12'** needs to be translated along its horizontal axis in preferably a reciprocal motion over a range of 4 mm for example. Mechanically, the linear translational scanning motion is less complicated than the radial scanning motion. In addition, linear translational scanning is better suited for endomicroscopy in organs having a small inner diameter such as blood vessels. However, for some larger organs, such as the large intestine, linear translational scanning is not as well suited due to positioning difficulties.

In a further alternative embodiment, both of the scanning motions may be combined to produce an endomicroscopy device having helical scanning. The helical scanning motion would comprise the rotational movement of the mirror **16** in combination with the linear translation of the mirror **16**, the focusing lens **14** and the fiber bundle tip **16**. Such an endomicroscopy device may be more suitable for imaging certain types of organs such as the human large intestine. The helical scanning

endomicroscopy device may be implemented by linearly translating the apparatus shown in Figure 1a.

In yet another alternative embodiment, the fiber bundle tip **12** may be altered to employ a Micromachined Electro-Mechanical System (MEMS) driving mechanism. Since the aforementioned embodiments require some form of motion for the mirror **16**, all embodiments require mechanical driving mechanisms. Accordingly, a motor is situated outside of the endoscope and a mechanical drive-train mechanism or wire is placed along the entire length of the endoscope. However, the multi-channel fiber optical design is not restricted to such mechanical driving means. In fact, due to the extremely small spatial resolutions realizable by the multi-channel system, adverse effects, such as vibration induced polarization dependence, from the mechanical drive means, may limit the full potential of the present invention if a mechanical drive means is utilized. Therefore, a MEMS electrical driving mechanism may be employed where electrically-driven, micro-mechanical optical devices are used to facilitate the scanning. This implementation may potentially circumvent the adverse effects that may be caused by a mechanical driving mechanism since the MEMS implementation reduces vibrations along the axis of the device except in the vicinity of the object which is being translated such as the mirror **16**. The MEMS implementation may also offer advantages in terms of miniaturization and performance.

In a further alternative embodiment, the fiber bundle tip may not require the mirror **16**. The combination of the fiber bundle tip **12** and the focusing lens **14** may be pivotally attached. Accordingly, through a pivoting motion, the combination of the fiber bundle tip **12** and the focusing lens **14** may be adapted to direct a plurality of focusing points along portions of a plurality of surfaces extending into the sample to construct the B-scan image **30** of the scan area **28**.

In yet another embodiment, the mirror **16** may be a surface of a prism. The rest of the apparatus would follow as previously described and shown in Figures 1a to 1d.

It should further be understood that the optical path can be straight, bent or curved. Furthermore, the optical path may be a 3 dimensional path having a length, width and height. Depending on the scanning motion (i.e. radial, linear or helical), the orientation of the surface, upon which the focal points reside, may also vary. Furthermore, the optical path may comprise optical radiation from one optical radiation source or a plurality of optical radiation sources (i.e. a plurality of light sources or a plurality of fibers each transmitting optical radiation).

Referring now to Figures 2b and 2c, a magnified view of the fiber bundle tip **12** comprising the multiple single mode fibers **10** is shown. Each of the multiple single mode fibers **10** comprises a cladding **10a** around a core **10b** having diameters of, for example, 40 μm and 5 μm respectively. The ends of the multiple single mode fibers **10** may be stepped by 40 μm so that the focal points of the optical radiation through each of these fibers are spaced apart. However, a step spacing other than 40 μm may also be used.

Referring now to Figure 3, A-scans for each of the multiple single mode fibers **10**, in the fiber bundle tip **12**, are acquired over approximately the entire 2 mm imaging depth, but retained only over a short axial range of approximately 40 μm near the focal point of each fiber where the beam diameter is close to a minimum (indicated at **34**) and does not vary substantially with axial position. This range of 40 μm, in this exemplary design, is indicated at **31**. The A-scans are performed simultaneously by each of the multiple single mode fibers **10** within the fiber bundle tip **12**. Effectively, the multiple A-scans cover the entire depth of 2 mm in the sample tissue at different radial directions, but for each of the multiple single mode fibers **10**, only sections of the respective A-scan in a corresponding 40 μm depth-of-focus **31** are used to build up the image. As shown in the focal zone **31**, each of the beams **21b**, **22b** and **23b** show a distinct "hourglass" shape for the focal points **38**, **37** and **36**, in known manner. For each of the beams **21b**, **22b** and **23b**, the far field beam spread is indicated by lines **32** and the near field beam spread is indicated by lines **34**.

The purpose of rotating the mirror **16** is to create radial (i.e. lateral) scans in a direction that is perpendicular to the A-scan direction to create a B-scan image, i.e. the scan area **28** of Figure 1. The resultant radial scan pattern of the focal points of the individual fibers from the multiple single mode fibers **10** is illustrated in Figure **4**. It is worth noting that a continuous scan surface is only present when the cleaved face of the mirror **16** is faced substantially in the direction of locations "A" and "C", where B-scan images should be taken. At other locations on the radial scan pattern, a "dead space" between the individual A-scans is too large to allow for sufficient sampling of the tissue. Therefore, the present invention comprises a sector-scan imaging device, to scan a sector substantially in the "A" or "C" locations, with a sector angle of about 20°, within which a 2 mm by 2 mm image is obtained. In this example, with the given geometry, a larger sector angle will produce "dead spaces" which are too large to form a suitable cross-sectional image.

Figures 4b and 4c show beam focal points **36**, **37** and **38** from both a top view and an end view respectively. As shown, and corresponding to earlier figures, the individual focal points **36**, **37** and **38** are spaced apart in the radial plane perpendicular to the axis **20**. As Figure 4c shows, in an end view along the axis **26**, the focal points **36**, **37** and **38** are spaced apart in terms of depth but overlap to create a continuous scanning surface or scan area **28**.

If, the cleaved face of the mirror **16** is faced substantially in the direction of the locations indicated at "B" and "D", in Figure 4a, which is perpendicular to the scanning surface or scan area **28**, then the patterns shown in Figure 4d (a top view of the pattern) and Figure 4e (a side view of the pattern) are obtained. Here, the focal points are indicated at **40**, **41** and **42**. As shown in Figure 4d, the focal points **40**, **41** and **42** are each in an individual plane **40'**, **41'** and **42'** which are spaced apart corresponding to the spacing of the fibers in the fiber bundle tip **12**. The planes **40'**, **41'** and **42'** are perpendicular to the axis **20**. In Figures 4b to 4e, arrows **44** indicate the direction of the radial scan.

For the linearly translated system shown in Figure 1d, there are no "dead spaces" and thus linear translation can produce images suitable images approximately 2 mm by 2 mm in size.

In the exemplary design of the endomicroscopic system, the maximal speed of tissue motion, due to physiological motion, was chosen as 5 mm/s for *in vivo* imaging. A near diffraction-limited focusing lens (i.e. a lens which approximates an ideal lens by providing very small focal points) was chosen as the focusing lens **14**. The near diffraction-limited focusing lens was supplied by Melles Griot Inc. In addition, each single mode fiber, from the plurality of single mode fibers **10**, had a core diameter of 5 microns (i.e. $\varnothing_c \approx 5$ µm) and was operated at a wavelength of 0.86 µm. Furthermore, the design incorporates an approximate core index of $n_c = 1.447$ and a difference in the refractive index between the core and the cladding of $\Delta n = 0.005$. Using these values, the NA of the fiber is then given by:

$$NA \approx n_c(2\Delta n)^{1/2} = 0.145 \quad (1)$$

and the acceptance angle, θ_a, of the fiber is given by:

$$\theta_a = \sin^{-1}(NA) = 8.32° = 0.145 \text{ rad} \quad (2)$$

The design further incorporates the concept of an ideal lens which is used to focus optical radiation, from the plurality of single mode fibers **10**, at a magnification of 1 to 1 and that the far field beam divergence angle is similar to θ_a. Then, for light beam radiation with a center wavelength λ_o, the beam diameter at the focal point is given by:

$$\varnothing_f = 2w_o = 2\,\frac{\lambda_o}{\pi\theta_a} = 3.95\mu m \approx \varnothing_c \quad (3)$$

The spot diameter $\varnothing_f$ is approximately equal to the core diameter ($\varnothing_c$=5µm) which results in efficient optical coupling. The depth of focus is $2\frac{\pi w_0^2}{\lambda_o} = 27.2$ mm and the beam diameter at the ends of the focal zones for focal points **36**, **37** and **38** is given by:

$$\varnothing_f' = 2\sqrt{2}\,w_0 = 5.59 \text{ mm} \quad (4)$$

Since the $\varnothing_f$ and $\varnothing_f'$ parameters are defined in terms of amplitudes, within 40 µm of the focal point in the axial direction, the beam diameter based on

light intensity (i.e. the square of the light amplitude) may actually be smaller than 5 μm.

The above calculation is based on ideal optics operating on the principle optical axis. Using an off-the-shelf lens system with ∅ = 5 mm, f = 5 mm, and a working distance of 8.2 mm, it has been found that the off-axis angle required to cover a 2 by 2 mm image is about 5° using commercial ray-tracing software. At approximately an 80% fill factor of the focusing lens **14**, the ray-tracing results show the on-axis RMS focal point to be 5.3 μm in radius, and the 5° off-axis RMS focal point to be 10.3 μm in radius. A custom designed lens system should have better performance.

As illustrated in Figure 1, the working distance of the entire optical system, i.e. the distance from the focusing lens **14** to the focal point of the apparatus is determined by the focal length of the lens system, the diameter of the focusing lens 14 and the gap between the focusing lens **14** and the mirror **16**. Using the off-the-shelf lens system discussed above, the working distance is about 2.35 mm. The distance from the center of the image to the rotational axis of the mirror **16** is about 5.47 mm. To obtain a 2 mm scan in the radial direction, the sector scanning angle should be approximately ±10.4°, or about 20° in total, as determined by the geometry of the optical system.

Currently existing *in vivo* OCT systems perform radial scans at 4 to 8 revolutions per second (RPS) to yield a biologically acceptable 4 to 8 frames per second. For the design of the present embodiment, 4.4 RPS is chosen as the rotational speed. The rotational speed depends on the repetition rate of the A-scans and the number of A-scans required to obtain a 5 μm lateral resolution. Therefore, the imaging speed of the apparatus of the present invention is 4.4 frames/s while other imaging speeds may be chosen based on different end-user applications. The imaging time for each individual frame is 12.6 ms, as determined by the rotation speed and the sector scanning angle. Therefore, for a given frame, the system is acquiring signals for 12.6 ms and the time between frames is about 215 ms during which data processing is performed. These parameters are dependent on

the performance of the optical delay generator (which is described later) that is used in the system.

While the above calculations were made based on a light source operating at a light wavelength of 860 nm and custom made single mode fibers, implementation using a light source operating at other wavelengths, such as 1300 nm, and off-the-shelf fiber may also be possible. Figure 5a shows a beam spot diagram for a 5 channel fiber bundle tip operating at a wavelength of 1300 nm and using off-the-shelf fibers (Corning SMF-28). The fiber bundle tip has a fiber step size of 125 μm. The light beams from these fibers, focused by a lens having a 5 mm diameter and a 4.5 mm focal length, cover a focal zone of approximately 0.65 mm. The resulting lateral imaging resolution is approximately 10 μm. Figure 5b shows a beam spot diagram for a 15 channel fiber bundle tip operating at a wavelength of 890 nm and using custom designed fibers having a core diameter of 5 μm and a cladding diameter of 40 μm. This fiber bundle tip has a fiber step size of 40 μm. The beams spots of only the central 5 channels are shown. The resulting lateral imaging resolution is approximately 5 μm over a focal zone of approximately 0.65 mm.

Figure 5c shows beam spot diameter versus distance along the focal zone for the 5 channel fiber bundle tip of Figure 5a. Figure 5c shows that the beam spot diameter is consistently less than 15 μm over the entire 0.65 mm focal zone. Figure 5d shows beam spot diameter versus distance along the focal zone for the 15 channel fiber bundle tip of Figure 5b. Figure 5d shows that the beam spot diameter is approximately 5 μm over the entire 0.65 mm focal zone.

Referring now to Figure 6, the overall general layout of the basic optical elements of the apparatus of the present invention comprises a plurality of optical sources **50**, a plurality of tree couplers **52**, a plurality of 3 dB couplers **54**, a fiber bundle tip **56**, a plurality of detectors **58**, a plurality of demodulators **60** and an optical delay generator **64**. The plurality of optical sources **50**, which may be lasers, are connected to the plurality of tree couplers **52**. More than one laser may be needed to ensure that

adequate optical radiation is provided to each of the fibers (i.e. channels) in the tip **56**. Each tree coupler **52** couples a respective optical source **50** to a subset of the plurality of 3 dB couplers **54**. The plurality of 3 dB couplers **54** are connected to the fiber bundle tip **56** for onward transmission of approximately half of the light radiation from the plurality of optical sources **50**. The fiber bundle tip **56** includes fiber bundle tip **12** and the other optical elements of Figure 1 (i.e. the focusing lens **14** and the mirror **16**). The other half of the radiation from the plurality of optical sources **50** is reflected back to detectors **58** which in turn are connected through the demodulators **60** to a computer **62** which functions to process the sampled data to generate the B-scan image **30**. The optical delay generator **64** is used by the 3 dB couplers **54** to provide a delayed reflected signal to the detectors **58**. The sample being investigated by the tip **56** is indicated at **65**.

In the layout shown in Figure 6, 1 dB or 10 dB optical couplers and the like may be used in place of the 3 dB couplers **54**. Furthermore, the intensity of the optical radiation transmitted to each of the 3 dB couplers **54**, and consequently each fiber, by the tree couplers **52** need not be the same and in fact is chosen depending on whether the 3 dB coupler provides optical radiation to a fiber (i.e. channel) that facilitates a deep or shallow scan into the tissue. High intensity optical radiation is needed to scan deeply into the tissue. Accordingly, tree couplers **52** and 3 dB couplers **54** that feed optical radiation to fibers that scan deeply into the tissue are adapted to provide larger amounts of optical radiation.

Figures 7a and 7b show the optical delay generator **64** in greater detail. The optical delay generator **64**, similar to those in existing *in vivo* OCT systems, is used to perform the A-scans using the coherence envelope of each individual fiber. The optical delay generator **64** comprises a grating **66**, a lens **67**, a scanning mirror **68** and a mirror **70**. Rapid depth scanning can be achieved with the optical delay generator **64** by dispersing quasi-monochromatic light from the multiple single mode fibers **10** in the fiber bundle tip **12** onto the diffraction grating **66** and focusing the dispersed light onto the oscillating mirror **69**. This has the effect of applying a linear ramp in the frequency or Fourier domain as described by G. J. Tearney,

B.E. Bouma and J. G. Fujimoto ("High-speed phase and group delay scanning with a grating based phase control line" Nature Medicine **4**(7), 861-865 (1998)). With recombination of the reflected wavelengths at the diffraction grating **66**, a real space-time delay is created. The angle of the scanning mirror **68** is rapidly oscillated through several degrees of rotation creating a rapidly varying time delay in the reference arm which allows for fast, repeated depth scanning of a sample.

The optical radiation **70** from one fiber from the multiple single mode fibers **10** is shown in Figure 7a. The optical radiation **70** is dispersed into spectral components represented by spectral components **71**, **72** and **73** by the grating **66**. Spectral component **71** represents the lowest wavelength in the optical radiation **70**; spectral component **73** represents the highest wavelength in the optical radiation **70**; and spectral component **72** represents the center wavelength in the optical radiation **70**. These spectral components of the optical radiation **70** are vertically aligned in the optical delay generator **64**. In a similar fashion, optical radiation from other fibers from the multiple single mode fibers **10** are dispersed and vertically aligned, with a vertical spacing between the dispersed optical radiation from the different fibers. The offset of the center wavelength of the dispersed optical radiation from the pivot axis of the scanning mirror **68**, for a given fiber, is represented by x_d which facilitates phase modulation of the dispersed optical radiation from each of the multiple single mode fibers **10**. Alternatively, if x_d were zero then a phase modulator would be needed, for each of the single mode fibers **10**, to phase modulate the optical radiation from each of the single mode fibers **10**. This has the advantage of allowing for a reduction in size of the scanning mirror **68** which in turn allows for a higher frame rate to be used. Furthermore, the phase modulator is electrically controlled which allows for very stable signals are generated

Referring now to Figure 7b, the multiple single mode fibers **10** are aligned in the fiber bundle tip **12**, such that dispersed optical radiation from each of the multiple single mode fibers **10** is vertically aligned on the scanning mirror **68** as rows **75**, **76**, **77** and **78**. Alternatively, other ordered arrangements may also be used for the spectral components of the optical

radiation from each fiber from the multiple single mode fibers **10** such as columns.

As illustrated in Figure 6, a single optical delay generator may be used to introduce delay in multiple fibers. The limiting factor in determining the number of channels that may be coupled to a single optical delay generator is the physical size of the scanning mirror which is in turn limited by the resonance frequency of the optical delay generator. Commercially available resonance optical scanners can operate up to 16 kHz. Accordingly, a size of 4 mm by 5 mm may be used for the scanning mirror **68**. Since the fiber bundle array is about 2 mm in size, it is possible to fit the entire array onto one optical delay generator. Therefore, for the embodiment of the present invention, a single optical delay generator is used having an optical scanner operating at f_r = 16 kHz with an optical scan angle α of $\pm$ 2°. The embodiment also incorporates a grating pitch of p = 3.33 μm, a center wavelength of λ_0 = 0.86 μm and a focal length of f_l = 21 mm. Accordingly, the free space group path length difference Δl_g is given by (from Rollins et al. 1998):

$$\Delta l_g = 4\alpha(f_l \frac{\lambda_0}{p} - x_d) = 0.618 \text{ mm} \quad (5)$$

which is also 1.24 mm peak to peak. In equation 5, x_d = 1 mm is the displacement between the λ_0 spectral line and the pivoting axis on the resonance mirror. The peak A-scan speed is given by:

$$V_{Amax} = 2\pi\Delta l_g f_r = 62.1 \text{ m/s} \quad (6)$$

and the A-scan speed varies according to equation 7.

$$V_A = V_{Amax}\cos(2\pi f_r t) \quad (7)$$

Choosing a source with a coherence length l_c of 5 μm and a Gaussian emission spectrum, the equivalent emission bandwidth is given by:

$$\Delta\lambda = \beta\frac{\lambda_0^2}{l_c} = 98 \text{ nm} \quad (8)$$

where b = 0.66 for a Gaussian envelope.

The size of the resonant mirror is determined next. For an optical delay generator with a grating having a first order diffraction, the diffraction angle is given by:

$$\theta(\lambda) = \sin^{-1}(\lambda/p) \quad (9)$$

The spread of the spectrum from $(\lambda_0 - \Delta\lambda/2)$ to $(\lambda_0 + \Delta\lambda/2)$ at the Fourier plane of the lens is given by:

$$\Delta x = 2 f_l \left[\theta(\lambda_0 + \Delta\lambda/2) - \theta(\lambda_0 - \Delta\lambda/2)\right] = 1.3 \text{ mm} \quad (10)$$

Since the mirror width is 4 mm, one can fit the spectrum on one side of the resonant mirror with the displacement x_d having a value of approximately 1 mm. This is illustrated in Figures 7a and 7b. The carrier frequency of an individual channel of the system is given by (Rollins et al. 1998):

$$f_c = (4x_d\alpha 2\pi f_r/\lambda_0)\cos(2\pi f_r t) \quad (11)$$

which is 16.3 MHz at the maximum.

The bandwidth of the interferogram (i.e. the interference fringe pattern) is given by:

$$\Delta f = \frac{\Delta\lambda}{\lambda_0^2} 4\pi\alpha f_r 2\left(f_l\lambda_0/p - x_d\right)\cos(2\pi f_r t) \quad (12)$$

which is 8.4 MHz at the maximum.

Since $f_c(t) > \Delta f(t)$, proper demodulation can be performed by conventional rectifying and low-pass filtering, although a sharp frequency cut-off is needed. It is preferable to set up the individual channels of the system such that $D_A = 40$ µm (the depth of the A-scan performed by a single channel) coincides with the maximum carrier frequency, so that the variation in carrier frequency over D_A is minimized. The carrier frequency varies sinusoidally in time given by:

$$\Delta f_c = f_c\{1 - \cos[\sin^{-1}(D_A/\Delta l_p)]\} = 34 \text{ kHz} \quad (13)$$

which is about 0.2% of f_c.

At other locations, the signal can still be properly demodulated, but the variation in carrier frequency will be larger. The demodulators **60** may incorporate an analog high-speed rectifier and a 10-pole low-pass filter to demodulate the signal. Effectively, the signal is frequency down-shifted

such that the signal is centered at DC and has a bandwidth of Δf. The demodulated envelope signal is then digitized at an appropriate sampling rate. Current existing data acquisition (DAQ) cards operate at 30 MegaSamples per second (MS/s) with an SNR of about 60 dB. Choosing a Gaussian shape for the interferogram spectrum with Δf = 8.4 MHz, the 60 dB point is at about 14.5 MHz. Accordingly, the Nyquist rate for digitizing such a signal is approximately 29 MS/s. Therefore, current existing DAQ cards will be able to digitize the envelope signal without aliasing.

Given a sampling rate of 30 MS/s for digitizing the envelope signal at the maximum carrier frequency, the spatial sampling interval in the axial direction is: $\Delta_{axial} = V_{Amax}/S$ = 2.07 μm. As shown in Figure 8, a scan path **80** is indicated showing A-scans alternately going up and down through the sample. Sampling points are indicated at **82**. The axial spacing of 2.07 μm is indicated at **84**. The spatial sampling interval in the lateral direction is determined by the lateral or B-scan velocity and the resonant frequency of the optical scanner in the optical delay generator **64**. At the center of the image, where the radial distance r is 5.47 mm from the rotational axis of the mirror, the radial sampling interval is given by:

$$\Delta_{radial} = {}^{V_{radial}}\!/_{2f_r} = {}^{2\pi\Omega r}\!/_{2f_r} = 4.73\ \mu m \qquad (14)$$

This interval is indicated at **86** in Figure 8. For the fiber scanning the shallowest depth, the spatial lateral sampling interval is 3.86 μm and for the deepest channel it is 5.59 μm. Therefore, the pixel size at the center of the image is 2.07 by 4.73 μm in the axial and lateral direction respectively. The lateral pixel size varies across the depth of the image from 3.86 to 5.59 μm. By varying the rotational speed of the mirror **16**, the lateral sampling interval can be changed, at the expense of frame rate. If a higher resonance frequency optical scanner is used, the sampling interval may also be reduced.

For a pulsed optical source (e.g. a 15 to 20 fs pulsed laser emitting light with a wavelength of 860 nm), the coherence length will be approximately 4.5 to 6 μm. Since the spatial sampling interval in the axial

direction is about 2 μm, which is smaller than half of the coherence length, the image is reasonably sampled in the axial direction. Using a near diffraction-limited focusing lens as the focusing lens **14**, the beam spot size should be about 5 μm. Since the spatial sampling interval in the lateral direction varies from 3.86 to 5.59 μm, the image is slightly under sampled, given that the beam waist size is about 5 μm. However, the spatial sampling interval is not equivalent to the final image resolution, which is also influenced by local contrast and noise levels. Local contrast is the difference in reflectivity between two points in the sample that show up as adjacent pixels in the image. If the two points have similar reflectivity, i.e. low local contrast, it will be difficult to resolve these points.

Imaging speed should be fast enough to reduce motion blurring. Given that the target speed (i.e. tissue motion) is typically 5 mm/sec, then within a frame time (an elapsed time of 12.6 ms), the target can move up to 63 μm in a particular direction which is much larger than the designed 5 μm resolution. In the present embodiment, the A-scan is performed simultaneously in all channels such that one line of the image is formed within 0.6 μs which is the time required to scan the coherence gate through a 40 μm distance. The time between two consecutive A-scans is about 16 μs, which is determined by the rotational speed of the mirror **16** of the system and the number of A-scans per image. Thus, the resultant image should be crisp since the motion during 16 μs is 0.08 μm which is much less than the resolution. Accordingly, there should be no motion blurring in the image but a motion artifact may still exist. The resultant motion artifact may be a geometric deformation of the features being imaged that may be as large as 63 μm depending on the size of the feature and the target velocity. This motion artifact is due to the effect that the air-tissue interface has on the optical radiation from the plurality of optical sources **50**.

As illustrated in Figure 9, the focal point of an individual fiber of the apparatus, inside the tissue being imaged, can vary depending on the distance d_0 of the location of the focal point in the tissue, whether the tissue surface had a refractive index of 1, and the actual refractive index of the

tissue (which is typically approximately 1.4). Accordingly, the actual focal point is at a distance d_f below the tissue surface given by:

$$d_f = d_0 \frac{\tan\theta_1}{\tan\theta_2} = d_0 \frac{\tan\theta_a}{\tan\left[\sin^{-1}\left(\frac{n_1}{n_2}\sin\theta_a\right)\right]} \qquad (15)$$

where θ_1 is assumed to be equal to θ_a, the acceptance angle of the individual fibers and θ_2 will be determined by the refractive index $n_1 = 1$ (i.e. air) outside the tissue and $n_2 = 1.4$ inside the tissue.

The coherence gate location varies according to:

$$d_c = \frac{n_1}{n_2} d_0 \qquad (16)$$

Accordingly, due to the fact that optical radiation travels more slowly in a medium with a larger refractive index there is an optical path mismatch between the focal point and the coherence gate of an optical beam which is matched in a medium with $n_1 = 1$ (i.e., with no tissue present). This mismatch is:

$$\Delta d = n_2(d_f - d_c) = \frac{n_2 d_0 \tan\theta_a}{\tan\left[\sin^{-1}\left(\frac{\sin\theta_a}{n_2}\right)\right]} - d_0 \qquad (17)$$

A tissue refractive index of $n_2 = 1.4$ yields $\Delta d \approx 0.97\, d_o$. This mismatch problem is common for all high-NA OCM systems and many existing high-NA OCM systems use some form of dynamic compensation, i.e., changing the reference path length dynamically to compensate for Δd, however, such dynamic compensation is difficult with a high imaging speed. Accordingly, one aspect of the embodiment of the present invention is to use 'flexible triggering' of the detected interferogram signal.

As shown above, the free space group path length difference is $2\Delta l_g = 1.24$ mm peak to peak, which is much larger than the useful A-scan range of only 40 μm. This leaves room for dealing with the mismatch since one then can trigger to obtain the interferogram only when the coherence gate is passing through the focal point.

As shown in Figure 9, the working distance for each fiber channel, d_w, varies with n_2, which is approximately constant Therefore, if one knows

where the tissue surface is, d_0 can be determined and in turn Δd can be determined.

Referring to Figure 10, showing a perspective view of a tissue surface and an arbitrary axial line **90**, channel 1, which is designated to scan the surface of the tissue, is the first to pass through the axial line **90**, in the scan area **28**. The focal points of channels 1 and 2 are indicated at **91** and **92** in a schematic representation **94** of the optical radiation from the multiple single mode fibers **10** (i.e. channels) passing through the axial line **90**. The focal point of the last channel, i.e. channel 50 in this example, is indicated at **95** and is designated to scan the deepest layer of the tissue in the image. The overall profile of the representation **94** defines a flexible trigger zone, within which the coherence gate and the focal length can be matched. One of the 50 channels, i.e. channel "v", will experience a large and distinctive specular reflection since the air-tissue interface approximates a mirror and reflects incident light. Underneath the tissue surface, the tissue acts as a turbid media which scatters and absorbs incident optical radiation. Thus, channel "v" will determine d_0 for this particular axial line **90** since all of the channels before channel "v" will return a signal that is at noise level. Accordingly, the "flexible triggering" method comprises comparing the detected reflected optical radiation for adjacent channels to locate the tissue surface by identifying the channel in which there is a large increase in reflectance compared to its 'neighboring' channels. This information is then passed on to each of the subsequent channels and the trigger point for each channel is set accordingly to reduce mismatch between the focal point and the coherence gate.

As an example, if channel "v" is channel 13 then the apparatus is calibrated such that channels 1 to 12 are set to scan free space above the tissue surface, channel 13 to scan the tissue surface, and subsequent channels are set to scan deeper tissue, with no mismatch between the focal point and the coherence gate of the optical beam of each channel. During imaging, a tolerance of $\Delta d_0 = \pm 0.5$ mm of the location of the tissue surface can be allowed as indicated at **96** in Figure 10. This tolerance is related to

the A-scan performance and the frequency response of the envelope detector as will now be explained.

Given Δd_o = 0.5 mm, the mismatch that needs to be compensated for is given by:

$$\Delta d' = 0.693 \times 0.5 \approx 0.347 \text{ mm} \quad (18)$$

This means that instead of triggering the interferogram signal at the maximum carrier frequency, the actual carrier frequency needs to be:

$$f_c' = f_{cmax} \cos(\sin^{-1}(\Delta d'/\Delta l_g)) = 13.5 \text{ MHz} \quad (19)$$

which is about 83% of the maximum carrier frequency with the interferogram signal bandwidth changing accordingly. Although the envelope detector's frequency response can be tuned dynamically, it is simpler and faster for the envelope detector to have a fixed response but it was designed for a 17% tolerance of the cut-off frequencies. In this way, the entire flexible triggering scheme contains only fixed components and all of the compensation is performed electronically to satisfy the high imaging speed requirement.

The optical components shown in Figure 6 can be chosen as follows. Based on Boppart, S.A., Bouma, B.E., Pitris, C., Southern, J.F., Brezinski, M.E., and Fujimoto, J.G. (*In vivo Cellular Optical Coherence Tomography Imaging*, Nature Medicine, **Vol. 4 No.7**:861-865, July 1998), an SNR of greater than 100 dB can be achieved in a non-endoscopic OCT system using 2 mW of incident power on the tissue to allow for imaging to a depth of approximately 2 to 3 mm. The optical source used was a Kerr-lens mode-locked solid-state Cr^{4+}: forsterite laser operating at a 1280 nm center wavelength with a coherence length of 5.1 μm. However, the embodiment of the present invention is not limited to this type or any other particular type of source, such as a broadband superluminescent diode. For instance, another possibility is a white-light emission Cr:LiSAF optical source with a bandwidth of approximately 100 nm centered at 860 nm which will provide a coherence length of approximately 4.5 to 6 μm. This diode-pumped, solid-state, mode-locked laser should operate with a pulse-repetition rate of about 100 MHz and an average power of 30 mW when operated at 860 nm.

The pulse energy variation should be less than 1%. Several (e.g., 2 or 4) of these lasers as indicated at **50** in Figure 6 are needed to provide the total power requirement of the 50 channels. The channels scanning the deeper portion of the tissue will need about approximately 1 to 2 mW of incident power per channel and the channels scanning the shallower portion will need less. The tree couplers **52** can be configured to split the source power to match these requirements. Since the maximum carrier frequency is 16.3 MHz, each interference fringe will contain at least 6 laser pulses. Therefore the fringe pattern should be adequately sampled.

For each channel, a separate photo receiver or detector **58** may be used to detect the interference fringes. The maximum detector bandwidth is 125 MHz, although in the apparatus of the present invention, a detector bandwidth of 30.8 MHz may be sufficient, as determined by the carrier frequency and the bandwidth of the interferogram.

An alternate embodiment of the present invention involves the concept of sharing optical components to reduce device complexity and cost. Referring to Figure 11a, a typical single channel interferometer **150** with balanced detection in which the AC component of the interferogram is separated from the DC component of the interferogram and only the AC component is amplified is shown. The single channel interferometer **150** comprises an IR broadband light source **L**, a visible wavelength guide light **G**, a balanced detector **BD**, a polarization controller **PC**, a phase modulator **ϕMOD** and an optical delay generator **ODG** which are connected through a network of optical fibers and 3 dB couplers **140**, **142** and **144**. The "x" denotes a dead end in the fiber network. The visible wavelength guide light **G** may be a green laser which indicates the direction in which the single channel interferometer **150** is pointing (i.e. it indicates what will be imaged). The single channel interferometer **150** is connected to a sample **S**.

The design of Figure 11a can be extended to construct a two channel interferometer **160** as shown in Figure 11b. The subscripts denote the components that are in the two channels. A component without subscripts indicates that the component is used in both channels. The two

channel interferometer **160** comprises a laser **L'**, a visible wavelength guide laser **G'**, a 2 to 1 tree coupler **TC1**, polarization controllers PC_1, PC_2 and phase modulator **ϕMOD'**, variable delay elements VD_1 and VD_2, an optical delay generator **ODG'**, detectors BD_1 and BD_2 and 3 dB couplers **162**, **164**, **166**, **168**, **170** and **172**. The variable delay elements VD_1 and VD_2 are introduced to adjust the coherence gate positions for each channel. The two channels are coupled to samples S_1 and S_2 which may be two points at different locations in a tissue sample. The light source **L'** is shared between the two channels in this case, with the optical power in channel 1 being twice that in channel 2. Therefore, channel 1 should be used to scan a deeper region of tissue than channel 2. The 1 to 2 tree coupler **TC1** is used so that both channels can share the same reference arm (comprising the phase modulator **ϕMOD'** and the optical delay generator **ODG'**). The ability to share the same reference arm allows one phase modulator to be used to phase modulate the optical radiation from the multiple single mode fibers **10** (i.e. all the channels). Note that the two channels are combined into one fiber by the tree coupler **TC1** and then fed to the same phase modulator **ϕMOD'**. Accordingly, cost and complexity of the two channel interferometer **160** is reduced.

Based on Figure 11b, it is conceivable that a general optical network can be used to construct an N channel OCT system such as optical network **180** shown in Figure 11c. The optical network **180** comprises an optical network for an n^{th} channel **182** and a reference arm **184** that is shared by all n channels. The optical network for the n^{th} channel **182** comprises a detector BD_n, 3 dB couplers **194**, **196** and **198** and a sample arm comprising a polarization controller PC_n and a variable delay element VD_n connected to a sample S_n. The optical network for the n^{th} channel **182** receives optical source radiation **186** from the $n\text{-}1^{th}$ channel and transmits optical source radiation **188** to the $n+1^{th}$ channel via 3 dB coupler **194**. The optical network for the n^{th} channel **182** receives guide light power **190** from the $n\text{-}1^{th}$ channel and sends guide light power **192** to the $n+1^{th}$ channel via 3 dB coupler **196**. In this embodiment, a light source (not shown) may be

shared between each of the N channels with a power distribution that follows a geometric series or another suitable power partition scheme. The reference arm **184**, comprising an N to 1 tree coupler **TCn**, a phase modulator **ϕMOD"** and an optical delay generator **ODG"**, is shared between each of the N channels.

Each of the schematics shown in Figures 11a, 11b and 11c, suffer from the fact that a portion of the optical radiation of the interference pattern, from the interference between the reflected optical radiation from the sample and reference arms, which is sent from the 3 dB coupler connected to the detector is lost. In this case 50% of the optical radiation of the interference pattern is lost since a 3 dB coupler is used. For instance in Figure 11a, only 50% of the optical radiation of the interference pattern is sent from 3 dB couplers **140** and **142** to the detector **BD**. This makes if more difficult to detect the interference pattern especially for interference patterns with low intensities. To address this, a non-reciprocal optical device, such as an optical circulator may be used to send, to a detector, the portion of the optical radiation that would have been lost if only a 3 dB coupler were used.

Referring to Figures 12a, 12b and 12c, alternate embodiments of a single channel OCT device **200**, a two channel OCT device **210** and an optical network for an N channel OCT device **220** are shown comprising optical circulators. In Figures 12a, 12b and 12c, the optical circulators **C**, C_1, C_2 and C_n are used to salvage and direct the optical radiation of the interference pattern to the detectors **BD**, BD_1, BD_2 and BD_n respectively to provide a larger intensity interference signal for detection. The rest of the components in these embodiments are similar to those in the of the single channel OCT device **150**, the two channel OCT device **160** and the optical network for the N channel OCT device **180** shown in Figures 11a to 11c. The concept of using optical circulators to salvage optical radiation and provide the salvaged optical radiation to a detector may also be applied to the apparatus of Figure 6 in which optical circulators could be placed between the 3 dB couplers and the detectors.

The schematic shown in Figure 11c and 12c leads to an elegant design, however, parallel interferometers that share components (i.e. a phase modulator) may produce prohibitive amounts of channel cross talk which may consequently lead to image degradation. However, with fiber length mismatching between channels, cross talk may be effectively handled. Electronic cross-talk can be handled using standard shielding and grounding techniques. The following describes the optical cross-talk.

Referring now to Figure 13a, a two channel OCT system **230** was assembled to investigate channel cross talk. The two channel OCT system **230** comprises a laser L_E, detectors D_1 and D_2, beam splitters BS_1 and BS_2, a 1 to 2 tree coupler TC_E, a phase modulator PM_E, an optical delay generator ODG_E, beam collimators BC_1 and BC_2 and two mirrors S_{1E} and S_{2E} which simulate samples. In the two channel OCT system **230**, the desired imaging signals come from the channel 1 and channel 2 optical paths. The desired imaging signal for channel 1 occurs when light from the optical pathway:

$$L_E \rightarrow BS_1 \rightarrow S_1 \rightarrow BS_1 \rightarrow D_1 \quad (20)$$

interferes coherently with light from the optical pathway:

$$L_E \rightarrow BS_1 \rightarrow ODG_E \rightarrow BS_1 \rightarrow D_1 \quad (21)$$

and is detected by the detector D_1. The desired imaging signal for channel 2 occurs when light from the optical pathway:

$$L_E \rightarrow BS_2 \rightarrow S_2 \rightarrow BS_2 \rightarrow D_2 \quad (22)$$

interferes coherently with light from the optical pathway:

$$L_E \rightarrow BS_2 \rightarrow ODG_E \rightarrow BS_2 \rightarrow D_2 \quad (23)$$

and is detected by the detector D_2. Furthermore, OCT imaging in the two channels occurs only when the optical distance $BS_1 \rightarrow S_1$ is equal to the optical distance $BS_1 \rightarrow ODG_E$ and when the optical distance $BS_2 \rightarrow S_2$ is equal to the optical distance $BS_2 \rightarrow ODG_E$. Otherwise, image degradation could occur from constructive interference of light reflected from two (or more) different paths that are not the desired imaging paths stated above.

Based on the optical network shown in Figure 13a, there may be two major classes of potential cross talk. The primary source of cross talk may be coherent light that is reflected (from a mirror or the sample) from

one channel's beam splitter into the other channel's beam splitter and detector. Such cross talk would have intensities equal to the imaging signal intensities and could potentially cause significant image degradation. Reflection from one channel to the other could occur at the optical delay generator ODG_E or at the samples S_1 or S_2. Therefore, light from the optical pathway:

$$L_E \rightarrow BS_1 \rightarrow S_1 \rightarrow BS_1 \rightarrow D_1 \quad (20)$$

may interfere with light from the optical pathway:

$$L_E \rightarrow BS_2 \rightarrow ODG_E \rightarrow BS_1 \rightarrow D_1 \quad (24)$$

Alternatively, light from the optical pathway:

$$L_E \rightarrow BS_2 \rightarrow S_2 \rightarrow BS_2 \rightarrow D_2 \quad (22)$$

may interfere with light from the optical pathway:

$$L_E \rightarrow BS_1 \rightarrow ODG_E \rightarrow BS_2 \rightarrow D_2 \quad (25)$$

Sample arms 1 and 2 would not normally be separated as they are in Figure 13a because the sample arms would be aimed at different points (i.e. different depths) on a tissue sample. When the samples are not separate, reflection could occur from channel 1 into channel 2 and vice-versa. In such a case, light from the optical pathway:

$$L_E \rightarrow BS_2 \rightarrow S_2 \rightarrow BS_1 \rightarrow D_1 \quad (26)$$

may interfere with light from the optical pathway:

$$L_E \rightarrow BS_1 \rightarrow ODG_E \rightarrow BS_1 \rightarrow D_1 \quad (21)$$

Alternatively, light from the optical pathway:

$$L_E \rightarrow BS_1 \rightarrow S_1 \rightarrow BS_2 \rightarrow D_2 \quad (27)$$

may interfere with light from the optical pathway:

$$L_E \rightarrow BS_2 \rightarrow ODG_E \rightarrow BS_2 \rightarrow D_2 \quad (23)$$

It should be recalled that reflection may also occur at undesirable locations such as beam splitters and connector insertion points. Conceivably, such reflections may contribute to image noise if the light from these pathways produced interference fringes having a significant intensity. However, this kind of noise may be secondary to the channel cross talk previously described because of its lower intensity.

Analysis of the system revealed that the worst-case scenario for interference of such back-reflections involves one reflection from a connector. For example, light from the following optical path:

$$L_E \rightarrow BS_1 \rightarrow S_1 \rightarrow BS_1 \rightarrow D_1 \quad (20)$$

may interfere with light from the optical pathway:

$$L_E \rightarrow BS_2 \rightarrow ODG_E \rightarrow PM_E \rightarrow ODG_E \rightarrow BS_1 \rightarrow D_1 \quad (28)$$

There are four possible outcomes for the interference of light from any two pathways and the outcome depends on path length difference. Firstly, if the path lengths are identical, then the intensity of the interference fringes at the detector will be greater than the true signal intensity based solely on the sample reflectivity. This sort of image noise would not be detectable as noise and would alter the measured sample intensity throughout the image. Fortunately, the probability of the path lengths matching exactly is remote. A second possibility is that the path lengths could match to within the coherence length of the light source. This situation would result in an increase in the width of the interference fringe envelope and consequently degradation in axial resolution. This situation is unlikely, but it may be detected by measuring the full-width-half-maximum of the mirror surface depth profile. A third possibility involves the path lengths differing by a distance greater than the coherence length of the source L_E and less than the scanning depth of the optical delay generator ODG_E. This situation may manifest as two separate coherence envelopes within one depth sweep by the optical delay generator ODG_E. The final and most likely possibility is that the path lengths differ by more than the scanning depth of the optical delay generator ODG_E and no noise or extraneous interference fringes will be detected by the system.

The primary type of channel cross talk should be unlikely because of fiber optic manufacturing. Optical path lengths $BS_1 \rightarrow ODG_E$ and $BS_2 \rightarrow ODG_E$ are essentially predetermined by the lengths of the fiber pigtails coming from beam splitters BS_1 and BS_2. Optical path lengths $BS_1 \rightarrow S_1$ and $BS_2 \rightarrow S_2$ are deliberately matched to the predetermined corresponding reference arm lengths. Typically manufactured fiber lengths differed by several tens of millimeters which is at least one order of magnitude greater

than the scanning depth of the optical delay generator ODG_E. Therefore, this type of cross talk should not be a problem in a dual channel system.

In the case of insertion point reflections, if the optical distance $PM_E \rightarrow ODG_E$ matched the path length difference between optical paths $BS_1 \rightarrow S_1$ and $BS_2 \rightarrow ODG_E$, then interference fringes and image degradation may occur. Again, this sort of secondary noise should be unlikely because the fiber lengths are about 300 mm while the optical delay generator ODG_E scans through only a couple of millimeters. Furthermore, the intensity of such interference fringes would be lost in the system noise. Secondly, the equipment used has a maximum 0.6 dB insertion loss (in other words a maximum of reflection of 0.6 dB) and therefore such a signal is below the detection limits used in the setup of Figure 13a.

To demonstrate that two channels can use the same fiber and optical components, the OCT system **230** was evaluated. The sample arm mirrors S_1 and S_2 were placed such that the sample arm optical path length and the optical delay generator ODG_E reference arm optical path length matched for each channel and a set of interference fringes were seen at each of the detectors D_1 and D_2. The sample arms for samples S_1 and S_2 were kept separate for alignment purposes and to eliminate the possibility of light from channel 1 reflecting into the fiber containing channel 2 and vice-versa. Although an optical delay generator could be used to produce both phase modulation and group delay (Tearney et al. 1997), with the setup shown in Figure 13a, the optical delay generator ODG_E was used for group delay (i.e. depth scanning) while the phase modulator PM_E in the reference arm was used to produce phase delay.

In the experimental setup of Figure 12a, the light source L_E comprised a 1310 nm, 9 mW light source (model BBS1310) made by AFC Technologies Inc. The central wavelength of the light source L_E was 1310 nm with a measured spectral spread of ± 40 nm. The measured coherence length of the light source L_E was 10 µm. The detectors D_1 and D_2 were 155 Mbps Perkin Elmer InGaAs photodiode receivers with a detection band centered at 1310 nm having a bandwidth greater than or equal to 100 nm.

The phase modulator PM_E was a JDS Uniphase 43 MHz phase modulator. The beam splitters BS_1 and BS_2 were made by MetroTek. OZ Optics manufactured the beam collimators BC_1 and BC_2. Alternate suitable components may be used from these or other suppliers.

The optical delay generator ODG_E dispersed the collimated light using a 150 line/mm diffraction grating blazed for 1310 nm which was made by CVI Spectral Products. A Melles Griot glass doublet lens with a 30 mm diameter and 100 mm focal length was used to focus light onto the oscillating mirror. EOPC (Electro-Optical Products Corporation) manufactured the resonant scanner that operated at 8 kHz and scanned through a $\pm$ 1° mechanical or a $\pm$ 2° optical angle. This angular setting corresponded to a depth scan of about 1 mm in the sample arms for the samples S_1 and S_2. Scanning depth is an important consideration in terms of mismatching the optical lengths of the two channels. For instance, if the optical path lengths differ by more than 1 mm then cross talk between the two channels should be minimal and proper shielding and grounding techniques should address electronic cross-talk as well.

Figures 13b and 13c show results from experiments conducted on the setup shown in Figure 13a. Figure 13b shows the oscilloscope trace from the detectors D_1 and D_2 in channel 1 and channel 2. Figure 13b shows that the interference fringes occur at different points in the cycle of the optical delay generator ODG_E which reflects the slightly different positioning of the two channels within the cycle of the optical delay generator ODG_E, i.e. the sample arm mirrors S_1 and S_2 were deliberately offset by a small amount to simulate imaging at different depths. Figure 13b shows that there is a strong imaging signal in each of the channels and no evidence of any cross talk. The arrows **232** and **234** indicate reflection from two different sample points which could correspond to two different points in a tissue sample. Furthermore, the full-width-half-maximum of the envelope of each detected pulse corresponded to the coherence length of the light source L_E which indicates that the light signal in each channel originated from the light source L_E. Figure 13b shows the experimental results when one of the

sample points was moved relative to the other sample point. In this case, cross-talk was also not observed.

In another embodiment of the invention, the fiber optic network, previously disclosed herein, is incorporated into an endoscope so that the multi-channel OCT methodology may be used clinically. Due to the size of the fiber bundle tip **12** of the apparatus, the fiber bundle tip **12** will not fit into the working channel of a conventional diagnostic endoscope (although it may be incorporated into the larger-diameter therapeutic endoscopes). Therefore, an alternate design approach was taken. Instead of designing the fiber bundle tip **12** to accommodate the working channel of a conventional diagnostic endoscope, all of the functionality of a conventional diagnostic endoscope was designed around the fiber bundle tip **12**. As shown in Figure 14, one embodiment of a GI endoscope **300** (corresponding to the tip **56** of Figure 6) incorporating the endomicroscope of the present invention is approximately 11 mm in diameter. This is slightly larger than the conventional diagnostic endoscope which is 8 - 9 mm in diameter. The GI endoscope **300** has the endomicroscopy capability disclosed above in addition to conventional forward-viewing white light imaging. Therefore, a user of the GI endoscope **300** should be able to obtain a 2 by 2 mm cross-sectional image as illustrated in Figure 16.

The GI endoscope **300** includes a 2.7 mm diameter suction/biopsy channel **302**. The end of the suction/biopsy channel **302** is bent so as to present an opening **304** directed towards the tissue area of interest **306**. The axis of the suction/biopsy channel **302** may be on the order of 6.7 mm from the center of the tissue area of interest **306**. Two channels **308** and **310** are provided for white light illumination and a channel **312** is provided for white light endoscope forward viewing. Each of the channels **308**, 310 and 312 may have a diameter of 2.7 mm. A small channel **314** is also provided for an air or water nozzle.

In accordance with the present invention, a side-viewing Endoscopic Coherent Optical Microscope (ECOM) **316** is provided in the GI endoscope **300**. The side-viewing ECOM **316** includes a drive mechanism **318** for rotating the mirror **16** (not shown in Figures 14 and 15). As

mentioned previously, radial, translational or helical scanning may be employed. Furthermore, as previously mentioned, a MEMS drive mechanism may be used instead of a mechanical drive mechanism. The side-viewing ECOM **316** is configured to scan through the tissue area of interest **306** having the depth set by the boundaries **320** and the angular extent set by the boundaries **322**. Additionally an optical window **324** may be provided for the side-viewing ECOM **316** (see Figure 14).

The forward-viewing white light channel **312** is updated at a rate of 30 frames/sec. The cross-sectional images obtained by the side-viewing ECOM **316** are updated at 4.4 frames/sec. All imaging channels are displayed simultaneously. The images that may be generated by the GI endoscope **300** are illustrated in Figures 16 and 17. Figure 16 shows a simulated image of a human colon epithelium incorporating the expected spatial resolution which may achievable with the side-viewing ECOM **316**. Figures 17a and 17b are a comparison of microscopy imaging versus *in vivo* OCT imaging. Figure 17a has two panels which each show a microscopy image of sweat ducts in the human skin. Figure 17b has three panels which each show an *in vivo* OCT image of sweat ducts in the human skin. The *in vivo* OCT images were generated with a light source operating at a wavelength of 1300 nm.

Typical maneuvers or use of the GI endoscope **300** by an endoscopist will incorporate the following steps:

a) Following the steps of a general endoscopy procedure, the GI endoscope **300** is inserted under the guidance of the conventional forward-viewing white light channel **312**. This maneuver should be no different from that of currently available GI endoscopes.

b) When the endoscopist needs to make microscopic examinations, he/she first pushes the GI endoscope **300** into contact with the wall of the lumen as shown in Figure 13. The optics are designed such that when the GI endoscope **300** is in contact with the tissue, the correct working distance of the entire optical system is obtained. Although the GI endoscope **300** is in contact with the

wall, the part of the tissue under microscopic examination is not, as illustrated in Figure 15. Therefore, the surface features of the tissue are not distorted by contact pressure. However, this does not imply that the GI endoscope **300** can only be operated in a contact mode. In fact, the GI endoscope **300** may be operated in a non-contact mode, as long as images are formed, which is dictated by whether the previously described dynamic triggering algorithm has found an air-tissue interface. If the air-tissue interface lies within the working distance of the system then the interface should be specific and easily detected since the interface produces clear peaks in the detected light pattern as previously described in the 'flexible triggering' method.

c) If the endoscopist needs to examine a region adjacent to the area imaged in step (b), then the endoscopist can torque the GI endoscope **300** and rotate the field of view to a new location.

The best techniques currently in use for visualization of the gastrointestinal (GI) tract include endoscopic ultrasonography (EUS) and magnification endoscopy (ME). The resolution of high-frequency EUS, approximately 70 to 100 mm, is insufficient for the identification of many conditions that perturb tissue microstructure, most notably subtle pathologic changes arising within the superficial layers of the GI tract (mucosa and submucosa). ME, with a magnification of up to 170X, provides excellent images of fine superficial mucosal patterns but subsurface structures and lesion staging cannot be determined. Accordingly, tissue biopsy and histology currently remain the standard of care for detecting microscopic diseases involving the GI tract.

The side-viewing ECOM **316** disclosed herein may achieve real-time, 2 mm deep cross-sectional images of the GI wall at a resolution of 5 µm in both axial and transverse (lateral) dimensions. For reference, gastrointestinal epithelial cells average 7 to 10 µm in size which increases further as dysplastic or neoplastic transformation ensues. In the GI tract, a depth of view at 2 mm is nevertheless sufficient to detect mucosally-based

diseases as well as any neoplastic invasion into the underlying submucosa, which is of important for prognostic and therapeutic purposes. The image resolution of the side-viewing ECOM **316** may correspond to observing an *unstained* histology slide under a 100X (total magnification) microscope. Accordingly, many important entities such as dysplasia (cellular neoplastic alterations) or neoplastic violation of structures such as the lamina propria or muscularis mucosae may be discernible with the side-viewing ECOM **316**.

The present invention may allow for *in-situ* diagnosis of diverse *microscopic* mucosal pathologies and lesion staging. In essence, this "optical biopsy" technique may replace, or at the very least, guide the standard biopsy and histology method. This may translate into reducing unnecessary biopsy samples and tissue processing, decreasing patient risk and increasing sampling rate and diagnostic yield thus providing immediate diagnostic feedback both to the physician and the patient and targeting biopsies (which in itself may become a therapeutic maneuver in some cases). Pre-neoplastic GI conditions such as Barrett's esophagus, chronic ulcerative colitis, early flat adenomas, or foci of aberrant colonic crypts, to name a few, may be applicable to the side-viewing ECOM **316**. Currently, detection and surveillance of neoplastic progression within these conditions are suboptimal due to their microscopic nature.

Secondly, the side-viewing ECOM **316** may serve as a functional imaging system permitting monitoring of neoplastic and non-neoplastic tissue alterations over time. For instance, the recovery of the structure of small intestinal villi and reduction in inflammatory cells may be monitored by the side-viewing ECOM **316** in diverse malabsorptive disorders of the gut such as gluten-sensitive enteropathy, tropical sprue and intestinal infestation. The natural history of many mucosal diseases at the microscopic level may also be assessed in a minimally invasive manner. The ability to monitor structural cellular changes that are occurring *in vivo* with time may provide important physiologic information on cellular function and insight into cellular pathologic transformation.

Thirdly, the side-viewing ECOM **316** may be used in the monitoring of tissue post therapy. *In vivo* microscopic evaluation of surgical resection margins or treatment margins during post-therapeutic surveillance of cancer resection or assessment of the adequacy of photodynamic therapy of mucosal preneoplastic conditions are only some examples.

Applications in other medical specialties may also be possible. It should be understood by those skilled in this art that the multichannel OCT apparatus disclosed herein may have application in a large number of medical specialties such as dermatology, hematology, oncology (medical and radiation), ophthalmology, urology, surgery, respirology and gastroenterology.

The multichannel OCT system disclosed herein may be altered to further improve system performance. For instance a modification that may be made would be to employ coded transmission for the optical radiation which is radiated from the optical sources. This technique may increase the image resolution by increasing the SNR of the optical radiation of the interference pattern obtained in channels which suffer from poor SNR.

It should be understood that various modifications can be made to the preferred embodiments described and illustrated herein, without departing from the present invention, the scope of which is defined in the appended claims. For instance, in each of the schematics, herein disclosed, other optical couplers may also be used in place of the 3 dB couplers.

CLAIMS:

1. An apparatus for optical examination of a sample, the apparatus comprising:

an optical source means for providing a plurality of separate optical radiation sources;

a first optical path extending from the source means;

a focusing means in the first optical path for focusing optical radiation from the optical radiation sources into a plurality of respective focal points located on a surface within the first optical path to provide substantially continuous coverage of a selected portion of the first optical path, whereby, in use, a sample can be located at least partially within said selected portion, thereby permitting simultaneous scanning of a plurality of points within the sample.

2. An apparatus as claimed in claim 1, wherein the optical source means comprises a primary optical source and optical coupling means connecting the primary optical source to the optical radiation sources and comprising a plurality of optical fibers.

3. An apparatus as claimed in claim 2, wherein the plurality of optical fibers terminate in a fiber bundle tip, wherein ends of the optical fibers in the fiber bundle tip are stepped relative to one another along the first optical path and wherein optical radiation from each optical fiber is focused to a different focal point.

4. An apparatus as claimed in claim 1, 2 or 3, which includes a rotatable mirror in the first optical path, for deflecting radiation from the optical radiation sources to permit rotational movement of the surface.

5. An apparatus as claimed in claim 1, 2 or 3, which includes a mirror in the first optical path and wherein the optical source means, the

focusing means and the mirror, in combination, may be linearly translated to permit linear movement of the surface.

6. An apparatus as claimed in claim 1, 2 or 3, which includes a rotatable mirror in the first optical path and wherein the optical source means, the focusing means and the rotatable mirror, in combination, may be linearly translated to permit helical movement of the surface.

7. An apparatus as claimed in claim 4, 5 or 6, wherein the surface is a complex surface.

8. An apparatus as claimed in claims 4, 5 or 6, wherein the mirror is a surface of a prism.

9. An apparatus as claimed in claims 4 or 6, including a micromachined electro-mechanical system coupled to the mirror for rotating the mirror.

10. An apparatus as claimed in claim 5 or 6, including a micromachined electro-mechanical system for linearly translating the optical source means, the focusing means and the mirror.

11. An apparatus as claimed in claim 2, 3 or 4, which further includes a plurality of optical couplers between the primary optical source and the optical fibers, an optical delay generator coupled to the optical couplers and detector means coupled to the optical couplers, wherein the optical couplers transmit a portion of the radiation from the primary optical source along the first optical path and a portion of the radiation from the primary optical source to the optical delay generator, the optical delay generator providing a second optical path, wherein an interference effect occurs between radiation returned along the first and second optical paths to the optical couplers and the optical couplers transmit the radiation returned along the first and second optical paths to the detector means.

12. An apparatus as claimed in claim 11, which includes a plurality of primary optical sources and a plurality of tree couplers, each tree coupler being associated with one primary optical source and coupling said one primary optical source to at least one of the optical couplers.

13. An apparatus as claimed in claim 12, which includes a plurality of optical circulators, placed between the optical couplers and the detectors for providing salvaged optical radiation to the detectors.

14. An apparatus as claimed in claim 11, wherein a plurality of optical fibers couple the optical couplers to the optical delay generator, the optical delay generator having a grating and a scanning mirror, the scanning mirror having an axis, wherein the grating separates optical radiation from each optical fiber into spectral components linearly oriented on the scanning mirror, wherein the midpoint of said spectral components is offset from the axis of the scanning mirror by a distance x_d to phase modulate said spectral components.

15. An apparatus as claimed in claim 11, which includes a first plurality of optical fibers for coupling each optical coupler to a phase modulator and a second plurality of optical fibers for coupling each phase modulator to the optical delay generator, the optical delay generator having a grating and a scanning mirror, the scanning mirror having an axis, wherein for each optical fiber, the phase modulator phase modulates the optical radiation and said grating separates said phase modulated optical radiation into spectral components which are linearly oriented on said scanning mirror, the midpoint of said spectral components being centered on the axis of said scanning mirror and wherein the spectral components from each optical fiber is spaced apart from the spectral components of the optical radiation from the other optical fibers.

22. An N channel apparatus as claimed in claim 21, wherein the sample arm comprises a polarization control means, a variable delay element and a sample.

23. An N channel apparatus as claimed in claim 20, wherein the reference arm comprises a tree coupling means, a phase modulating means and an optical delay means.

24. A two channel apparatus, for optical examination of a sample, said two channel apparatus comprising two optical networks as claimed in claim 20, 21, 22, 23, an optical source and a visible light source for guiding the orientation of the two channel apparatus.

25. A method for optical examination of a sample, the method comprising:

(a) providing radiation from a plurality of separate optical radiation sources, along a first optical path;

(b) providing focusing means in the first optical path;

(c) focusing the optical radiation from the optical sources into a plurality of respective focal points along a surface within the first optical path to provide substantially continuous coverage of a selected portion of the first optical path; and

(d) providing a sample located at least partially within the first optical path; and

(e) simultaneously scanning a plurality of points within the sample.

26. A method as claimed in claim 25, which includes providing radiation from a primary optical source and transmitting the radiation along a plurality of optical fibers to a plurality of separate optical radiation sources.

27. A method as claimed in claim 26, which includes terminating the plurality of optical fibers in a fiber bundle tip, providing the ends of the

optical fibers in the fiber bundle tip in a common plane and stepping the ends of the optical fibers relative to one another, along the first optical path, and focusing radiation from the optical fibers through a common lens.

28. A method as claimed in claim 27, which includes:
(a) providing a rotatable mirror in the first optical path;
(b) deflecting the first optical path;
(c) causing the plurality of focal points to be located on a surface;
(d) performing an axial scan;
(e) rotating the mirror to move the surface; and,
(f) repeating step (d) at least two times and performing step (e) between each repetition.

29. A method as claimed in claim 27, which includes:
(a) providing a mirror in the first optical path;
(b) deflecting the first optical path;
(c) causing the plurality of focal points to be located on a surface;
(d) performing an axial scan;
(e) linearly translating, in combination, the focusing means, the plurality of optical radiation sources and the mirror to move the surface; and,
(f) repeating step (d) at least two times and performing step (e) between each repetition.

30. A method as claimed in claim 27, which includes:
(a) providing a mirror in the first optical path;
(b) deflecting the first optical path;
(c) causing the plurality of focal points to be located on a surface;
(d) performing an axial scan;
(e) simultaneously rotating the mirror and linearly translating, in combination, the focusing means, the plurality of optical radiation sources and the mirror to move the surface; and,
(f) repeating step (d) at least two times and performing step (e) between each repetition.

31. A method as claimed in claims 28, 29 or 30, which includes providing a surface of a prism as the mirror.

32. A method as claimed in claims 28, 29 or 30, which includes supplying radiation from the primary optical source through a plurality of couplers to the optical fibers, providing an optical delay generator connected to the optical couplers and providing a second optical path, permitting radiation to be transmitted back along the first and second optical paths to the couplers, for forming interference, and transmitting radiation received from the first and second optical paths at the optical couplers to detection means for detection of the interference pattern.

33. A method as claimed in claim 32, which includes providing a plurality of primary optical sources and, for each primary optical source, a respective tree coupler, and coupling each primary optical source through said respective tree coupler to each of the optical couplers.

34. A method as claimed in claim 32, which includes providing optical circulator means between the optical couplers and the detection means for providing salvaged optical radiation to the detection means.

35. A method as claimed in claim 33, which includes providing the apparatus as an endoscope adapted for examining an internal cavity of the body, including at least one of: at least one channel for white light illumination, a white light endoscope forward viewing channel, a suction/biopsy channel and a channel for one of an air nozzle and a water nozzle.

36. A method as claimed in claims 30, 31 or 32, wherein there is a change in refractive index between a medium containing the optical radiation sources and the sample and for each focal point, a distance mismatch due to the change in refractive index between the coherence gate

of each optical radiation source and the focal point in the sample due is obtained according to the steps of:

(a) scanning optical radiation from the plurality of optical radiation sources in said first optical path such that the focal points of the optical radiation sources are aligned along a path extending from the medium containing the optical radiation sources into the sample;

(b) detecting the reflected optical radiation for each focal point; and,

(c) locating the focal point for which there is a large change in reflected optical radiation compared to neighboring focal points,

whereby, the focal point located in step (c) indicates the location of the interface between the sample and the medium containing the optical radiation sources.

37. A method as claimed in claim 36, wherein the method further comprises repeating steps (a) to (c) for each axial scan to obtain proper spatial resolution for the selected scan zone.

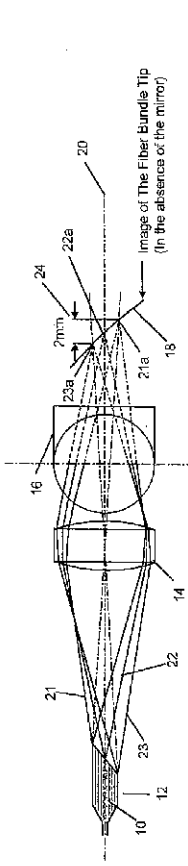

Figure 1a

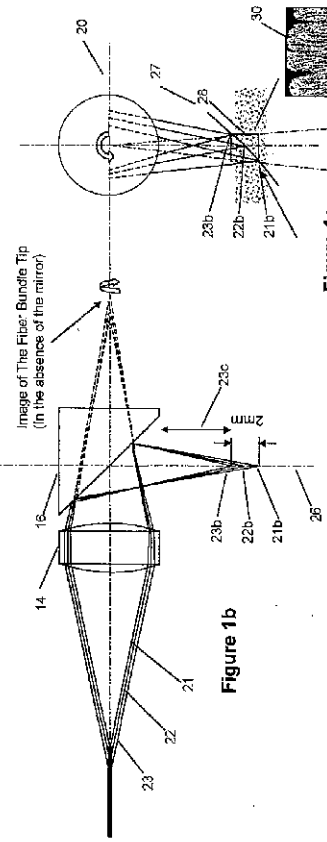

Figure 1b

Figure 1c

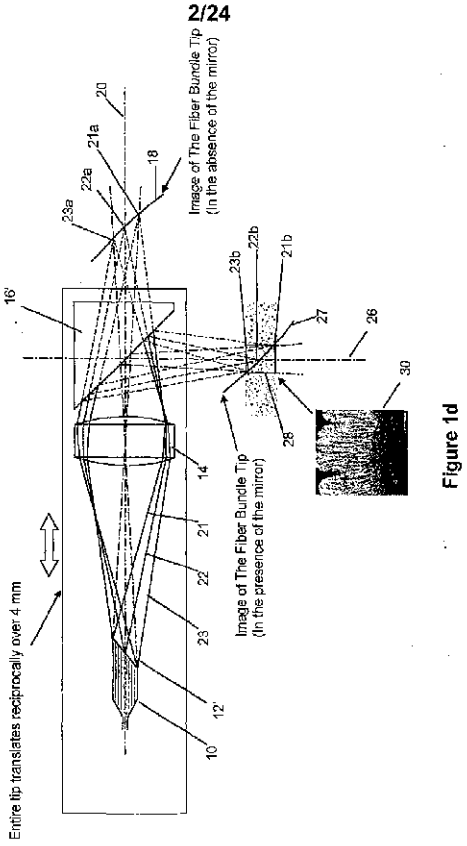
Image of The Fiber Bundle Tip
(In the absence of the mirror)
20
21a
18
22a
23a
16'
23b
22b
21b
27
26
30
28
14
21
22
23
12'
10'
Image of The Fiber Bundle Tip
(In the presence of the mirror)
Entire tip translates reciprocally over 4 mm

Figure 1d

Figure 2a

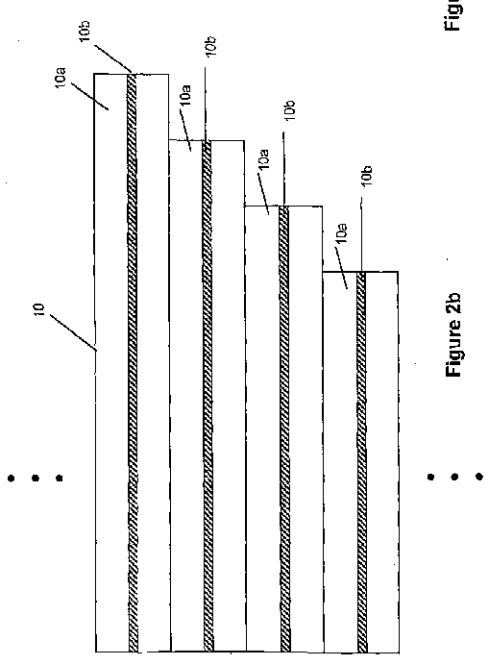

Figure 2b

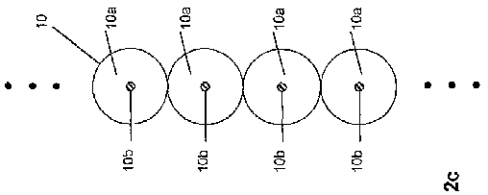

Figure 2c

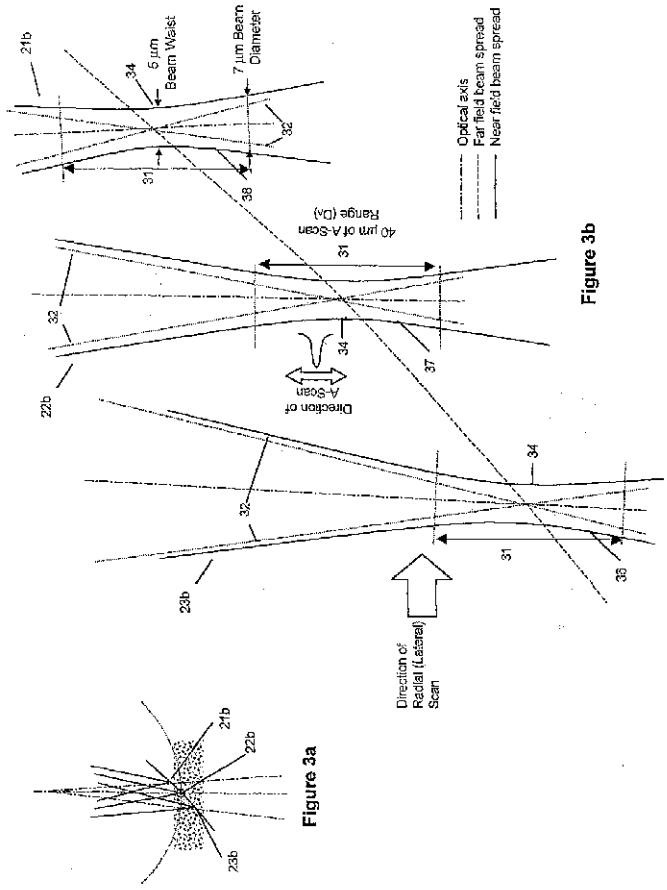

Figure 3b

Figure 3a

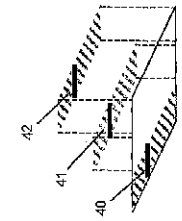

Figure 4f

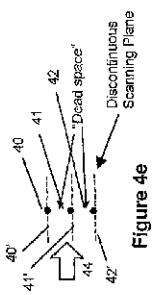

Figure 4e

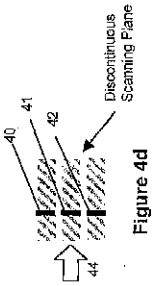

Figure 4d

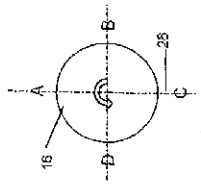

Figure 4a

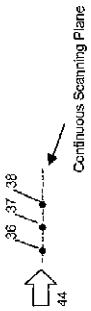

Figure 4b

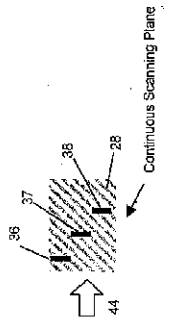

Figure 4c

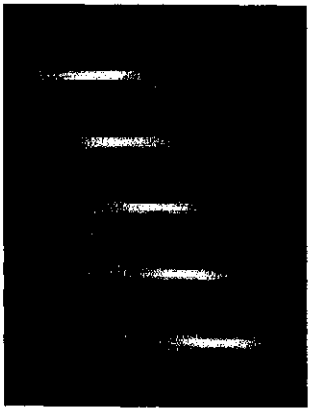

Figure 5b

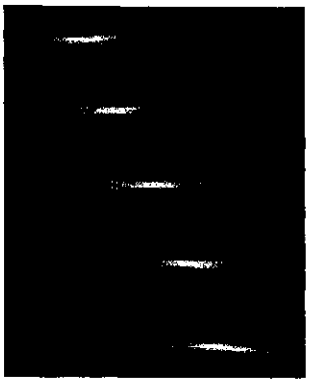

Figure 5a

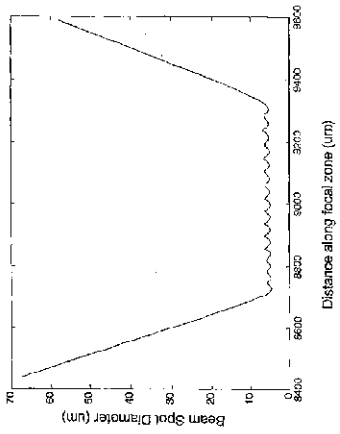

Figure 5d

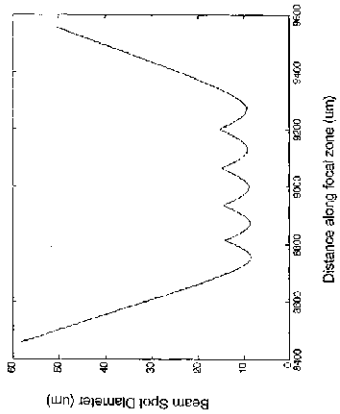

Figure 5c

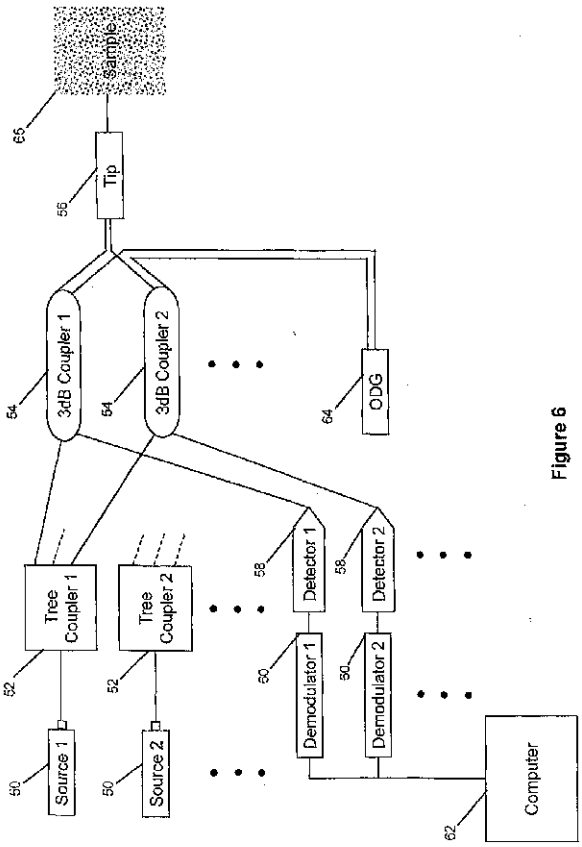
Sample
65
Tip
56
3dB Coupler 1
54
3dB Coupler 2
54
ODG
64
Tree Coupler 1
52
Tree Coupler 2
52
Detector 1
58
Detector 2
58
Demodulator 1
60
Demodulator 2
60
Source 1
50
Source 2
50
Computer
62

Figure 6

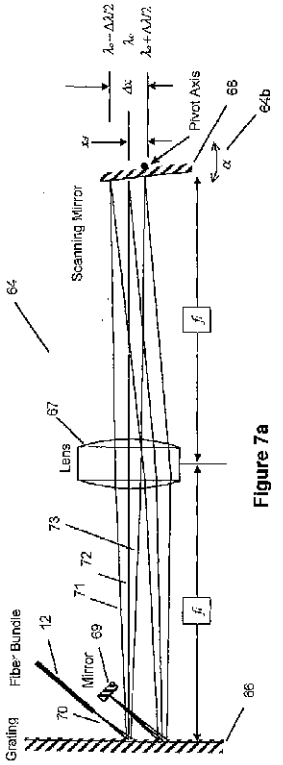

Figure 7a

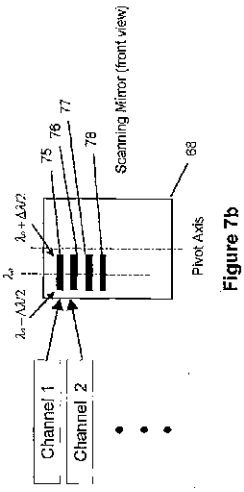

Figure 7b

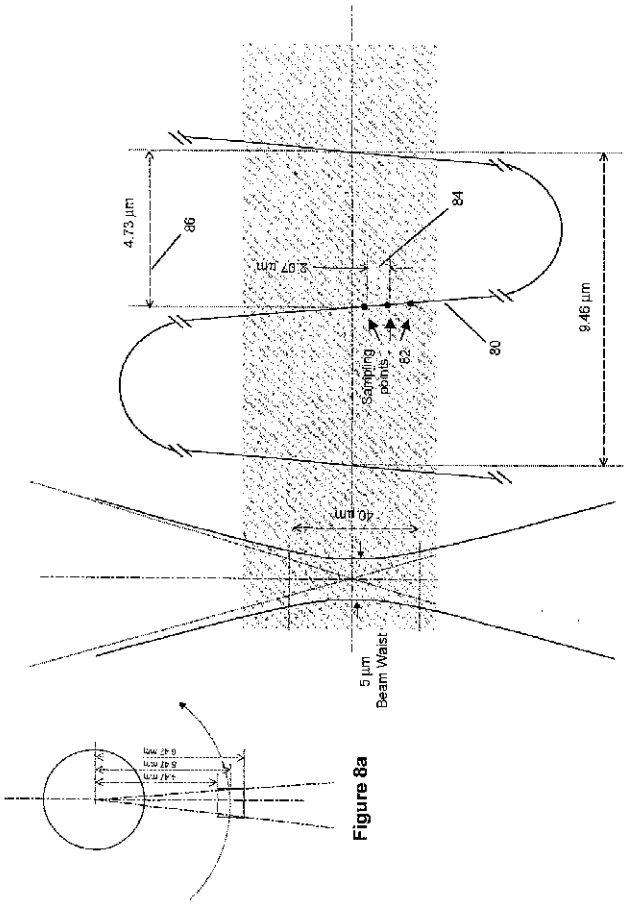

Figure 8b

Figure 8a

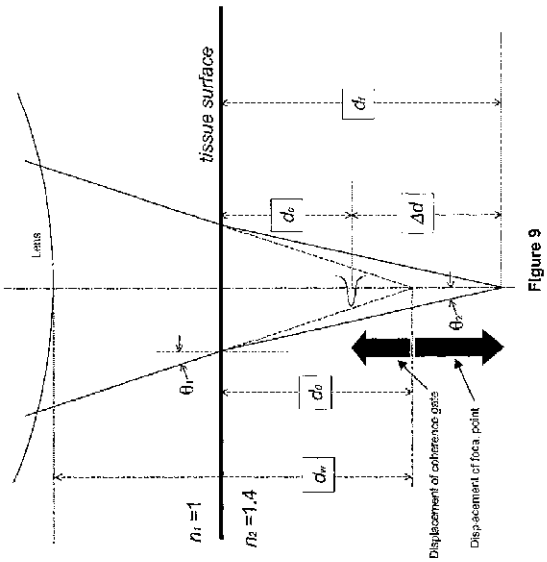
tissue surface
Lens
d_f
d_o
Δd
θ_2
θ_1
d_o'
d_w
$n_1 = 1$
$n_2 = 1.4$
Displacement of coherence gate
Displacement of focal point

Figure 9

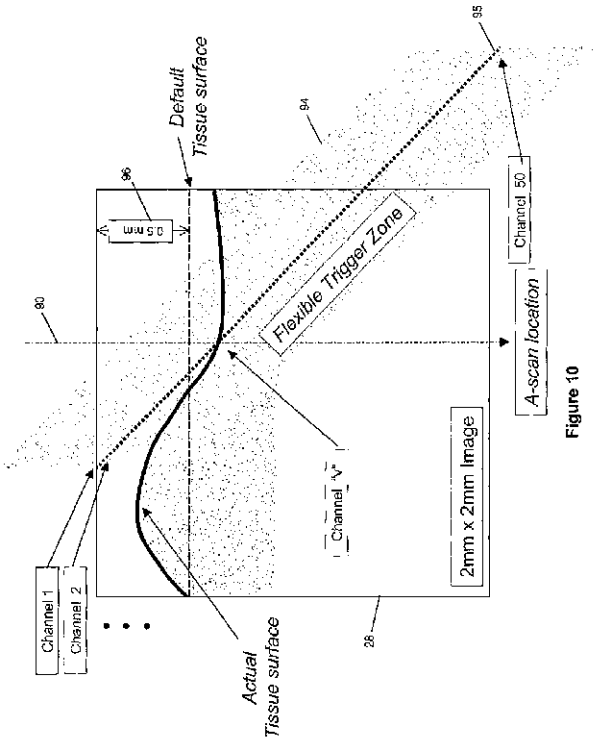
Default
Tissue surface
94
95
96
0.5 mm
Flexible Trigger Zone
Channel 50
A-scan location
80
Channel 1
Channel 2
Channel "n"
2mm x 2mm Image
28
Actual
Tissue surface

Figure 10

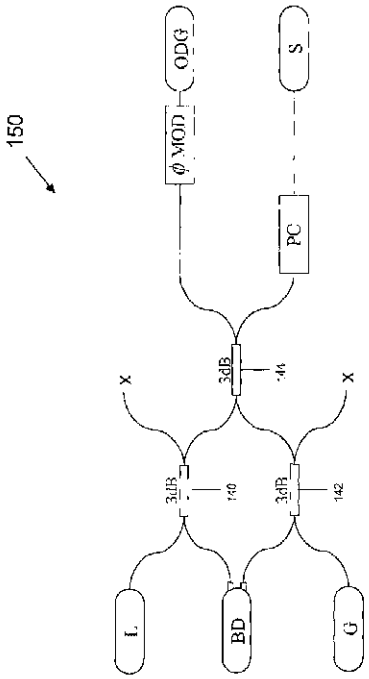

"Prior Art"

Figure 11a

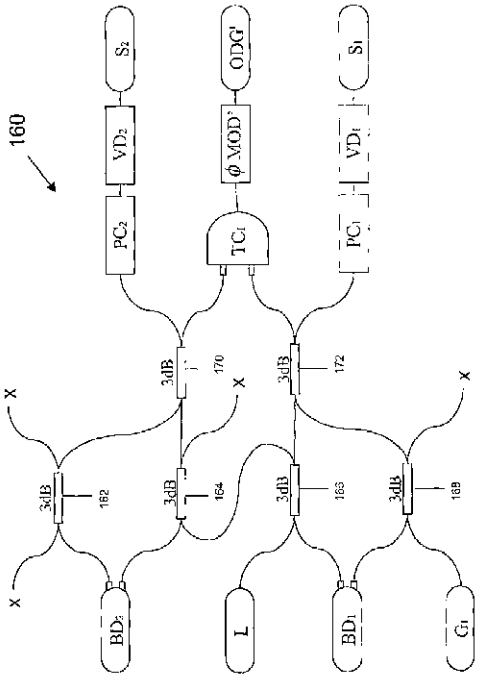
160
S2
VD2
PC2
ODG'
φ MOD'
TC1
S1
VD1
PC1
3dB
170
172
162
164
163
169
X
BD2
L
BD1
G1

Figure 11b

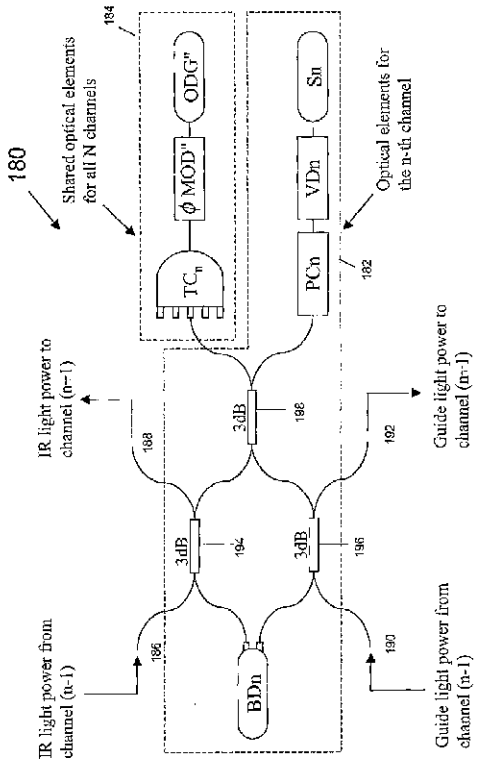
180
Shared optical elements for all N channels
184
ODG"
ϕ MOD"
TCn
Sn
VDn
PCn
Optical elements for the n-th channel
182
IR light power to channel (n-1)
188
3dB
198
Guide light power to channel (n-1)
192
3dB
194
3dB
196
IR light power from channel (n-1)
186
BDn
190
Guide light power from channel (n-1)

Figure 11c

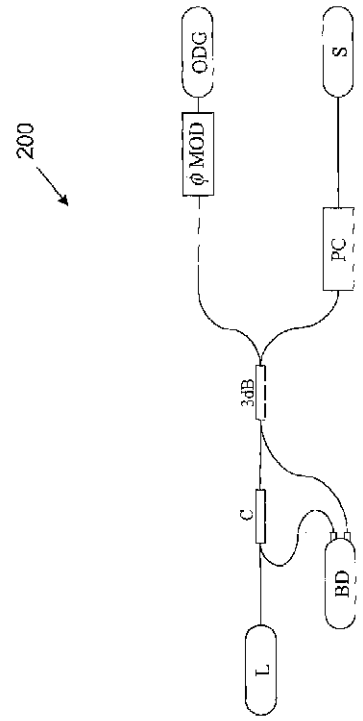

"Prior Art"

Figure 12a

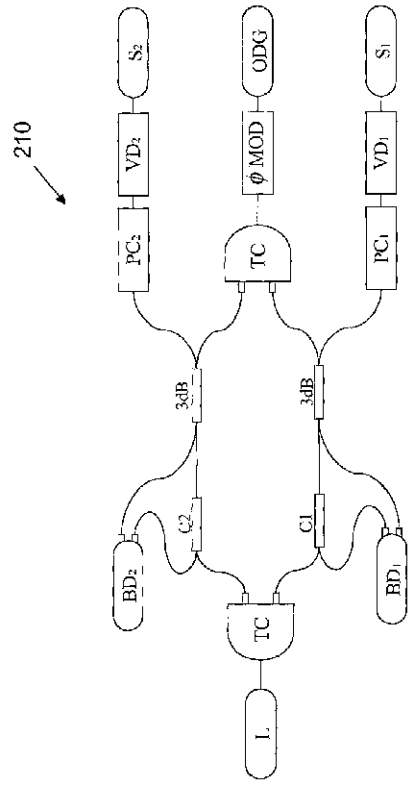

Figure 12b

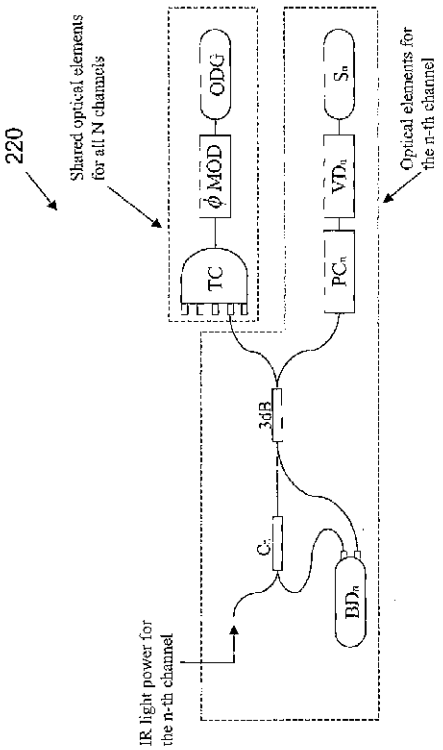
220
Shared optical elements for all N channels
Optical elements for the n-th channel
TC
ϕ MOD
ODG
PC_n
VD_n
S_n
3dB
C_n
BD_n
IR light power for the n-th channel

Figure 12c

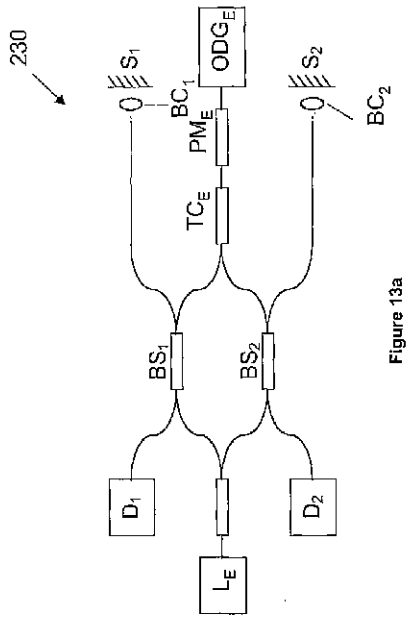

Figure 13a

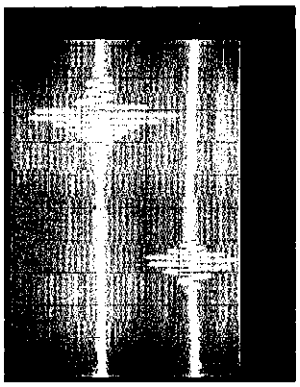

Figure 13c

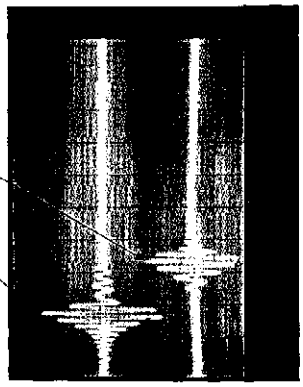

Figure 13b

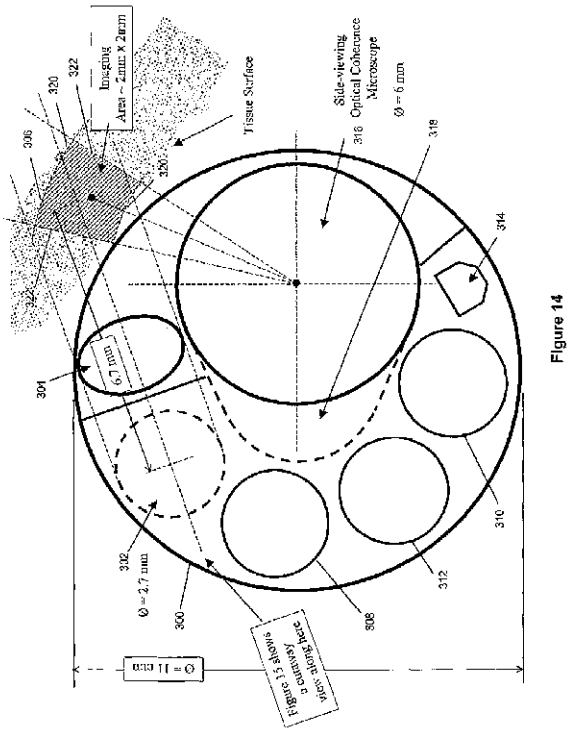
Imaging Area ~ 2mm x 2mm
Tissue Surface
Side-viewing Optical Coherence Microscope
Ø = 6 mm
306
320
322
316
318
314
301
6.7 mm
310
312
308
302
Ø = 2.7 mm
300
Figure 3 cutaway view through here
Ø = 11.6mm

Figure 14

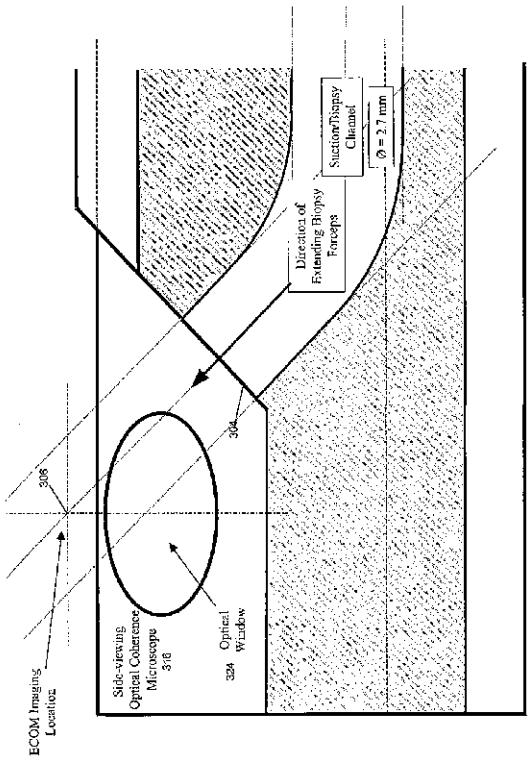
Suction/Biopsy Channel
Ø = 2.7 mm
Direction of Extending Biopsy Forceps
304
308
Side-viewing Optical Coherence Microscope 316
Optical Window 324
ECOM Imaging Location

Figure 15

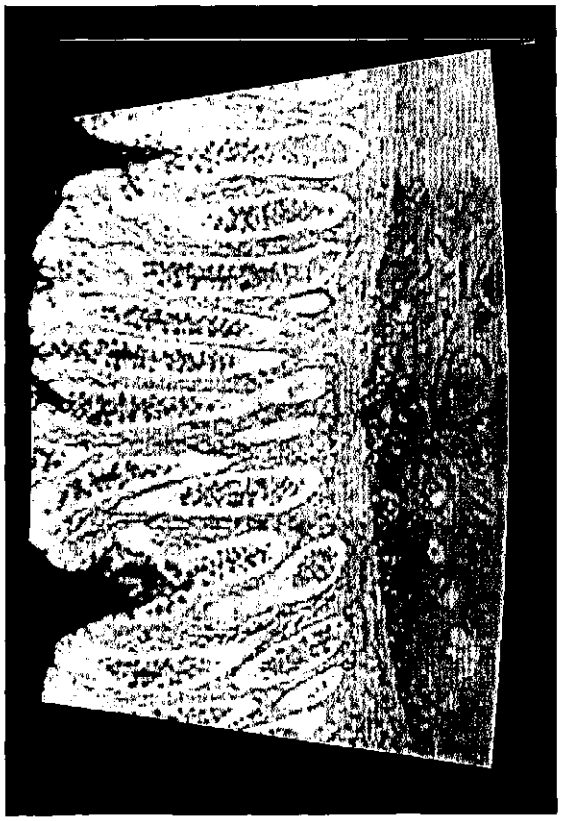

Figure 16

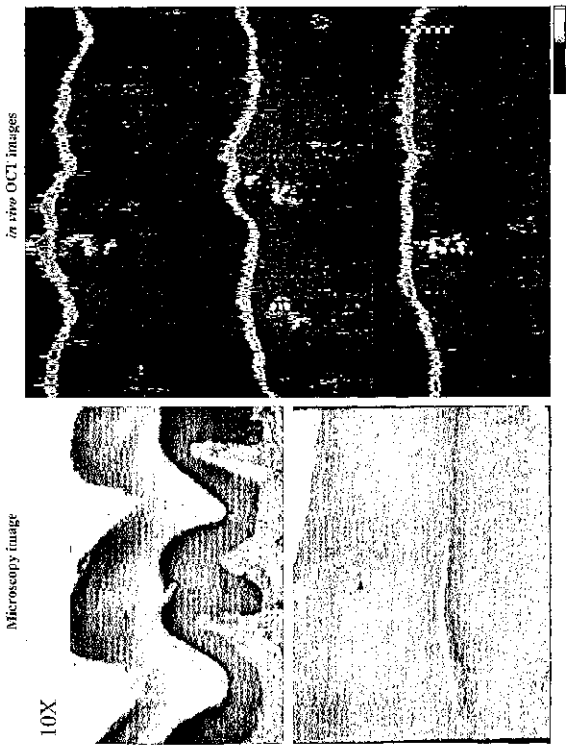

Figure 17b

Figure 17a

【国際調査報告】

INTERNATIONAL SEARCH REPORT

International application No.

A. CLASSIFICATION OF SUBJECT MATTER

According to International Patent Classification (IPC) or to both national classification and IPC

B. FIELDS SEARCHED

Minimum documentation searched (classification system followed by classification symbols)

Documentation searched other than minimum documentation to the extent that such documents are included in the fields searched

Electronic data base consulted during the international search (name of data base and, where practicable, search terms used)

C. DOCUMENTS CONSIDERED TO BE RELEVANT

Category*	Citation of document, with indication, where appropriate, of the relevant passages	Relevant to claim No.

☐ Further documents are listed in the continuation of Box C. ☐ See patent family annex.

* Special categories of cited documents:
"A" document defining the general state of the art which is not considered to be of particular relevance
"B" earlier document but published on or after the international filing date
"L" document which may throw doubts on priority claim(s) or which is cited to establish the publication date of another citation or other special reason (as specified)
"O" document referring to an oral disclosure, use, exhibition or other means
"P" document published prior to the international filing date but later than the priority date claimed

"T" later document published after the international filing date or priority date and not in conflict with the application but cited to understand the principle or theory underlying the invention
"X" document of particular relevance; the claimed invention cannot be considered novel or cannot be considered to involve an inventive step when the document is taken alone
"Y" document of particular relevance; the claimed invention cannot be considered to involve an inventive step when the document is combined with one or more other such documents, such combination being obvious to a person skilled in the art
"&" document member of the same patent family

Date of the actual completion of the international search	Date of mailing of the international search report
Name and mailing address of the ISA/	Authorized officer
Facsimile No.	Telephone No.

Form PCT/ISA/210 (second sheet) (July 1992)

フロントページの続き

(81)指定国 AP(GH,GM,KE,LS,MW,MZ,SD,SL,SZ,TZ,UG,ZW),EA(AM,AZ,BY,KG,KZ,MD,RU,TJ,TM),EP(AT,BE,CH,CY,DE,DK,ES,FI,FR,GB,GR,IE,IT,LU,MC,NL,PT,SE,TR),OA(BF,BJ,CF,CG,CI,CM,GA,GN,GW,ML,MR,NE,SN,TD,TG),AE,AG,AL,AM,AT,AU,AZ,BA,BB,BG,BR,BY,BZ,CA,CH,CN,CO,CR,CU,CZ,DE,DK,DM,DZ,EE,ES,FI,GB,GD,GE,GH,GM,HR,HU,ID,IL,IN,IS,JP,KE,KG,KP,KR,KZ,LC,LK,LR,LS,LT,LU,LV,MA,MD,MG,MK,MN,MW,MX,MZ,NO,NZ,PL,PT,RO,RU,SD,SE,SG,SI,SK,SL,TJ,TM,TR,TT,TZ,UA,UG,US,UZ,VN,YU,ZA,ZW

(72)発明者 ヤン，ヴィクター シャオ ドン
カナダ国 エム５エス ３エル１ オンタリオ州 トロント ハーボード ストリート ６０ ユニット ９３６ビー
(72)発明者 ヴィトキン，アイ アレックス
カナダ国 エム６ピー １イー５ オンタリオ州 トロント グレンレイク アヴェニュー １３０
(72)発明者 ウォンキーソン，ルイエ
アメリカ合衆国 ミネソタ州 ５５９０１ ロチェスター セカンド ストリート エヌダブリュ ２１１ アパートメント ５０２
(72)発明者 カツ，シャロン
カナダ国 エム４エム ２エックス２ オンタリオ州 トロント ウィニフレッド アヴェニュー ７７
(72)発明者 ゴードン，マーガレット レスリー
カナダ国 エム４ピー ２エヌ４ オンタリオ州 トロント デイルウッド ロード ６１
(72)発明者 ウィルソン，ブライアン シー
カナダ国 エム６アール ２ワイ６ オンタリオ州 トロント インディアン グローヴ ８５
(72)発明者 モク，アルヴィン ホー クァン
カナダ国 エル４ビー ３シー５ オンタリオ州 リッチモンド ヒル スパディナ ロード １８７

Ｆターム(参考) 2G059 BB12 EE09 FF01 FF03 GG01 GG03 GG06 HH01 HH02 HH06
JJ05 JJ11 JJ12 JJ13 JJ15 JJ17 JJ22 KK03 MM01 MM08
MM09
2H040 BA01 CA02 CA11
4C061 CC06 DD03 FF46 FF47 HH51 LL01 WW10 WW20
5C024 BX02 CX00 CY00 EX41 EX48 EX54 JX02

专利名称(译)	用于高分辨率相干光成像的方法和设备		
公开(公告)号	JP2004502957A	公开(公告)日	2004-01-29
申请号	JP2002509751	申请日	2001-07-10
[标]申请(专利权)人(译)	大学健康网络		
申请(专利权)人(译)	盐湖城大学健康网络		
[标]发明人	ヤンヴィクターシャオドン ヴィトキンアイアレックス ウォンキーソンルイエ カツシャロン ゴードンマーガレットレスリー ウィルソンブライアンシー モクアルヴィンホークァン		
发明人	ヤン,ヴィクター シャオ ドン ヴィトキン,アイ アレックス ウォンキーソン,ルイエ カツ,シャロン ゴードン,マーガレット レスリー ウィルソン,ブライアン シー モク,アルヴィン ホー クァン		
IPC分类号	G01N21/17 A61B1/00 A61B1/05 A61B5/00 G01N21/47 G02B6/04 G02B23/26 H04N5/335		
CPC分类号	A61B5/6852 A61B1/00096 A61B1/00172 A61B1/05 A61B5/0066 G01N21/4795		
FI分类号	G01N21/17.620 A61B1/00.300.D G02B23/26.B H04N5/335.V		
F-TERM分类号	2G059/BB12 2G059/EE09 2G059/FF01 2G059/FF03 2G059/GG01 2G059/GG03 2G059/GG06 2G059/HH01 2G059/HH02 2G059/HH06 2G059/JJ05 2G059/JJ11 2G059/JJ12 2G059/JJ13 2G059/JJ15 2G059/JJ17 2G059/JJ22 2G059/KK03 2G059/MM01 2G059/MM08 2G059/MM09 2H040/BA01 2H040/CA02 2H040/CA11 4C061/CC06 4C061/DD03 4C061/FF46 4C061/FF47 4C061/HH51 4C061/LL01 4C061/WW10 4C061/WW20 5C024/BX02 5C024/CX00 5C024/CY00 5C024/EX41 5C024/EX48 5C024/EX54 5C024/JX02		
代理人(译)	佐久间刚		
优先权	60/217090 2000-07-10 US		
其他公开文献	JP2004502957A5		
外部链接	Espacenet		

摘要(译)

提供了一种用于检查样品的表面下微结构的方法和设备。来自多个光学辐射源的辐射沿第一光学路径行进。在第一光路中，装置将来自每个光源的光学辐射聚焦成沿第一光路的多个相应焦点，以提供第一光路的选定部分的基本上连续的覆盖。然后，沿着第一光路的所选部分扫描在延伸到样品中的所选长度内的第一光路上的样品。

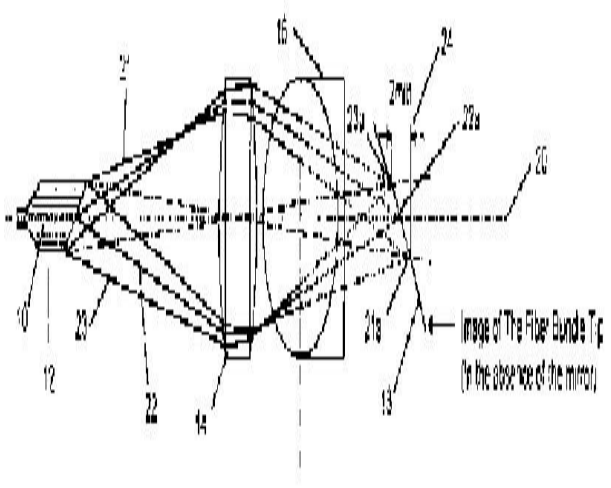
16
24
2
23a
22a
20
10
26
21a
Image of The Fiber Bundle Tip
(In the absence of the mirror)
12
22
14
13